2019

UNIVERSITY OF CRETE
SCHOOL OF SCIENCES AND ENGINEERING
DEPARTMENT OF PHYSICS

POSTGRADUATE PROGRAM:
"Photonics and Nanoelectronics"

MASTER THESIS

Chemical synthesis of ZnO nanostructures, following environmental friendly approaches and study of their structural and optical properties.

Author:
Evangelia G. Petromichelaki

Supervisors:

Prof. Alexandros Georgakilas,
University of Crete

Dr. George Kenanakis,
Researcher, IESL-FORTH

2019

UNIVERSITY OF CRETE

SCHOOL OF SCIENCES AND ENGINEERING

DEPARTMENT OF PHYSICS

POSTGRADUATE PROGRAM:
"Photonics and Nanoelectronics

MASTERS THESIS

Chemical synthesis of ZnO nanostructures, following environmental friendly approaches and study of their structural and optical properties.

Author:
Evangelia G. Petromichelaki

Thesis examination committee:

1. Prof. Alexandros Georgakilas at Department of Physics, University of Crete.
2. Dr. George Kenanakis, Researcher at Institute of Electronic Structure & Laser, Foundation for Research and Technology.
3. Prof. Demetrios Anglos at Department of Chemistry, University of Crete.

Acknowledgements

First, I would like to express my sincere gratitude to my advisor Dr. George Kenanakis, Researcher at the Institute of Electronic Structure and Laser (IESL) of Foundation of Research and Technology Hellas (FORTH), member of the Photonic-, Phononic-, and Meta-materials (PPM) group, who guided me throughout the experimental procedures and provided me with all the necessary information.

Furthermore, I would like to thank all the other members of the PPM Group, for their invaluable help, cooperation and support in my work.

Moreover, I would like to thank Mrs. Alexandra Manousaki for her help on the characterization of the samples using the electron microscopy, as well as Mrs. Maria Androulidaki, for her priceless contribution on the photoluminescence measurements and their analysis.

Finally yet importantly, I would like to thank Prof. Alexandros Georgakilas, of the Physics department of University of Crete, for the supervision of this work.

Abstract

This Master thesis focuses on the chemical synthesis of zinc oxide (ZnO) nanostructures, following environmental friendly approaches, with emphasis on their structural and optical properties.

The synthesis of ZnO nanostructures was based on an aqueous solution chemical (ACG) method, a low cost, environmental friendly technique that does not require any complicate or expensive equipment, at mild temperatures. Moreover, it is the first time that ZnO was synthesized following the ACG approach at temperatures as high as 195°C max., using eco-friendly solvents, such as water or mild alcohol solutions.

Subsequently, in comparison to other research groups, edible alcoholic distillations were used as solvents, in order to synthesize different morphologies of ZnO, enriched with dopants coming from the characteristic ingredients of each drinking alcohol.

Last but not least, we present nano- and micro-structures of ZnO that have been synthesized using metallic zinc, in the form of powder, in various solvents, without further annealing. These samples resulted in sharp photoluminescence characteristic peaks at room temperature, with intensities much higher than the ones recorded so far.

The morphology and the structural properties of the synthesized ZnO nanostructures were studied by means of scanning electron microscopy (SEM) and X-ray diffraction (XRD), respectively, while their optical properties were examined through photoluminescence (PL) spectroscopy measurements. Their structural properties disclose a hexagonal wurtzite structure, while photoluminescence spectroscopy measurements reveal that the as-grown ZnO samples exhibit strong UV emission, which corresponds to the near band edge emission of ZnO.

It is concluded that ZnO nanostructures can be synthesized based on an environmental green synthesis approach, using non-toxic reagents, exhibiting remarkable PL properties.

Keywords: ZnO; nanostructures; aqueous chemical growth (ACG); green synthesis; photoluminescence (PL)

Περίληψη

Η παρούσα διπλωματική εργασία εστιάζει στη χημική σύνθεση νανοδομών οξειδίου του ψευδαργύρου (ZnO), ακολουθώντας φιλικές προς το περιβάλλον προσεγγίσεις, δίνοντας έμφαση στη μελέτη των δομικών και οπτικών ιδιοτήτων τους.

Η σύνθεση των νανοδομών ZnO βασίστηκε σε μια χημική μέθοδο, με υδατικά διαλύματα (ACG), χαμηλού κόστους και φιλική προς το περιβάλλον, που δεν απαιτεί πολύπλοκο ή ακριβό εξοπλισμό, σε ήπιες συνθήκες πίεσης και θερμοκρασίας. Επίσης, για πρώτη φορά πραγματοποιήθηκε σύνθεση του ZnO σε ποικιλία νανοδομών χρησιμοποιώντας την ίδια χημική τεχνική σε θερμοκρασίες που δεν υπερβαίνουν τους 195°C, και διαλύτες φιλικούς προς το περιβάλλον, όπως νερό ή ήπια αλκοολικά διαλύματα.

Συνεχίζοντας, σε σχέση με άλλες ερευνητικές ομάδες χρησιμοποιήθηκαν αλκοολικά αποστάγματα γεωργικής προελεύσεως σε μία προσπάθεια σύνθεσης ZnO διαφόρων μορφολογιών με προσμίξεις που προέρχονται από τα χαρακτηριστικά συστατικά των πόσιμων αλκοολών.

Τέλος, παρουσιάζουμε νανο- και μίκρο δομές ZnO που έχουν συντεθεί χρησιμοποιώντας μόνο μεταλλικό ψευδάργυρο σε νερό, χωρίς ανόπτηση ή περαιτέρω επεξεργασία, που δίνουν οξείες κορυφές φωτοφωταύγειας σε θερμοκρασία δωματίου, με εντάσεις πολύ μεγαλύτερες από τις μέχρι τώρα καταγεγραμμένες

Οι νανοδομές ZnO μελετήθηκαν όσον αφορά τα μορφολογικά και δομικά χαρακτηριστικά τους, με χρήση ηλεκτρονικής μικροσκοπίας σάρωσης (SEM) και περιθλασιμετρίας ακτίνων-Χ (XRD) αντίστοιχα, ενώ οι οπτικές τους ιδιότητες, μελετήθηκαν μέσω μετρήσεων φασματοσκοπίας φωτοφωταύγειας (PL). Η δομική μελέτη αποκαλύπτει την εξαγωνική κρυσταλλική δομή του βουρτσίτη, ενώ οι μετρήσεις φωτοφωταύγειας υπέδειξαν ότι τα δείγματα ZnO παρουσίασαν έντονη εκπομπή στο υπεριώδες, που αντιστοιχεί στη χαρακτηριστική εκπομπή του ZnO.

Από αυτή την εργασία συμπεραίνουμε ότι είναι εφικτή η σύνθεση νανοδομών ZnO, ακολουθώντας μια φιλική προς το περιβάλλον προσέγγιση χρησιμοποιώντας μη τοξικά αντιδραστήρια, φιλικά προς το περιβάλλον, με αξιοσημείωτες ιδιότητες όσον αφορά την φωτοφωταύγεια.

Λέξεις – κλειδιά: ZnO, νανοδομές, σύνθεση σε υδατικά διαλύματα (ACG), «πράσινη» σύνθεση, φωτοφωταύγεια (PL)

Table of Contents

Acknowledgements i
Abstract ii
Περίληψη iii

Chapter 1 – Theoretical part 4
Introduction 4
1.1 Semiconductors 5
1.1.1 Applications of metal oxide semiconductors 6
1.2 Zinc oxide (ZnO) among other metal oxide semiconductors 7
1.1.1 Properties of ZnO 8
1.1.1.1 Crystal structure of ZnO 8
1.1.1.2 Mechanical properties of ZnO 9
1.1.1.3 Electrical properties of ZnO 9
1.1.1.4 Optical properties of ZnO [44] 9
1.1.2 Synthesis techniques of ZnO 11
1.1.2.1 Sputter deposition [46] 11
1.1.2.2 Thermal Evaporation [48] 12
1.1.2.3 Pulsed Laser Deposition, PLD [50] 13
1.1.2.4 Spin coating 14
1.1.2.5 Chemical Vapor Deposition, CVD 15
1.1.2.6 Aqueous Chemical Growth, ACG 16
1.2 The need of environmental friendly synthesis 19

Chapter 2 – Experimental 20
Introduction 20
2.1 Synthesis of ZnO 21
2.1.1 Reagents / Materials 22
2.1.2 Synthesis of ZnO with zinc salts and HMTA 22
2.1.3 Synthesis of ZnO with zinc salts and baking ammonia 24
2.1.4 Synthesis of ZnO with zinc powder and HMTA 25
2.1.5 Synthesis of ZnO with zinc powder and baking ammonia 26

2.2.6 Synthesis of ZnO using pure zinc powder 26
2.2 Characterization techniques 27
2.2.1 Electron Microscopy 27
2.2.2 Scanning Electron Microscopy, SEM 28
2.2.3 Energy Dispersive X-ray Analysis, EDX [76] 32
2.2.4 X-ray Diffraction, XRD 33
2.2.5 Raman Spectroscopy [84] 37
2.2.6 Luminescence 39
2.2.6.1 Photoluminescence, PL 41

Chapter 3 – Results and discussion 43
Introduction 43
3.1. ZnO structures synthesized using zinc salts and HMTA 44
3.1.1 Morphology – SEM 44
3.1.2 Qualitative elemental analysis – EDX 52
3.1.3 Structural characterization – XRD 53
3.1.4 Optical characterization – PL 54
3.2. ZnO structures synthesized with zinc salts and baking ammonia *57*
3.2.1 Morphology – SEM 57
3.2.2 Qualitative elemental analysis – EDX 64
3.2.3 Structural characterization – XRD 64
3.2.4 Optical characterization – PL 66
3.3. ZnO structures synthesized with zinc powder and HMTA 68
3.3.1 Morphology – SEM 68
3.3.2 Qualitative elemental analysis – EDX 71
3.3.3 Structural characterization – XRD 72
3.3.4 Optical characterization – PL 74
3.4. ZnO structures synthesized with zinc powder and baking ammonia 75
3.4.1 Morphology – SEM 75
3.4.2 Qualitative elemental analysis – EDX 78
3.4.3 Structural characterization – XRD 79
3.4.4 Optical characterization – XRD 81

3.5. ZnO structures synthesized only with zinc powder 82
3.5.1 Morphology – SEM 82
3.5.2 Qualitative elemental analysis – EDX 84
3.5.3 Structural characterization – XRD 85
3.5.4 Optical characterization – PL 87
3.5.5 Raman Spectroscopy 88
3.6. Analysis of the photoluminescence (PL) measurements 89

Chapter 4 – Conclusions 91

References 94

Chapter 1 – Theoretical part

Introduction

This chapter starts with a general theory of the electronic properties of semiconductors and the variety of their applications.

Thereafter, among several metal oxides, ZnO is introduced; at first, the importance of ZnO is presented, along with some of its characteristic properties, with emphasis on its crystal structure. Afterwards, some of the physical and chemical methods used for ZnO synthesis are presented, ending up to the Aqueous Chemical Growth (ACG), the method that was applied for the purposes of this Master thesis.

Finally, the importance and the necessity of an environmental friendly approach regarding the synthesis of metal oxide semiconductors is presented, concluding to a brief description of the green synthesis of ZnO that was held in the framework of this work.

1.1 Semiconductors

The solid-state materials are classified as insulators, semiconductors and conductors, depending on the conductivity (or resistivity) and the energy bands.

Semiconductors are materials whose electrical conductivity lies between the conductivity of conductors and insulators. They are not good conductors nor good insulators, hence their name "semi"-conductors. They are characterized by a small number of "free electrons", in contrast with the conductors and insulators that have a large number and very few free electrons, respectively. As a result, the insulators have electrical conductivity $\sigma < 10^{-8}\ S/cm$, semiconductors have $10^{-8}\ S/cm < \sigma < 10^{3}\ S/cm$ and at last for the conductors the electrical conductivity is $\sigma > 10^{3}\ S/cm$.

The electrical properties of a given material are depending on the electronic populations of the different allowed bands. Every solid has its own characteristic energy band structure, as it can be seen from the following figure.

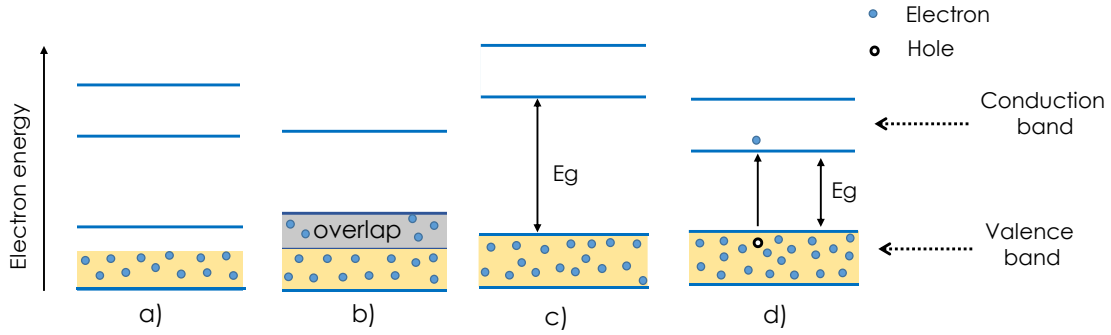

Figure 1.1 Energy band diagrams of a), b) a conductor, c) an insulator and d) a semiconductor

In conductors the valence band is either not fully occupied with electrons, or the filled valence band overlaps with the empty conduction band. Therefore, there is no energy gap E_g. On the other hand, insulators have filled valence bands and empty conduction bands, separated by a large band gap E_g (typically >4eV).

Finally, the semiconductors have a small band gap between valence and conduction bands (usually $E_g < 2$ eV), so it is possible for some valence electrons to gain energy from external sources (e.g. by thermal or optical excitation) and cross the gap between the valence and conduction bands. By this movement, they create a free electron in the

conduction band and a hole in the valence band for other valence electrons to move in.

1.1.1 Applications of metal oxide semiconductors

Nanotechnology is a field of intense interest and is one of the key innovations in 21st century's science. Nanotechnology refers to the synthesis and processing of materials in the nanometer scale; the produced materials are called nanomaterials and could be metals, metal oxide semiconductors, polymers etc.

As far as metal oxide semiconductors is concerned, several types have been synthesized in the nm-scale, like TiO_2 [1], VO_2 [2], V_2O_5 [3], WO_3 [4], CuO [5], Cu_2O [6], ZnO [7], etc., and they exist in a variety of different forms, morphologies, structures, and properties.

Metal oxide semiconductors have been widely studied, due to their applications in novel topics, such as environment, energy, electronic devices, health [8]; applications that are based on their remarkable electrical, mechanical, catalytic and/or optical properties.

The applications of the nanomaterials are also tightly connected with their morphology, size and surface area [9]. Several methods have been applied for the synthesis of metal oxide as thin films [10] and nanostructures. As far as nanostructures is concerned, various size and morphologies have been reported the last decades such as nanowires, nanorods [11], nanoneedles [12], nanocubes [13], nanoflowers [14], nanosheets [15], etc..

Typical applications of Metal oxides (MOx) include gas sensors [16], catalysts [17], solar cells [18], waste water treatment [19], "smart windows" [20], light emitting diodes [21], random lasers [22] and photoluminescence devices [23] and , electrochromic applications [24], etc.. Moreover, MOx have been used in biomedical [25] and antimicrobial [26] applications,.

1.2 Zinc oxide (ZnO) among other metal oxide semiconductors

ZnO has been one of the most studied materials for over two decades. It is a binary II-VI semiconductor material, with a wide and direct band gap of 3.37 eV, which luminesces in the ultraviolet region of the spectrum. Moreover, ZnO exhibits large exciton binding energy of 60 meV, which allows efficient excitonic emission at room temperature (RT) [27].

ZnO is a low cost, easily prepared, non – toxic material. Due to its low toxicity, ZnO has been listed as "Generally Recognized as Safe" (GRAS) by the US Food and Drug Administration (21CFR182.8991) [28].

ZnO is a highly preferred multitasking metal oxide having a list of attractive properties. Due to its large band gap and exciton binding energy, ZnO exhibits high photocatalytic activity [29], [30], UV filtering properties [31], anti – microbial activities [32], wound healing [33]. Because of its ability to block the UV light, it is used in sunscreens, cosmetics and in many biomedical applications [34]. Additionally, it has been used for gas sensors [35], transparent electrodes in solar cells [36], photoluminescence devices [37], laser diodes and short – wavelength light – emitting devices, possibly suitable for replacing GaN based devices [27].

Various methods have been used for the synthesis of ZnO; some of them are physical while some others are chemical. Examples of physical methods are Molecular Beam Epitaxy (MBE), Pulsed Laser Deposition (PLD), sputtering and thermal evaporation. On the other hand, chemical methods are employing sol – gel, spray – pyrolysis, Chemical Vapor Deposition (CVD), hydrolysis, Aqueous Chemical Growth (ACG), etc.

Every method has its advantages and disadvantages. Physical methods involve the use of costly equipment, significantly longer duration of synthesis, high temperature and pressure, while chemical methods involve the use of toxic chemicals, which can be proved hazardous for the person handling it and the environment. Advantages of the chemical methods are the non – complicated equipment and the shorter duration of the process.

The result of using different methods for the synthesis of ZnO is to have different morphologies and sizes (micro – and nano – structures), like flakes, hexagonal prismatic rods, wires, flowers, belts, rods, etc., [38]. ZnO has also been reported in the form of thin films [39], [40].

1.1.1 Properties of ZnO

1.1.1.1 Crystal structure of ZnO

Cubic zincblende and hexagonal wurtzite are the crystal structures most of the II-VI semiconductors crystallize in [27]. There are three crystal structures formed by ZnO: hexagonal wurtzite (*B*4), cubic zincblende (*B*3), and the rarely observed cubic rocksalt (*B*1), as schematically shown in Figure 1.2.

At ambient conditions, the thermodynamically stable phase of ZnO is wurtzite and thus the most common one. The zincblende structure can be stabilized by growing ZnO on substrates with cubic lattice structure, and the rocksalt (NaCl) structure may be obtained at relatively high pressures (10GPa) [41].

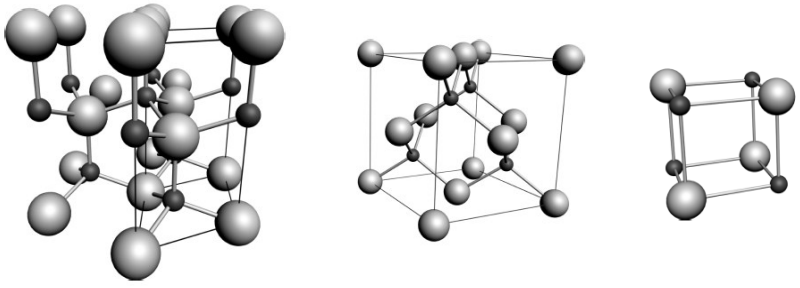

Figure 1.2 Representation of ZnO crystal structures a) hexagonal Wurzite (B4), b) cubic Zinc blende (B3), c) Cubic rocksalt (B1). Shaded grey and black spheres denote O and Zn, respectively. Only one unit cell is illustrated for clarity.(Obtained from Coleman V.A. and Jagadish C. [42])

Hexagonal and zincblende polymorphs have no inversion symmetry (reflection of a crystal relatively any given point does not transform it into itself). This and other lattice symmetry properties result in piezoelectricity of the hexagonal and zincblende ZnO, and in pyroelectricity of hexagonal ZnO.

The unit cell of the wurtzite structure has lattice parameters a=3.250Å and c=5.207Å, with their ratio c/a ~ 1.60 to be close to the ideal value for hexagonal cell c/a= 1.633. At the wurtzite structure, the Zn^{+2} cation is surrounded by four O^{-2} anions at the edges of a slightly deformed tetrahedron, and vice versa.

1.1.1.2 Mechanical properties of ZnO

ZnO is a relatively soft material having a hardness of 4.5 on the Mohs scale [43]. Its high heat capacity and heat conductivity with low thermal expansion and high melting temperatures makes it beneficial for ceramics. Piezoelectricity is also an important characteristic of ZnO, as it has one of the highest piezoelectric tensor compared to III-V semiconductors such as GaN and AlN. This property makes it important for many piezoelectrical applications, which require a large electromechanical coupling [42].

1.1.1.3 Electrical properties of ZnO

As it was previously mentioned, ZnO has a wide direct band gap of ~3.7 eV and large excitation binding energy of 60 meV, compared to thermal energy which is of the order of ~ 25 meV at room temperature. One of the reasons ZnO has been so attractive for electronic and optoelectronic devices is its large exciton binding energy. Moreover, the large band gap of ZnO offers the advantage of sustainment at large electric fields, operation at high temperature and high power, and lower noise generation [41].

1.1.1.4 Optical properties of ZnO [44]

The optical properties of ZnO, have been studied using photoluminescence, and absorption and are reflecting the direct band gap, a strongly bound exciton state, and gap states arising from point defects.

More specifically, the Photoluminescence (PL) spectra of ZnO structures have been widely studied. They exhibit a strong RT, near-band-edge UV photoluminescence peak at ~3.2 eV which is attributed to an exciton state, as the exciton binding energy is on the order of 60 meV. In addition, visible emission is also observed as a result of defect states.

The main parameters [45] of ZnO are summarized in table 1.1:

Table 1.1 *Main parameters of ZnO (redesigned from Norton, D. P. et al [45])*

Property	***Value***
Lattice parameters at 300 K :	
a	0.32495 nm
c	0.52069 nm
a/c	1.602 (1.633 for ideal hexagonal structure)
*u**	0.345
Density	5.606 g/cm^3
Stable phase at 300 K	wurtzite
Melting point	1975°C
Thermal conductivity	0.6, 1 – 1.2
Linear expansion coefficient (/°C)	a: 6.5 × 10^{-6}, c : 3.0 × 10^{-6}
Static dielectric constant	8.656
Refractive index	2.008, 2.029
Energy gap	3.37 eV (direct)
Intrinsic carrier concentration	< 10^6 / cm^3
Exciton binding energy	60 meV
Electron effective mass	0.24
Electron Hall mobility at 300 K for low n – type conductivity	200 cm^2/ V·s
Hole effective mass	0.59
Hole Hall mobility at 300 K for low p – type conductivity	5 – 50 cm^2/ V·s

*the u parameter is defined as the length of the bond parallel to the c axis

1.1.2 Synthesis techniques of ZnO

1.1.2.1 Sputter deposition [46]

Sputtering is a technique used to deposit thin films of a material onto a surface – substrate. During this process, particles are ejected from a target material after its bombardment with energetic particles. Sputtering only takes place when the kinetic energy of the bombarding particles is extremely high, much higher than normal thermal energies. This technique can be done either by using DC voltage (DC sputtering) or AC voltage (RF sputtering).

The sputtering process begins when the substrate to be coated is placed in a vacuum chamber. Subsequently, a gaseous plasma (usually Argon) is created and a negative voltage is applied to a target source material that will be deposited onto the substrate, causing the plasma to glow (figure 1.3). Free electrons flow from the negatively charged target source material in the plasma environment, colliding with the outer electronic shell of the Argon gas atoms, driving these electrons off due to their like charge. The inert gas atoms become positively charged ions attracted to the negatively charged target material at a very high velocity that "Sputters off" atomic size particles from the target source material due to the momentum of the collisions. These particles cross the vacuum deposition chamber of the sputter coater and are deposited as a thin film of material on the surface of the substrate to be coated.

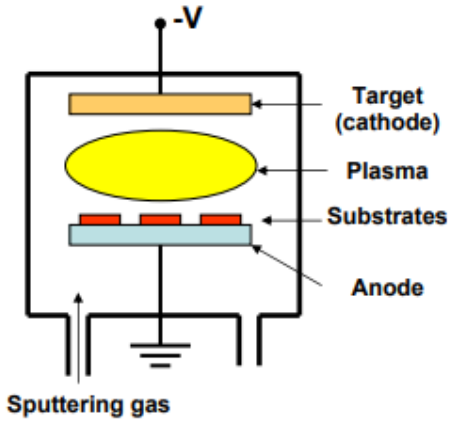

Figure 1.3 Schematic illustration of the sputtering process.(redesigned from [47])

1.1.2.2 Thermal Evaporation [48]

One of the common methods of Physical Vapor Deposition (PVD) is Thermal Evaporation. Thermal Evaporation uses metals or non – metals as the materials that can be applied, while the substrates can be semiconductor wafers, solar cells, optical components, or many other possibilities.

During thermal evaporation a solid material is heated, in a vacuum environment, upon the temperature it evaporates until vapor pressure is produced. Subsequently, the evaporated material traverses the chamber and finally it forms a thin film on a substrate, which is placed towards the heated material.

A scheme of the deposition equipment is showed in the figure 1.4.

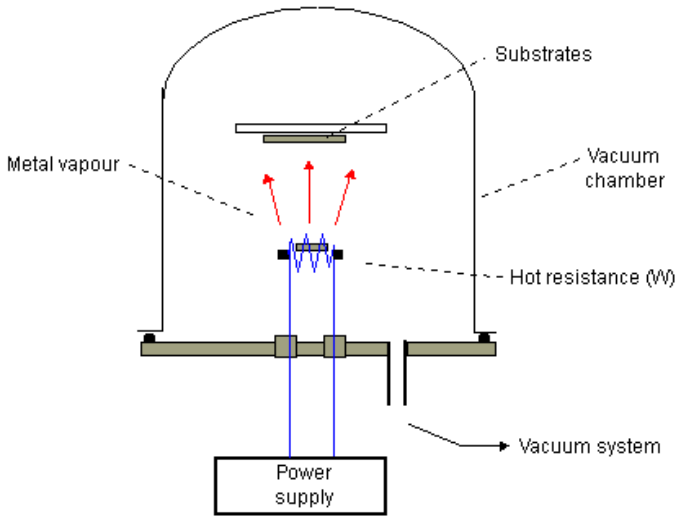

Figure 1.4 Schematic illustration of a typical evaporation deposition equipment (obtained from web page [49])

1.1.2.3 Pulsed Laser Deposition, PLD [50]

Pulsed laser deposition (PLD) can be considered as a special case of evaporation; local heating with a laser causes evaporation. The main difference with classical evaporation is the formation of clusters, ions and the high initial energy of these ions. A laser pulse is used for ablation of target material producing a local plasma. This results in a plasma, containing energetic clusters and macro particles.

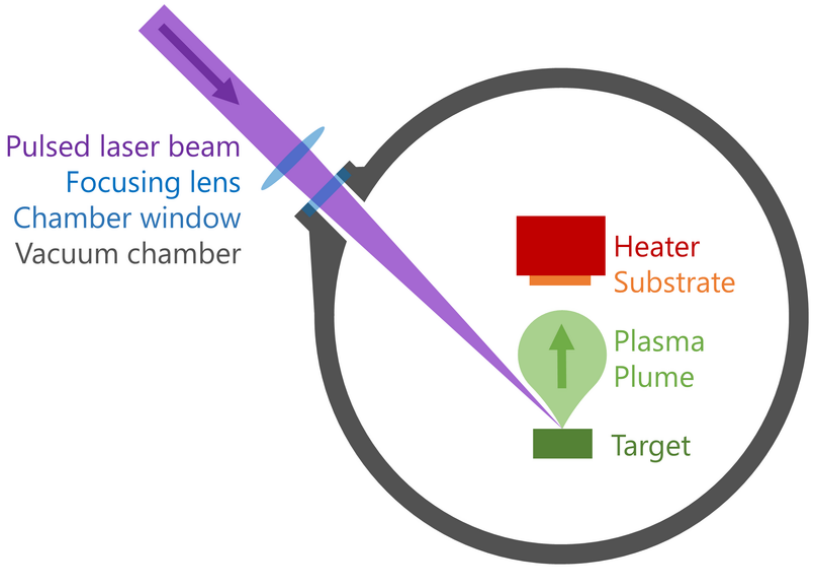

Figure 1.5 Schematic diagram of the Pulsed Laser deposition system (obtained from Wikipedia [51])

Specifically, a high-power pulsed laser beam is focused inside a vacuum chamber to strike a target of the material that is to be deposited on the surface of the substrate. This material is vaporized from the target (in a plasma plume) which deposits it as a thin film on a substrate (such as a silicon wafer facing the target). This process can occur in ultra-high vacuum or in the presence of a background gas, such as oxygen which is commonly used when depositing oxides, to fully oxygenate the deposited films.

1.1.2.4 Spin coating

Spin coating is a method for application of thin, uniform films to flat substrates. The machine used for spin coating is called spin coater.

At first, a small amount of solution is placed on the substrate and the substrate is then rotated at high speed and the fluid is spread by centrifugal force. Rotation is continued for some time, with fluid being spun off the edges of the substrate, until the desired film thickness is achieved. The solvent is usually volatile, in order to be simultaneously evaporated.

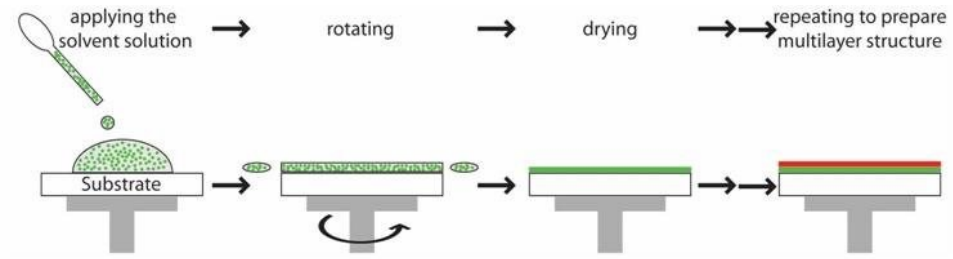

Figure 1.6 Schematic illustration of spin coating technique (obtained from S. Ahmadi-Kandajani et al. [52])

Spin coating permits to obtain homogeneous films of good optical quality, with thicknesses ranging from a few nanometers to few micrometers. The film thickness depends on the precursor solution composition and pre-aging treatment and it can be controlled, during the deposition procedure, varying the viscosity of the solution and the spinning rate [53].

The films are deposited at room temperature and then they are heated at temperatures higher than the evaporation point of the solvent, in order to dry properly.

This procedure can be repeated many times resulting in a multilayer structure with the preferred thickness.

1.1.2.5 Chemical Vapor Deposition, CVD

Chemical vapor deposition (CVD) is a chemical process used to produce high purity, high performance solid materials. Applications of CVD range from the fabrication of microelectronic devices to the deposition of protective coatings [54].

In a typical CVD process, the substrate is placed in a chamber at a specific temperature and then it is exposed to one or more volatile precursors, which react and decompose on the substrate surface to produce the desired deposit. During this process, volatile byproducts are also produced, but are removed by gas flow through the reaction chamber.

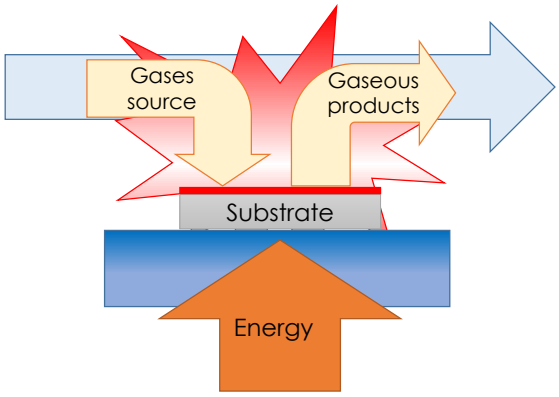

Figure 1.7 Chemical Vapor Deposition mechanism

A characteristic feature of the CVD technique is its excellent throwing power, enabling the production of coatings of uniform thickness and properties with a low porosity even on substrates of complicated shape. Another important feature is the capability of localized, or *selective* deposition, on patterned substrates.

A number of forms of CVD [55] are in wide use and are frequently referenced in the literature: Atmospheric pressure CVD (APCVD), Atomic layer CVD (ALCVD), Aerosol Assisted CVD (AACVD), Hot Wire CVD (HWCVD), Low-pressure CVD (LPCVD), Microwave plasma-assisted CVD (MPCVD), Plasma-Enhanced CVD (PECVD), Rapid thermal CVD (RTCVD), Remote plasma-enhanced CVD (RPECVD), Ultra-high vacuum CVD (UHVCVD).

1.1.2.6 Aqueous Chemical Growth, ACG

The Aqueous Chemical Growth (ACG) is a novel and inexpensive technique that produces thin films and coatings of metal oxide materials onto various substrates at low cost and mild temperatures [56].

This method allows the generation of advanced nano-, meso-, and micro-particulate thin films as well as two- and three-dimensional arrays, without any template, surfactant, or external field and without any specific requirements in substrate activation, thermal stability, or crystallinity. Given that the crystallites are nucleating and growing directly from the substrate at mild temperatures, a large choice of substrates (e.g. amorphous, single crystalline, polycrystalline, transparent, conducting, flexible etc.) is offered. Such diversity provides a higher degree of nanomaterials engineering and design.

The synthesis involves the hydrolysis-condensation of hydrated metal ions and complexes (inorganic polymerization) and their heteronucleation onto substrates.

Experimentally, the aqueous chemical growth method simply consists of heating an aqueous solution of metal precursors (salts or complexes) at a given ionic pH and ionic strength, in the presence of substrates at mild temperatures (below 100°C) in a closed bottle as illustrated in figure 1.8. Therefore, such method does not require expensive and complicated set-up or hazardous high-pressure containers.

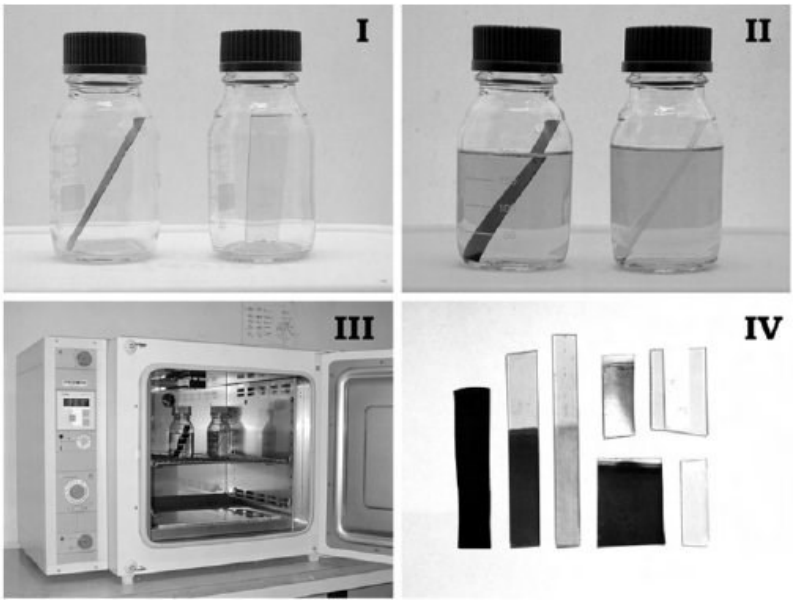

Figure 1.8 The aqueous chemical growth (ACG) thin film processing technique: I. Introduction of the bare substrates or thin films; II. Total (or partial) immersion of the substrates in selected aqueous solutions of metal salt precursors at room temperature; III. Heat treatment at constant temperature in a laboratory oven below 100°C; IV. Generation of nano-, meso-, and micro-particulate thin films of large physical area (obtained from L. Vayssieres [56])

It is entirely recyclable, safe, and environmental-friendly, since only water is used as solvent. Such a process avoids hazards, organic solvents and their critical evaporation and potential toxicity. In addition, since no organic solvents or surfactants are present, the purity of the as-prepared thin films is substantially improved. The residual salts are easily washed out by water due to their high solubility. In most cases, no additional heat or chemical treatments are necessary, which represent a significant improvement compared to the sol-gel process as well as surfactant, template and membrane-based synthesis methods. The utilization of temperature and chemical sensitive substrates required by certain applications is therefore allowed.

A crucial feature is the large-scale manufacturability of a synthesis technique. Many parameters have to been taken into account to identify such ability. However, up-scaling the ACG method is definitely realistic. First, the theoretical concepts as well as the experimental technique are applicable to all water-soluble metal ions likely to precipitate in solution. Second, the exclusive use of water as solvent, the mild temperatures required and the low cost of precursors (metal salts) make of such a technique, a suitable candidate for large-scale

manufacturing of low cost nanomaterials and devices. As it is, advanced thin films with physical areas as large as several tens of centimeters square are obtained. The utilization of larger containers and larger substrates will provide the ability to generate much larger physical areas.

Figure 1.9 presents the correlation of the surface coverage of thin films grown by ACG with the synthesis time. It can be seen that as the deposition time increases, the coverage of the film becomes higher.

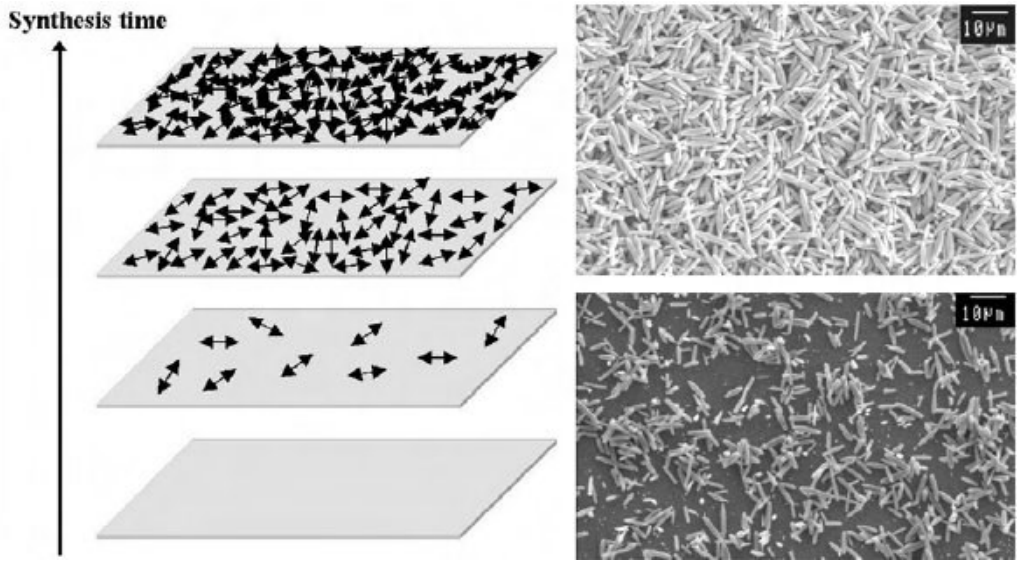

Figure 1.9 Schematic representation and SEM images of the effect of synthesis time on the surface coverage of thin films grown by ACG (obtained from L. Vayssieres [56])

1.2 The need of environmental friendly synthesis

Nowadays, MOx nanoparticles can be applied in several applications, varying from health and food industry, to space and aviation. This is exactly why one should explore the risks and benefits of nano-derived processes and products.

One critical parameter of nano-structured powders, films and devices is that during the applied CVD/PVD fabrication techniques, researchers tend to use hazardous substances and solvents. These substances can be surfactants, which act as capping agents, in order to stabilize and prevent the agglomeration of the nanoparticles, or as sculpturing agents that direct the growth direction of the particle. Toxicity risks arise as it is extremely difficult to remove all the chemical contaminants from the nanoparticles' surface and some of the chemicals reside in the materials [57].

Therefore, in order to reduce the toxicity concerns, many scientists turn to what it is called "green technology", which is less toxic, cost-effective, environmental friendly and safe.

The green methods for the synthesis of materials are gaining importance due to their simplicity and eco – friendliness. Green synthesis of metal oxide nanoparticles is advantageous over other conventional methods due to their nontoxic and environmental friendly protocols.

Various metal oxides such as ZnO, NiO, ZrO_2, TiO_2, CuO, Al_2O_3, SnO_2 and $CoFe_2O_4$ have been also synthesized from several research groups, following eco – friendly approaches [33], [58]–[63].

Among the MOx mentioned above, this Master thesis focuses on the synthesis of ZnO nanostructures following an environmental friendly approach, and on the study of their optical and structural properties.

At this point it is quite critical to mention that during the ZnO synthesis temperatures as high as 195°C were used, along with mild solvents such as water or edible alcoholic solutions (e.g. raki and ouzo) were used.

Chapter 2 – Experimental

Introduction

The purpose of this chapter is to present the experimental techniques involved on the synthesis and the characterization of the as-grown ZnO nanostructures, and is divided in two parts.

The first part concerns the chemical methods employed for the ZnO synthesis; several details are presented such as the reactants, the experimental procedure and their variations.

The second part, provides information about the techniques used for the samples' characterization.

2.1 Synthesis of ZnO

In this subsection, useful information, about the reactants and the synthesis of ZnO samples, are provided.

The general idea of this Master thesis was to synthesize, ZnO using chemical reactants and then try to substitute each one of them with nontoxic and mild reagents, following the Aqueous Chemical Growth (ACG) method. It should be noted that all the experiments were performed at relatively low temperatures.

During the synthesis of ZnO, the reaction mechanism, is the following [64], [65]:

$$Zn^{+2} + 2OH^{-} \leftrightarrow Zn(OH)_2 \leftrightarrow ZnO + H_2O \qquad \text{Reaction 2.1}$$

In reaction 2.1, the source of zinc cations is typically zinc salts, such as zinc nitrate ($Zn(NO_3)_2$), zinc acetate ($Zn(CH_3COO)_2$), or even metallic zinc. On the other hand, the hydroxyl anions can result from the presence of water, alcohol and other solvents containing hydroxyls. Moreover, OH^- can be formed by the reaction of an amine, such as Hexamethylenetetramine (HMTA, $(CH_2)_6N_4$), or even Ammonium carbonate ($(NH4)_2CO3$), with water.

First, pure chemical reactants, like $Zn(NO_3)_2$ or $Zn(CH_3COO)_2$ and HMTA, were used in different solvents (water, ethanol, etc.). The samples resulted from these experiments were used as reference samples, and for direct comparison with the ones from the literature.

The eco-friendly synthesis was achieved by substituting the chemical reactant of HMTA with Ammonium carbonate (baking ammonia sold in local market). The executed experiments were performed using the same solvents and under the same temperature conditions using both types of amines. To our best knowledge, it is the first time that baking ammonia is utilized for the synthesis of ZnO.

After using baking ammonia as OH^- source, the final step for green synthesized ZnO was to substitute the zinc source. As the literature states, ZnO is possible to be formed by oxidation of metallic Zn powder [66]–[70]. Thus, instead of using zinc salts, like $Zn(NO_3)_2$ or $Zn(CH_3COO)_2$, zinc metal was used, in the form of powder. In this case, various experiments were performed by using HMTA and baking ammonia dissolved in various solvents.

Moreover, regarding the zinc metal, several syntheses were executed, without the use of any type of amine.

More details about the synthesis procedure of ZnO structures are provided below.

2.1.1 Reagents / Materials

ZnO structures were grown following the Aqueous Chemical Growth (ACG) technique on Silicon (100) wafer using the following reagents:

- Zinc nitrate hexahydrate [$Zn(NO_3)_2 \cdot 6H_2O$, ≥ 99.99 %]
- Zinc acetate dihydrate [$Zn(CH_3COO)_2 \cdot 2H_2O$, ≥ 99.99 %]
- Hexamethylenetetramine [$(CH_2)_6N_4$, ≥ 99.0 %]
- Zinc powder

All reagents mentioned above were used without further purification and purchased from Sigma – Aldrich, except from zinc powder, which was purchased and used as obtained by Fluka.

Furthermore, nontoxic and daily use reactants were used in order to perform environmental friendly syntheses. More specifically, in addition to water, beverages such as soda water, leavening agents used in traditional puff pastry and cookie recipes such as baking ammonia, mild antiseptics such as hydrogen peroxide (2.8% w/w), ethyl alcohol based alcoholic beverages, like raki and ouzo (Greek products), were used for the synthesis of ZnO.

2.1.2 Synthesis of ZnO with zinc salts and HMTA

Before deposition, the Silicon (100) wafer pieces that were used as substrates, were cleaned with ethanol in order to remove any kind of dirt that could contaminate the grown ZnO.

Afterwards, the Si substrates were put in Pyrex glass bottles with polypropylene autoclave screw caps or in Teflon – lined stainless steel autoclaves, like these in figure 2.1. The type of container, was depending on the synthesis temperature and it will be specified below.

Figure 2.1 Left: Pyrex bottle with polypropylene autoclave screw cap (used at 95 °C), Right: The Teflon - lined stainless steel autoclave (used at 195 °C)

Every container was filled with 50 ml of equimolar (0.01M) aqueous solution of zinc nitrate hexahydrate ($Zn(NO_3)_2 \cdot 6H_2O$)and HMTA ($(CH_2)_6N_4$), and then it was placed in a common laboratory oven preheated at a specific temperature (95°C or 195°C) for 2 hours.

During the synthesis procedure, the chemical reaction of the reagents was noticeable (obviously in the case of the transparent Pyrex bottles), since small white particles, could be observed. After about 45 minutes being in the oven, a white layer of the precipitate was observed at the bottom of the bottle, as well as, a white thin layer on the silicon substrate.

After the pass of the desired growth time (2 hours), the substrates were collected and washed thoroughly with distilled water to eliminate the residual salts or amino complex and then dried at the same temperature.

Exactly the same procedure was followed for the case of zinc acetate dihydrate ($Zn(CH_3COO)_2 \cdot 2H_2O$).

For each zinc source used (zinc nitrate or zinc acetate), the oven was set at two different temperatures every time the experiment was held; at 95 °C and at 195 °C, respectively. The Pyrex bottles were used when the temperature was set at 95 °C, while the stainless steel autoclaves when the temperature was set at 195 °C.

The possible reaction mechanisms that take place in the formation of the ZnO structures are believed to be the following [64], [65]:

a) Dissociation of the precursors:

$$Zn(NO_3)_2 \leftrightarrow Zn^{2+} + 2NO_3^-$$

$$Zn(CH_3COO)_2 \leftrightarrow Zn^{2+} + 2CH_3COO^-$$

Reaction 2.2

b) Hydrolysis of HMTA:

$$(CH_2)_6N_4 + 6H_2O \leftrightarrow 6HCHO + 4NH_3$$

Reaction 2.3

$$NH_3+H_2O \leftrightarrow NH_4^+ + OH^-$$

c) Precipitation of Zn ions:

$$Zn^{+2} + 2OH^- \leftrightarrow Zn(OH)_2 \leftrightarrow ZnO + H_2O$$

Reaction 2.4

As already mentioned, all ZnO nano-structures were synthesized following the Aqueous Chemical Growth (ACG) technique. In the first place, the solvent used, for the preparation of the solutions, was water and then it was replaced by ethanol, raki and ouzo. Even though the solvents were different from water, the synthesis technique and the steps followed, were the same for all the solvents at both temperatures and zinc salt sources. After 2 hours of ZnO growth, the collected samples were washed with the solvent that was used each particular time.

In conclusion, ZnO samples were prepared in 2 hours by solutions of zinc nitrate or zinc acetate and HMTA, based on ACG method, in four solvents (water, ethanol, raki, ouzo) and at two different temperatures (95 °C, 195 °C) for each one of them.

2.1.3 Synthesis of ZnO with zinc salts and baking ammonia

After synthesizing ZnO with the conventional reagents, the base HMTA was simply substituted by the nontoxic baking ammonia, which has been listed as "Generally Recognized as Safe" (GRAS) by the US Food and Drug Administration (21CFR184.1137) [71].

Baking ammonia, also known as ammonium carbonate ($(NH_4)_2CO_3$), is a mixture of ammonium bicarbonate (NH_4HCO_3) and ammonium carbamate (NH_2COONH_4). It has been used as a primary leavening agent by bakers, before the advent of baking soda and baking powder, because under heating conditions it breaks into carbon dioxide (leavening), ammonia (needs dissipation) and water [72]:

$$(NH_4)_2CO_3 \leftrightarrow NH_3 + H_2O + CO_2$$

Reaction 2.5

As in the case of zinc salts the reaction continues as follows [65]:

$$NH_3+H_2O \leftrightarrow NH_4^+ + OH^- \quad \text{Reaction 2.3b}$$

$$Zn^{+2} + 2OH^- \leftrightarrow Zn(OH)_2 \leftrightarrow ZnO + H_2O \quad \text{Reaction 2.4}$$

All the steps of the synthesis method remained exactly the same. The laboratory oven was set again for 2 hours at two different temperatures (95 °C, 195 °C) for each solvent (water, ethanol, raki and ouzo).

2.1.4 Synthesis of ZnO with zinc powder and HMTA

After using baking ammonia as the source of the OH^-, zinc salts were substituted by zinc powder. As the reader will find out, the duration of the experiments was also changed when using zinc powder.

Zinc powder (1.8g) was dissolved in 35ml of distilled water. Then 0.05g HMTA was added to the above solution under continuous stirring. The resulting suspension was transferred into a Teflon – lined stainless steel autoclave, which contained the silicon substrate, and sealed tightly. After that, the autoclave was put in the laboratory oven at 195 °C for 24 hours.

After the pass of the desired growth time, the substrates were collected and washed thoroughly with the distilled water to eliminate the residual salts or amino complex and dried at the same temperature.

The possible reaction mechanism is believed to be the following [66]:

$$Zn + H_2O \rightarrow Zn^{2+} + H_2\uparrow + OH^- \quad \text{Reaction 2.6}$$

$$Zn^{2+} + OH^- \rightarrow Zn(OH)_4^{2-} \rightarrow ZnO + H_2O \quad \text{Reaction 2.7}$$

As in the case of zinc salts, except from distilled water, other solvents were also used; Ethanol, soda water, lemon soft drink and hydrogen peroxide (2.8% w/w) contributed to the fabrication of ZnO by following the ACG method. The collected samples were washed with the solvent that was used each particular time

Last but not least, HMTA was used in two different amounts. Experiments that 0.15g instead of 0.05g HMTA was also executed under exactly the same procedure using five different solvents (water, soda water, lemon soft drink, hydrogen peroxide).

2.1.5 Synthesis of ZnO with zinc powder and baking ammonia

In the following ZnO synthesis, zinc powder was used along with baking ammonia following a green synthesis approach.

First, zinc powder (1.8g) was dissolved in 35ml of the desired solvent. 0.05g baking ammonia was added to the above solution under continuous stirring. The resulting suspension was transferred into a Teflon – lined stainless steel autoclave, which contained a silicon substrate, and sealed tightly in a laboratory oven at 195 °C for 24 hours.

After 24 hours, the substrates were collected and washed thoroughly with solvent to eliminate the residual salts or amino complexes and dried at the same temperature.

Distilled water, ethanol, soda water, lemon beverage and hydrogen peroxide (2.8% w/w) were used as solvents for the syntheses described above.

2.2.6 Synthesis of ZnO using pure zinc powder

The final syntheses were carried out, dissolving pure zinc powder in a solvent (distilled water, ethanol, soda water, and hydrogen peroxide) without the presence of any amine, or catalyst of any kind.

Zinc powder (1.8g) was dissolved in 35ml of the desired solvent under vigorous stirring. The resulting suspension was transferred into a Teflon – lined stainless steel autoclave, which contained a silicon substrate, and sealed tightly in the laboratory oven at 195 °C for 24 hours.

After 24 hours, the substrates were collected and washed thoroughly with the solvent to eliminate the residual salts or amino complexes and dried at the same temperature.

2.2 Characterization techniques

For the purposes of this Master Thesis several techniques were performed for the characterization of the prepared samples.

For the morphological characterization of the samples Scanning Electron Microscopy (SEM) was used, while for their structural study X – ray Diffraction (XRD) was performed. The identification of ZnO was evaluated by means of Energy Dispersive X – ray Analysis (EDX), Raman Spectrometry and Photoluminescence (PL) spectroscopy.

2.2.1 Electron Microscopy

Electron microscopy has been the most often used imaging technology for scientists and engineers over the past decades, as it gives them the opportunity to observe and characterize even nanoscale materials [73].

The electron microscope uses a beam of electrons to illuminate the specimen and create an enlarged image, unlike the optical microscope that uses visible light. The resolving power of electron microscope is greater than that of light microscope, as a result of the shorter wavelength of the electrons, leading to much higher magnifications [74].

Electrons accelerated onto a specimen can interact with the atoms of the target-specimen in different ways (Figure 2.2) [75]. Accelerated electrons can pass through the specimen without interaction, undergo elastic scattering and can be inelastically scattered. Elastic and inelastic scattering result in a number of signals that are used for imaging, quantitative and semi-quantitative information of the target-specimen and generation of an X-ray source. Typical signals used for imaging include secondary electrons (SE), backscattered electrons (BSE), cathodoluminescence (CL), Auger electrons and characteristic X-rays.

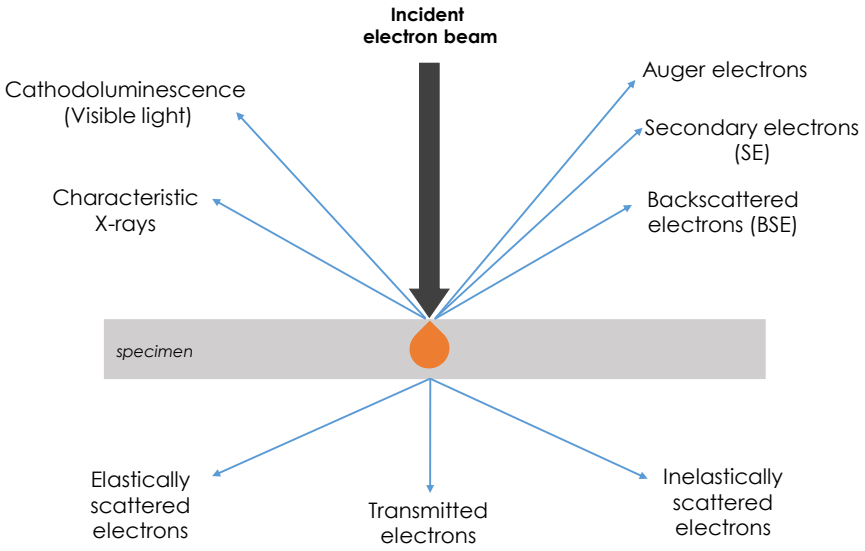

Figure 2.2 Types of interactions between the electrons and the specimen (redesigned by [75])

Several types of electron microscope have been developed to help investigate different aspects of a specimen. The Scanning Electron Microscope (SEM) is designed primarily to examine specimen surface. It generates highly focused beam of electrons, which impact on the specimen inside a vacuum chamber and the produced secondary electrons are being collected.

2.2.2 Scanning Electron Microscopy, SEM

The scanning electron microscopy (SEM) uses a focused beam of high-energy electrons to generate a variety of signals at the surface of the specimen. The signals that derive from electron-sample interactions reveal information about the sample including external morphology (texture), chemical composition, and crystalline structure and orientation of materials making up the sample.

The main components (Figure 2.3) of the SEM are:

- Source of electrons
- Column with electromagnetic lenses and apertures, down which the electrons travel.
- Specimen chamber
- Electron detectors

- Vacuum pump
- Computer and monitor to view the images

In a typical SEM, electrons are produced at the top of the column and are attracted by the anode, which is positively charged. Some of these accelerated electrons go right through the anode and pass through a combination of lenses and apertures, producing in this way a focused electron beam which hits the surface of the specimen. The electromagnetic lenses and apertures act to control the diameter of the beam as well as to focus the electron beam on the specimen and to affect the properties of the beam, respectively. The sample is mounted on a stage in the chamber area and both the column and the chamber are evacuated by a combination of pumps [73].

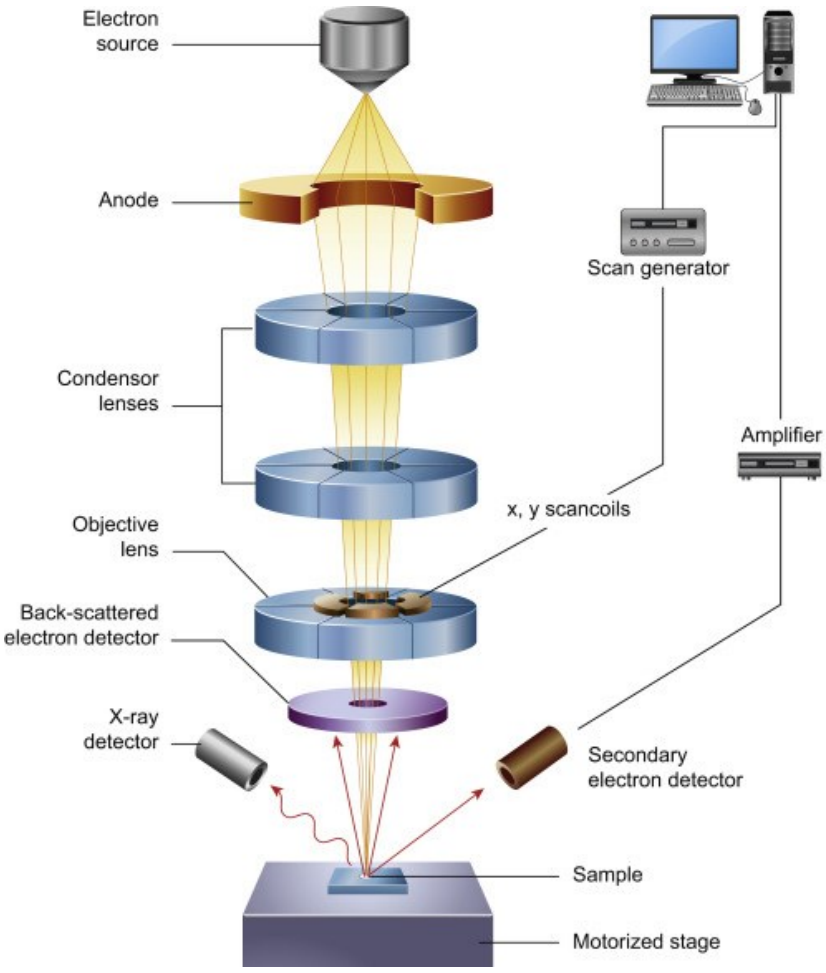

Figure 2.3 Schematic diagram of a SEM (obtained by [73])

As the electron beam strikes on the specimen surface, it interacts elastically or inelastically with the atoms of the sample and signals, in the form of backscattered electrons, secondary electrons (SE) and characteristic X-rays are emitted, and reveal information about the topography, composition, etc. of the organic or inorganic material. SEM utilizes both elastic and inelastic collisions, collecting the following signals [73]:

I. Secondary electrons:
Secondary electrons originate from the surface or the near-surface regions of the sample. They are a result of inelastic interactions between the primary electron beam and the sample and have lower energy than the backscattered electrons. Secondary electrons are most valuable for showing morphology and topography on samples.

II. Backscattered electrons:
Primary (high energy) electrons of the beam that after a series of elastic collisions in the specimen are emerged back out of the specimen surface. The intensity of the produced signal depends on the atomic number of the elements and the crystallographic orientation. This dependence from the atomic number makes backscattered electrons valuable for illustrating contrasts in composition in multiphase samples. Furthermore, signals from backscattered electrons can also provide beneficial information on topography, crystallography and the magnetic field of the sample.

III. Characteristic X-Rays:
When the incident beam strikes the sample creating secondary electrons, it leaves thousands of the sample atoms with holes in the electron shells where secondary electrons used to be. If these "holes" are in inner shells, the atoms are not in a stable state. To stabilize the atoms, electrons from outer shells will drop into the inner shells. However, because the outer shells are at a higher energy state, to do this the atom must lose some energy. It does this by releasing X-rays in a pattern that is “characteristic” to each element. The analysis of Characteristic X-rays leads to the chemical analysis of the surface.

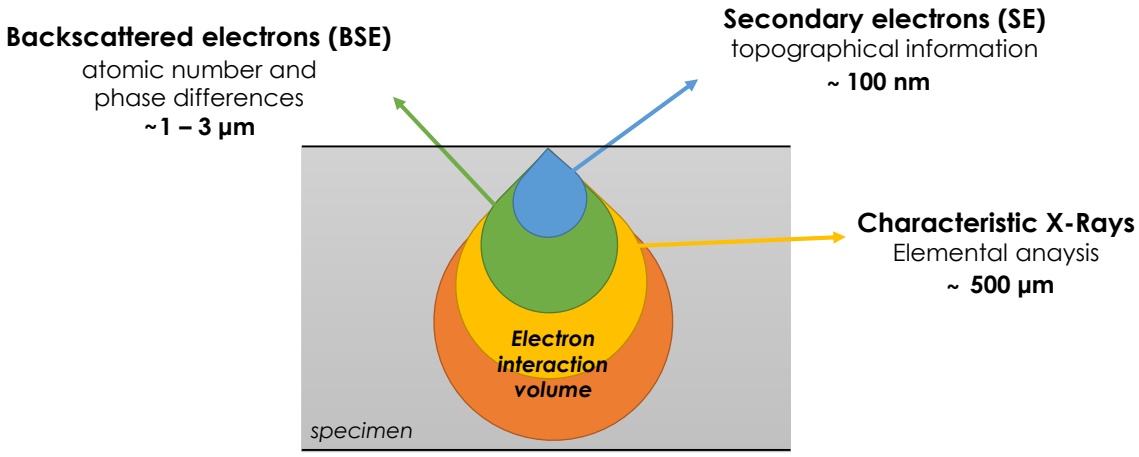

Figure 2.4 Signals emitted from different parts of the interaction volume (redesigned from [74])

SEM is an instrument that allows the observation and characterization of surfaces and its detection capacity is as much as 1µm from the sample surface. Secondary electrons and backscattered electrons are the frequently used signals by SEM users for imaging samples. Not all SEM users need the same type of information, so the capability of having many detectors makes SEM a highly versatile tool that can provide advantageous solutions for many different applications.

Last but not least, proper sample preparation plays a key role in obtaining the required information when using SEM. Some samples need to be coated in order to be conductive. Metals require no preparation due to their inherent ability to conduct electricity. However, non-metals need to be coated with a conductive material. Most often, a thin layer of gold (Au) works. This requires the use of a sputter-coater.

For the purposes of this Master thesis a JSM – 6390LV SEM of JEOL was used, as shown in figure 2.5.

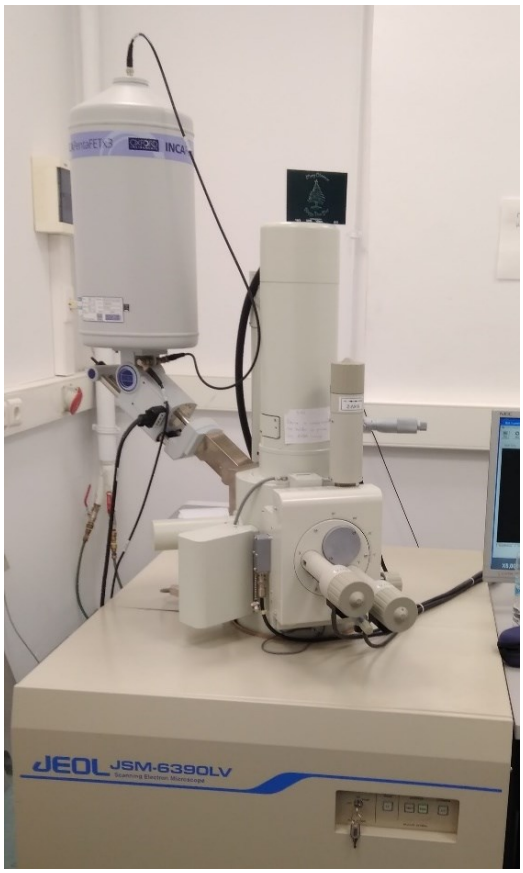

Figure 2.5 A JSM - 6390LV SEM of JEOL at the University of Crete

2.2.3 Energy Dispersive X-ray Analysis, EDX [76]

The Energy Dispersive X-ray Analysis, referred to as EDX, is an X-ray technique used in conjunction with SEM to identify the elemental composition of examined materials.

As the primary electron beam bombards the specimen, it emits X-rays which are detected by the homonymous detector and whose energy strongly depends from the examined material (section 2.2.1). The data generated by EDX analysis consist of spectra showing peaks corresponding to all the different elements making up the true composition of the sample being analyzed. An example of an EDX spectrum is shown in Figure 2.6. Every element has characteristic peaks of unique energy.

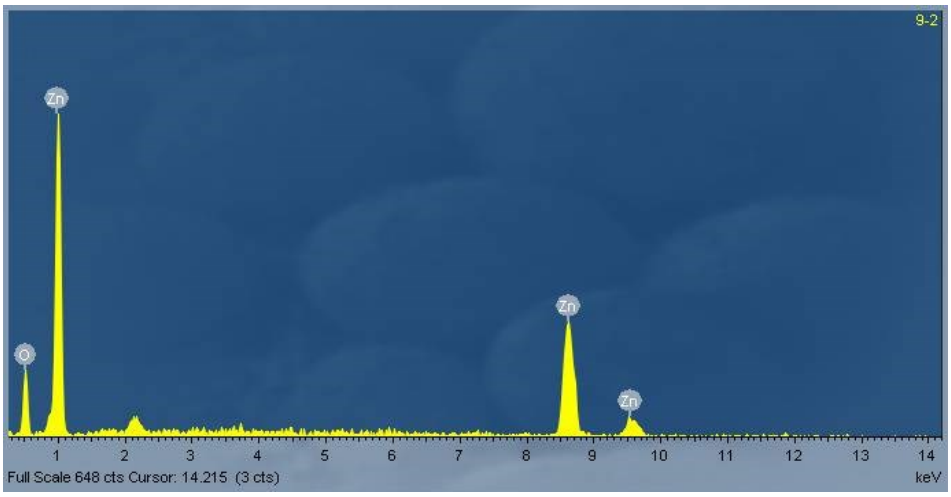

Figure 2.6 Typical EDX spectrum: y-axis depicts the number of counts and the x-axis the energy of the X-rays. The position of the peaks leads to the identification of the elements and the peak height helps in the quantification of each element's concentration

Moreover, EDX can be used for qualitative (the type of elements) as well as quantitative (the percentage of each element's concentration) analysis [76], [77].

2.2.4 X-ray Diffraction, XRD

X-ray Diffraction (XRD) is a technique that gives information about the structure and the crystallinity of the materials. Moreover, identification of compounds and characterization of the samples can be achieved by using XRD [78]. The XRD spectrum can be analyzed for the estimation of the lattice constant d, the dimensions of the unit cell, the crystallite's size, the defects, etc.

More specifically, the analysis of the materials with XRD, offers the user the opportunity to obtain information about:

1) The type of the crystals.
   The angle – intensity spectrum leads to the determination of the lattice constants.
2) The quality of the crystals.
   Many times, in the diffraction spectrum of several samples – materials it has been observed the presence of peaks at different diffraction angles than the ideal diffraction angles of each sample. Such deviations may be the result of changes in the stoichiometry of the materials.

3) The type of the crystal growth, according to which arises:
   a) a polycrystalline material with random growth direction of the crystalline grains.
   b) a polycrystalline material with preferable growth direction of the crystalline grains.
   c) a monocrystalline material.

4) The crystallite size.
   The crystallite size of a particular sample – material is computed from the FWHM of the main peak, according to the Scherrer's equation [79]:

$$d_g = \frac{0.9\lambda}{B \cos\theta_B} \qquad \text{eq (2.1)}$$

where, d_g : the crystallite size
λ : the X-rays' wavelength (= 0.154056 nm)
B : the FWHM of the main peak (in rad)
θ_B : the angle of the main peak.

The X-ray diffractometers consist of three basic components [78]:

- X-ray tube,
- Sample holder,
- X-ray detector.

X-rays are generated in a cathode ray tube by heating a filament to produce electrons. These electrons are accelerating by applying a voltage and bombarding the target material, which has a large atomic number. As these electrons strike on the target material, they excite the electrons of the inner shells of the target material and dislodge them and when outer shell electrons replace them, characteristic X-rays are produced.

The emitted X-ray spectrum consists of continuous radiation and characteristic peaks (Figure 2.7). The continuous spectrum arises due to the deceleration of the electrons hitting the target (called Bremsstrahlung radiation), while the presence of characteristic peaks depends on the atoms of the cathode sample [78]. The characteristic emission peaks are denoted as K_α, K_β, etc. The first letter concerns the

shell from where the electron is knocked out and the subscript is the number of the shells the electron changed during its transition [80].

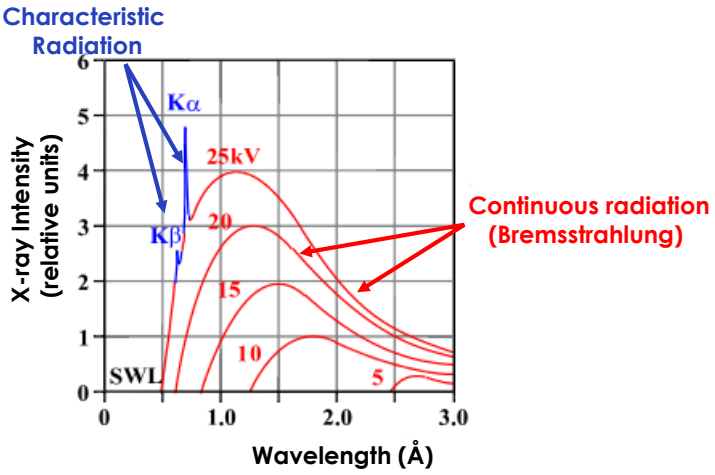

Figure 2.7 Spectrum of X-rays depending on the applied voltage (Mo-anode) (adapted from [81])

The XRD depends on the interaction of monochromatic X-ray with the sample. Since atoms are arranged periodically in a lattice, X-rays scattered from a crystalline solid can constructively interfere and produce a diffracted beam through these atoms.

According to the Bragg's law [82], constructive interference from parallel crystalline planes happens when the path length difference for beams diffracted from different atoms is an integral multiple of the X-ray wavelength:

$$n \cdot \lambda = 2 \cdot d \cdot \sin\theta \qquad \text{eq (1.4)}$$

where, n: integer (order of reflection)

λ: wavelength of the incident X-rays,

d: the interplanar spacing of the crystal,

θ: the angle of incidence,

as it is shown in figure 2.8 [83].

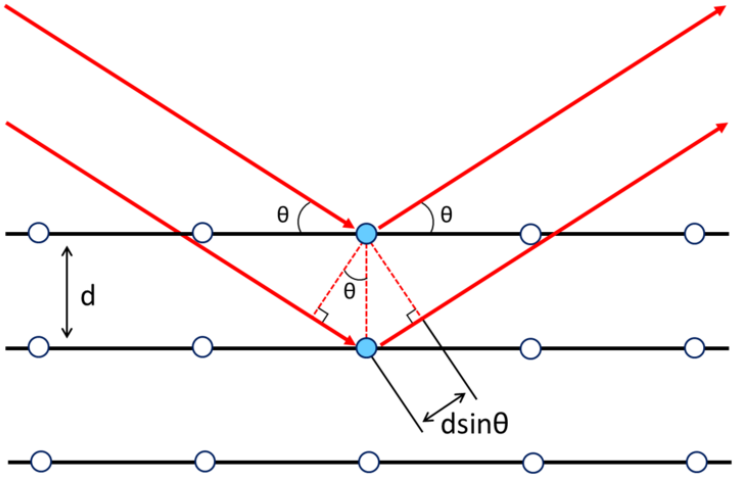

Figure 2.8 Diffraction of X - rays at crystal lattice (redesigned from [83]).

The features of a typical X-ray diffractometer are illustrated in figure 2.9. The rotation axis, O, of the diffractometer is perpendicular to the plane of the page. The sample S is placed on the sample holder, which can rotate around the axis O. The monochromatic X-ray beam is generated by the source T, and the intensities of diffracted beams are collected by a detector C. The sample, the X-ray source and the detector are all coplanar.

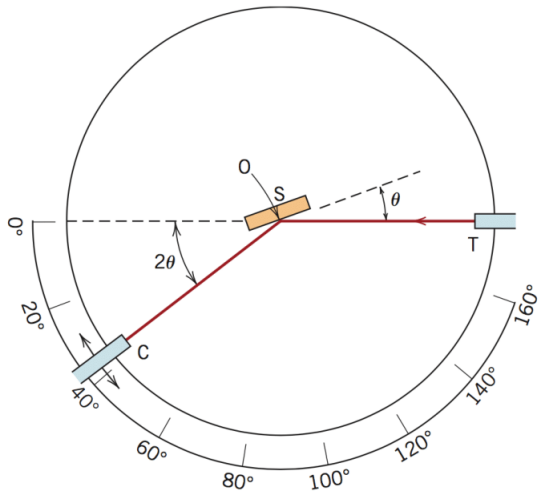

Figure 2.9 Schematic illustration of an X - ray diffractometer (obtained from [82])

The detector is placed on a movable carriage which can also rotate about the O axis. This detector is an electronic counter that converts the incoming diffracted X-rays to electrical pulses with the help of an electronic circuit.

The movable carriage and the sample are mechanically coupled such that a rotation of the sample through θ is accompanied by a 2θ rotation of the detector. This ensures that the incident angle is equal to the reflected angle and equal to the half of the total diffraction angle.

In this work the crystalline structure of the samples was investigated using a Rigaku (RINT-2000) X-ray diffractometer. XRD patterns were recorded

from 30° to 70° 2θ angles using CuKa radiation (λ=1.5405 Å) operated at 40kV and 82mA.

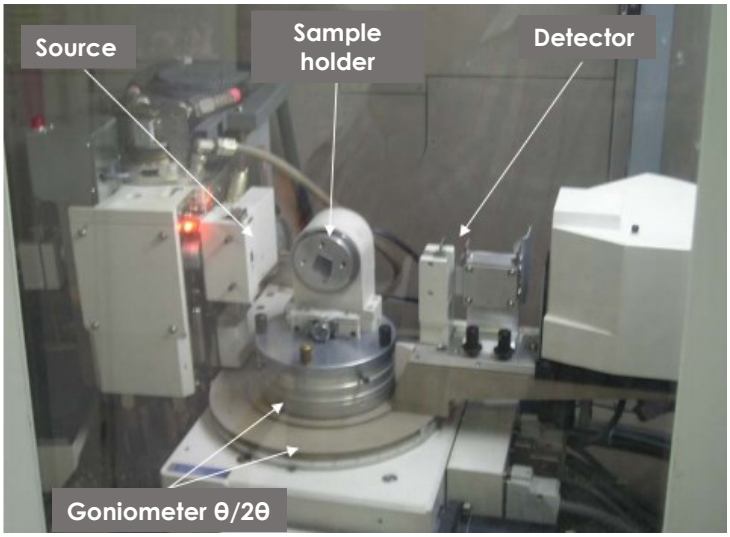

Figure 2.10 The Rigaku – Rint 2000 X-ray diffractometer at the IESL/FORTH

2.2.5 Raman Spectroscopy [84]

When a sample is exposed to a monochromatic light in visible region, the sample absorbs light and major portion of the light gets transmitted through the sample. However, a part of the incident light is scattered by the sample in all the directions.

The electrons have different vibrational levels that are defined by specific energy differences. When an incident monochromatic light interacts with an electron in the sample, the electrons absorbs energy from the incident photon and rises to a virtual state of energy. The energy transferred is given by the formula $E=hv_i$. An electron then falls back to an energy level by losing energy. If the energy lost equals to the energy of the incident photon $hv_s=hv_i$, the electron falls back to initial vibrational level, by emitting another photon. Since the energy lost is equivalent to the energy of the incident photon, the released photon has the same frequency as the incident photon. As the frequency is the same Rayleigh scattering occurs.

However, sometimes electrons when losing energy from the virtual state, can fall back to a different vibrational level. In this case, the energy lost by the electron is different than the energy absorbed from the incident photon $hv_s \neq hv_i$. As a result, the photon emitted by the electron has energy different than the incident photon. This is possible when the

frequency of the emitted photon is different than the incident photon. This gives rise to Raman scattering.

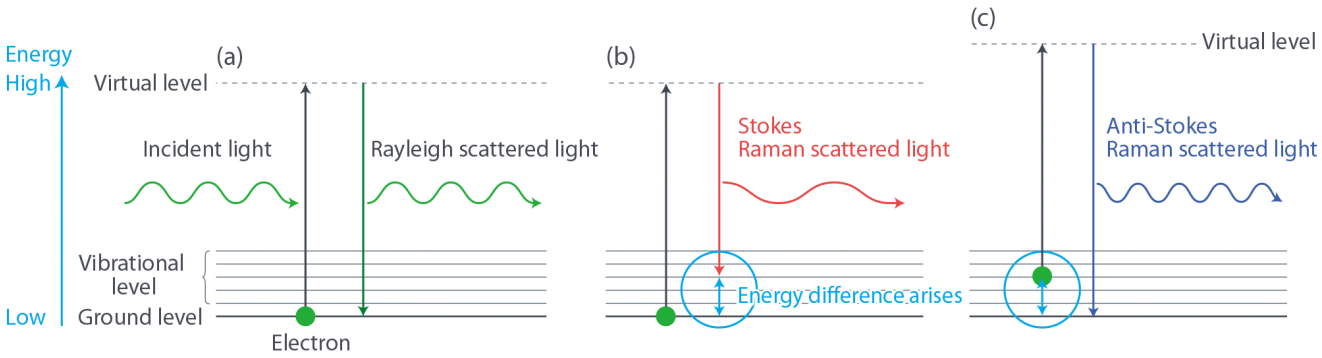

Figure 2.11 a) The Rayleigh and b), c) the Raman scattering processes (obtained from [85])

Depending on the final energy of the electron or the final vibrational level of the electron scattering can be separated into Stokes lines and anti – Stokes lines. If the frequency of the scattered photon is less than the frequency of the incident photon, Stokes lines are observed on Raman spectrum. This happens when the electron absorbs energy. Similarly, when frequency of the emitted photon is greater than the incident photon, anti – Stokes lines are observed. This means that energy is released by the electron.

Raman spectroscopy is a technique based on the analysis of the inelastically scattered light from the sample, produced by the interaction of the light with the atomic vibration levels. Usually, in a Raman spectroscopy experiment, the shift in energy between the incoming and inelastically scattered light is measured. The Raman effect was first observed in molecules by C.V. Raman in 1928, and nowadays Raman spectroscopy is a standard technique for the analysis of molecules, crystals and semiconductors [85].

A Raman spectrometer typically consists of three basic components:

1) The excitation source (laser),
2) The sample illumination system and light collection optics,
3) The detector.

A sample is normally illuminated with a laser beam in the ultraviolet (UV), visible (Vis) or near infrared (NIR) range. Scattered light is collected with

a lens and is sent through interference filter or spectrophotometer to obtain Raman spectrum of a sample.

The Raman spectrum gives the molecular fingerprint and it is characteristic for each molecular. Raman spectroscopy can be used to perform both qualitative and quantitative analysis on a sample. The study of the spectrum gives the opportunity to identify the rotational levels and thus a particular molecule (qualitative analysis). Similarly the intensity of a particular Raman line helps to determine the concentration of a molecule in a sample (quantitative analysis).

In this work the Raman spectra of the as-grown ZnO nanostructures were obtained using a Horiba LabRAM HR micro-spectrometer [86].

Figure 2.12 Horiba LabRAM HR Raman spectrometer (obtained from [86])

2.2.6 Luminescence

Luminescence is the general term used for describing the light emission of a material, which has previously interacted with an external source of energy, like a laser or even by applying electric field [86].

Depending on the excitation source, there are several types of luminescence [86]. Photoluminescence (PL) is caused by the absorption of photons from a monochromatic source, Cathodoluminescence (CL) results from electron beam, electroluminescence (EL) is excited by application of electric field and current and thermoluminescence is caused by heat excitation.

In the case of Photoluminescence, when a semiconductor, with a band gap energy Eg, is irradiated by a laser with energy hv>Eg, an electron is excited in the conduction band creating a hole in the valence band. An electron – hole pair is thus generated. The electrons and holes

thermalize to the lowest energy state of their respective bands via phonon emission and then they are recombining across the fundamental band gap or the defect levels within the band gap.

There are two basic mechanisms of recombination in semiconductors, namely radiative and non – radiative recombination. The radiative recombination is accompanied with photon emission with energy equal to or near the band gap energy of the semiconductor. On the other hand, in the non – radiative mechanism the energy is exchanged with the lattice as heat through phonon emissions within the defect states in the semiconductor. The defects in the crystal structure can be native defects, impurities and dislocations. The native defects include interstitials, vacancies and antisite defects. It is common such defects to form one or several energy levels within the forbidden gap of the semiconductor, which contribute to the radiative and non – radiative recombination. Energy levels within the energy band gap of the semiconductor are efficient recombination centers.

The non – radiative recombination cannot be detected by PL, and it occurs through the following mechanisms: Auger recombination, recombination at defects in the bulk and surface recombination.

The emission of electromagnetic irradiation, called luminescence can be achieved with the following radiative transitions [87]:

- Exciton recombination

Upon excitation at energy above the band gap, free electrons are created in the conduction band, as well as free holes in the valence band. This electron – hole pair is called free exciton and the exciton recombination leads to photon emission with energy hv=Eg-Ex, where Ex is the total energy of the exciton which can be in the ground or excited states. In the luminescence spectra of the semiconductor the exciton transitions appeared as sharp peaks.

In a semiconductor with impurities, the excitons are captured by the impurities and create the bound excitons. In the luminescence spectra the radiative transitions of the bound excitons are happening in lower energies than the free exciton.

- Band to band recombination

The recombination of free electrons in the conduction band with free holes in the valence band takes place when excitons cannot exist (high concentration of carries, high temperature). The electron which initially occupies a state in the conduction band transitions to a state in the valence band. Since the energy of the electron in the final state is lower than that at the initial state, the process is accompanied by energy release, typically in the form of photon.

- Transitions between donor – acceptor and impurity – band

The recombination of an e – h pair takes place, also, between donor – acceptor levels. This type of transition, called D – A transition, dominates at the luminescence spectra when the concentration of impurities is high and the semiconductor is under such conditions that allow the full occupation of the energy levels of acceptors and donors, from holes and electrons, respectively.
The D-A transitions can be observed at the luminescence spectra when the semiconductor is at low temperature and thus the D - A levels are not ionized.

Another radiative transition include the transition from impurity level (donor or acceptor) to energy band (Valence or conduction, respectively).

2.2.6.1 Photoluminescence, PL

Photoluminescence spectroscopy, is a powerful optical method for characterizing materials. It is a contactless, non-destructive method of probing the electronic structure of materials that has the ability to give large amount of information quickly and easy as the samples do not need any particular preparation [88].

The PL spectrum of semiconductors provide information about their physical properties and the behavior of charged carriers (band gap energy, defect levels, etc.).

The experimental set up that was used for the purpose of this Master thesis is presented in the figure below.

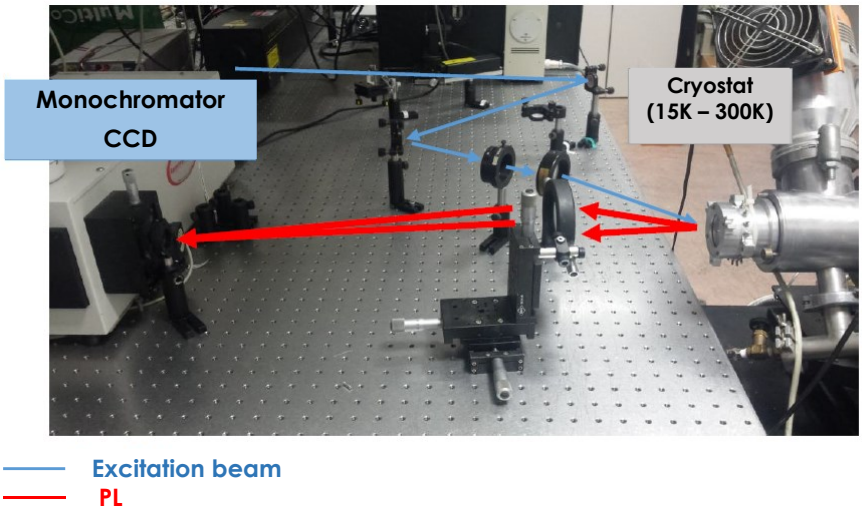

Figure 2.13 The experimental set up for the PL measurements at laboratory of the Microelectronics Research Group of IESL, FORTH and University of Crete

The PL set up was placed on an optical table. The photoluminescence measurements were carried out by using a He- Cd, cw laser at 325 nm with full power of 35 mW. The samples were placed in a high vacuum cryostat, which is cooled down to change the temperature from 13K to 300K. The emission spectrum is measured using a very sensitive, LN_2 cooled, CCD camera.

Chapter 3 – Results and discussion

Introduction

In this chapter we present the characterization of the nanostructured ZnO samples, as prepared using the ACG technique.

At each one of the ZnO samples, SEM was used in order to examine their morphology, while EDX spectroscopy provided their elemental analysis. Their structural properties were studied through XRD measurements, while their optical properties were studied through PL measurements.

3.1. ZnO structures synthesized using zinc salts and HMTA

In this set of experiments, the solutions of zinc nitrate or acetate and HMTA were prepared in water, ethanol, raki and ouzo in order to synthesize ZnO on Silicon (100) substrates, by means of chemical growth. Each synthesis was carried out at 95°C and 195°C.

The morphological and structural characteristics of the synthesized samples, as well as their optical properties are analytically presented below.

3.1.1 Morphology – SEM

- *Synthesis temperature: 95°C*

SEM images of the samples synthesized for 2 hours at 95°C using zinc nitrate or zinc acetate and HMTA are presented in Figure 3.1.

When water was used as a solvent, the presence of zinc nitrate with HMTA resulted in rodlike morphologies with hexagonal cross section, lying onto the substrate (figure 3.1a)). The average length and width are ~5μm and ~500nm, respectively.

On the other hand, the aqueous solution of zinc acetate and HMTA led to flowerlike architectures (figure 3.1b)), which consist of hexagonal nanorods with length of several microns (~2-3μm) and a typical width of about 200-300nm. Some individual rods can be, also, observed with mean length of ~2-3μm and width of about 300-400nm. Another difference when using Zn nitrate or zinc acetate, is that the substrate coverage changes from 80% to 90%, respectively. In both zinc sources the hexagonal cross section of rods, implies the wurtzite hexagonal structure of ZnO as it will be demonstrated by XRD pattern in following subsection.

Decomposition of zinc nitrate and HMTA in ethanol solvent ends up with the formation of co-existing flakes and flowerlike structures, which are composed of flakes (Figure 3.1c)). Their thickness ranges between 200-800nm, their edge length between 2-6μm and the substrate coverage is about 80%. Furthermore, when zinc nitrate was replaced by zinc acetate, nanospheres with mean diameter ~500nm were formed and the substrate coverage increased to nearly 98%.

Figures 3.1e) and 3.1f) depict the influence of raki on the morphology of the samples. It is observed that the substrate was covered by flake-like

structures in both zinc sources, while for the case of zinc acetate the textures ere more crinkly, and the flakes were denser.

Finally, when the reaction was performed by decomposing zinc nitrate and HMTA in ouzo, the shape of ZnO was flowerlike (Figure 3.1g)) consisting of nm-scale hexagonal rods of typical length and width of ~1μm and ~500nm, respectively. The shape changed to nanorods with hexagonal cross section under the presence of zinc acetate (Figure 3.1h)). The average length is ranging at 700-800nm, while the average width is about 200nm. The substrate coverage was decreased from 80% to 60%, respectively.

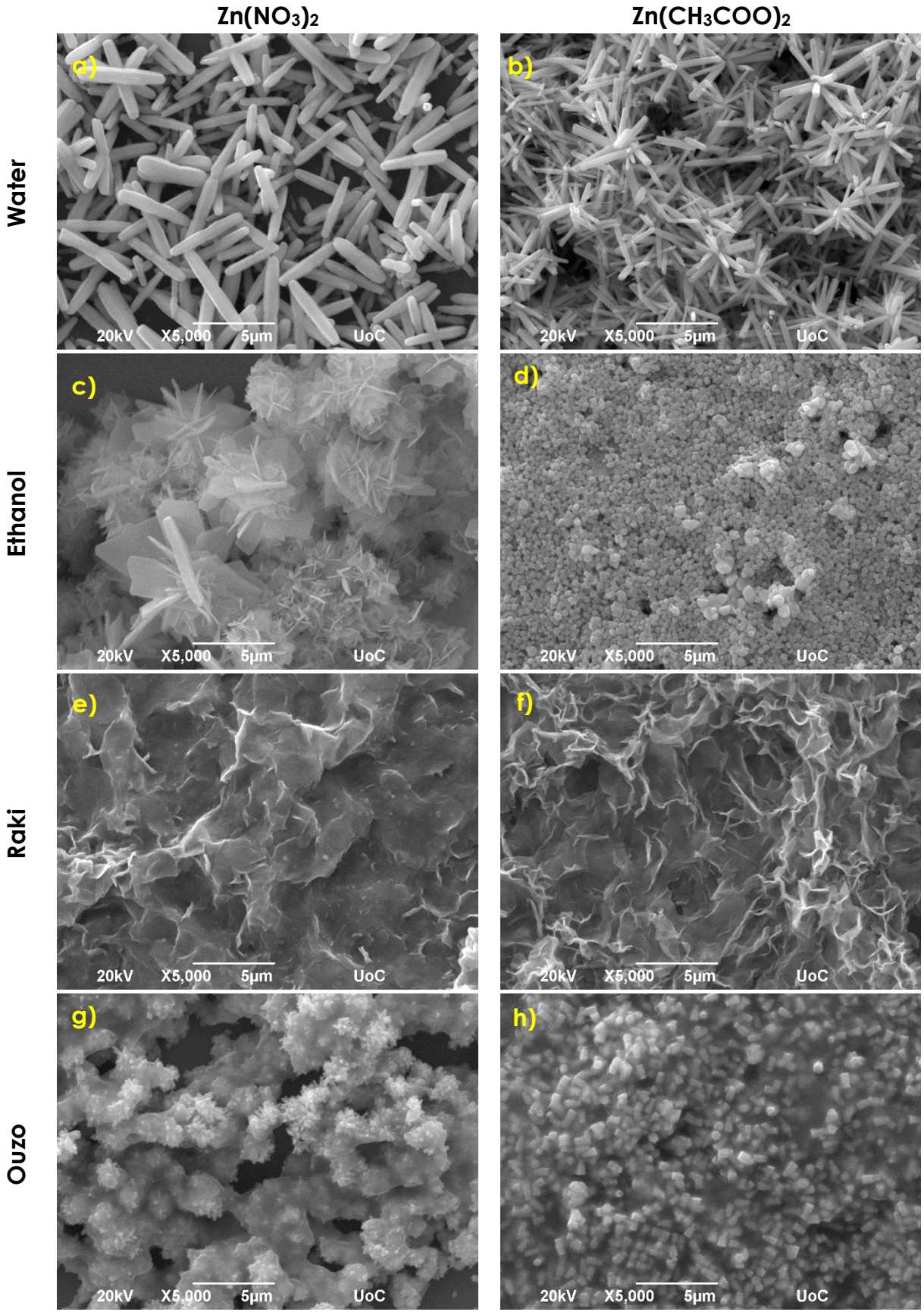

Figure 3.1 SEM images of ZnO samples synthesized at 95 °C with zinc nitrate or zinc acetate and HMTA

Moreover, in the case of water solvent, further experiments were carried out; Except from the equimolar aqueous solutions of zinc nitrate or acetate and HMTA, solutions with molar ratio 1:(1/6) of the above reagents were prepared and used for the ZnO structures' fabrication.

As it is depicted in figure 3.2, when varying the molar ratio, the morphology of deposits formed by each zinc precursor, do not differ from the equimolar reaction, but their size as well as the substrate coverage changes dramatically.

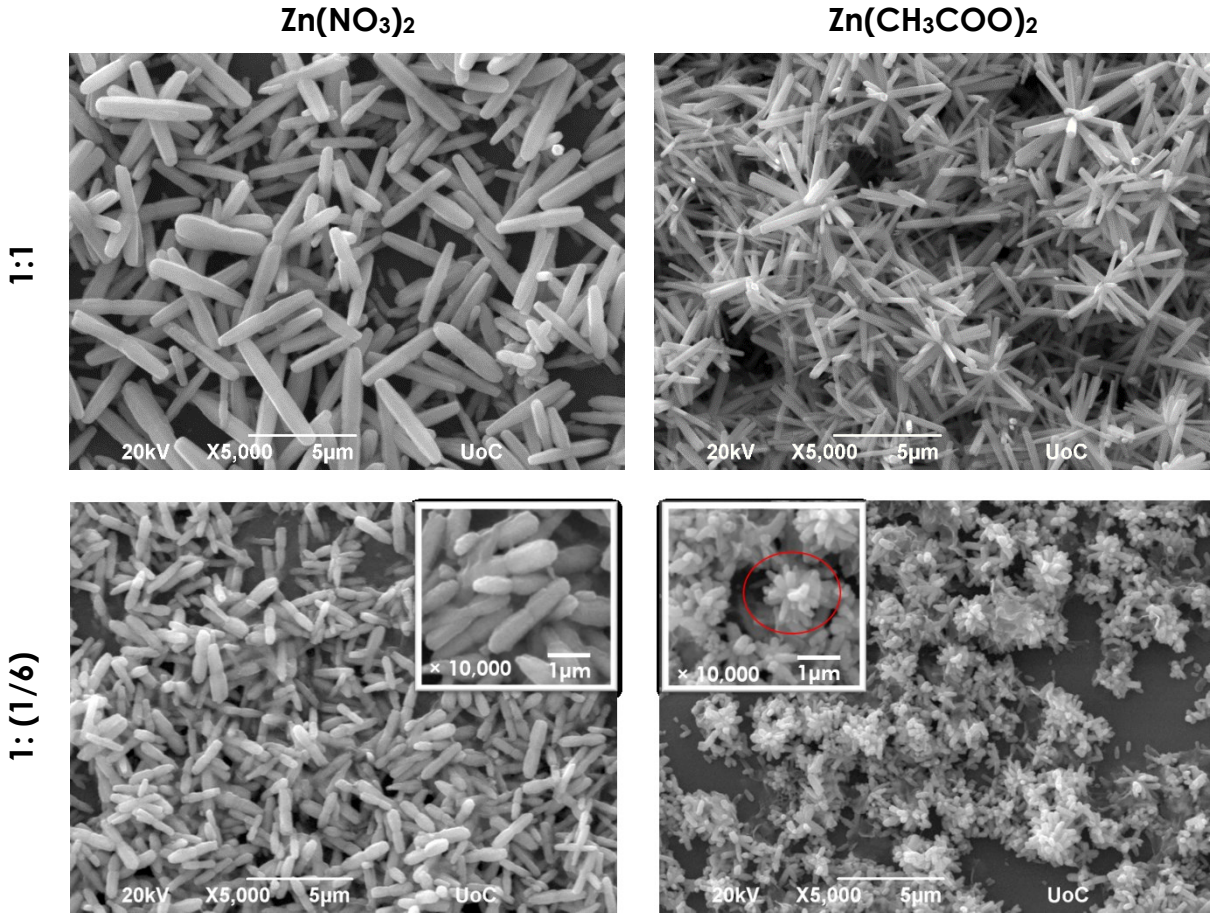

Figure 3.2 Comparison of ZnO samples prepared with different reagent's ratio in water solvent at 95 °C (The red circle denotes the flowerlike structure)

In the case Zn:HMTA ratio was 1:(1/6), the rodlike architectures have an average length and width of about 1-2μm and ~400nm, respectively. On the other hand, for the case of zinc acetate, the mean length and width of the rods composing the flowerlike structures were ~400nm and ~200nm. A direct comparison of these dimensions with the corresponding ones resulted from the equimolar reaction, prove that the morphologies are less developed.

In addition, when the equimolar reaction takes place, the substrate was well covered. The fact that the substrate coverage decreased, when the Zn:HMTA ratio was 1: 1/6, leads to the conclusion that the rate of the reaction is lower and that maybe more time would be necessary to achieve the same coverage like the case of the equimolar reaction.

- *Synthesis temperature: 195°C*

SEM images of the samples synthesized for 2 hours at 195°C with zinc nitrate or zinc acetate and HMTA are presented in figure 3.3.

Figure 3.3a) shows tip rod-like ZnO micro-structures resulted from aqueous solution of zinc nitrate and HMTA. Their length is about 1.5–3μm, while the width is ~700nm. There are also some bigger rod-like structures, having length of about 9μm. In the case of zinc acetate as zinc source (figure 3.3b)), the shape changes to flower-like, consisting of tip nanorods with average length 3-5μm and width ~600-700nm. Last but not least, there was a noticeably increase in substrate coverage from about 70% to 85%, when zinc acetate was used.

The decomposition of zinc nitrate and HMTA in ethanol results in coexistence of tip rods of length ~9μm and width ~2μm and flowerlike architectures, consisting of tip rods with length and width of about 7μm and ~2μm, respectively, as it is shown in figure 3.3c). When zinc nitrate is substituted by zinc acetate, the structures transform to spheres, with a mean diameter of about 500nm (figure 3.3d)). Additional to the shape difference, there is change and in the coverage of the substrate, as it increases from ~ 70% to 95%.

In case of raki as a solvent there is a remarkable change in the morphology. When zinc nitrate and HMTA are used at 195°C, ZnO structures are grown on Si(100), consisting of lying rod-like structures (figure 3.3e)), with hexagonal cross section, mean length of ~5μm and width of ~2μm. Quite similar morphologies were obtained when zinc acetate was used; twin hexagonal nut-like structures were observed (figure 3.3f)). A similar morphology of ZnO was previously observed by Jun Zhang et al. [89]. The average length and width of the twin hexagonal nutlike structures were ~4-5μm and ~2μm, respectively, while the substrate coverage, is increased from ~94% to 98%.

Finally, under the presence of ouzo, the zinc nitrate-HMTA reaction resulted in sphere-like morphologies composing of rods with mean length and width of ~2.5μm and 250nm, respectively, as it is observed in figure 3.3g). When zinc nitrate was replaced by zinc acetate, nanorods with hexagonal cross section, were formed, having a mean length of

~600nm and a width of ~200-300 nm (figure 3.3h)). The substrates' coverage increased from ~80% to 85%.

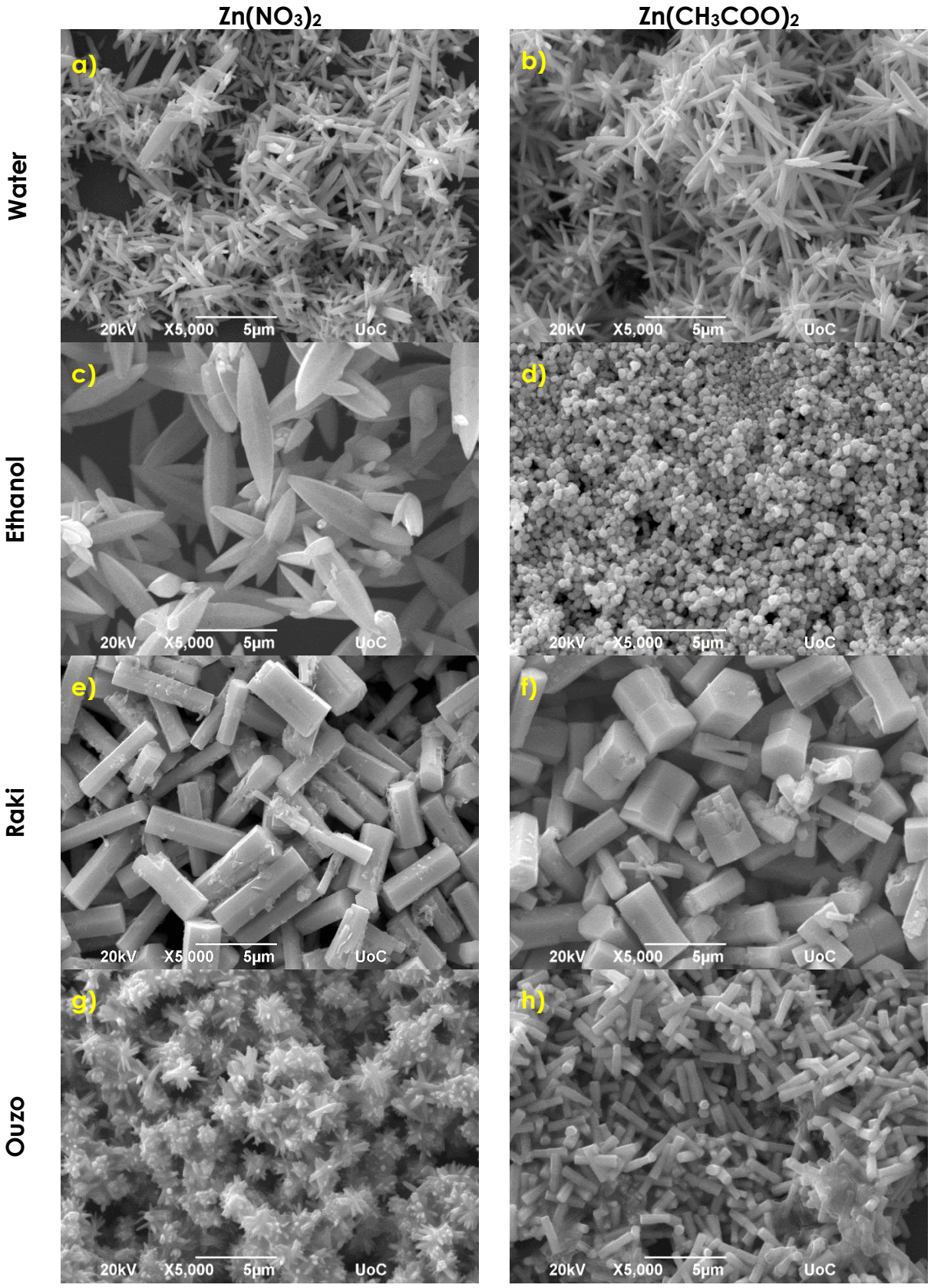

Figure 3.3 SEM images of ZnO samples synthesized at 195 °C with zinc nitrate or zinc acetate and HMTA

In conclusion, the SEM images above revealed the diversity in the morphology depending on whether zinc nitrate or zinc acetate was used.

Another crucial parameter that affects the morphology of the ZnO structures is the temperature; An increase of the temperature from 95°C to 195°C led to the formation of quite different morphologies, either on their shape, or on their geometry. As it was previously commented, in the case of raki, the flake-like structures obtained for 95°C (figure 3.1e)), were transformed to hexagonal rods for 195°C (figure 3.3e)), while for the case of ouzo the as-grown structures kept their original geometry, exhibiting quite bigger dimensions, as the growth temperature increased from 95°C to 195°C (figures 3.1h)-g), 3.3h)-g)).

In table 3.1 the morphologies of the produced structures as well as the reaction conditions are summarized.

Table 3.1 Summarized morphologies and reaction conditions when using HMTA

Morphology	Zinc source	Solvent	Temperature (°)
Rodlike	Zinc nitrate	Water	95
Flowerlike	Zinc acetate	Water	95
Tip rodlike	Zinc nitrate	Water	195
Flowerlike	Zinc acetate	Water	195
Flowerlike/Flakes	Zinc nitrate	Ethanol	95
Nanospheres	Zinc acetate	Ethanol	95
Tip rods/Flowerlike	Zinc nitrate	Ethanol	195
Spheres	Zinc acetate	Ethanol	195
Flakelike	Zinc nitrate	Raki	95
Flakelike	Zinc acetate	Raki	95
Rodlike	Zinc nitrate	Raki	195
Twin nutlike	Zinc acetate	Raki	195
Flowerlike	Zinc nitrate	Ouzo	95
Nanorods	Zinc acetate	Ouzo	95
Spherelike	Zinc nitrate	Ouzo	195
Nanorods	Zinc acetate	Ouzo	195

3.1.2 Qualitative elemental analysis – EDX

Energy Dispersive X-ray (EDX) analysis was performed for the qualitative elemental analysis of the samples. A typical example of an EDX spectrum is presented in figure 3.4.

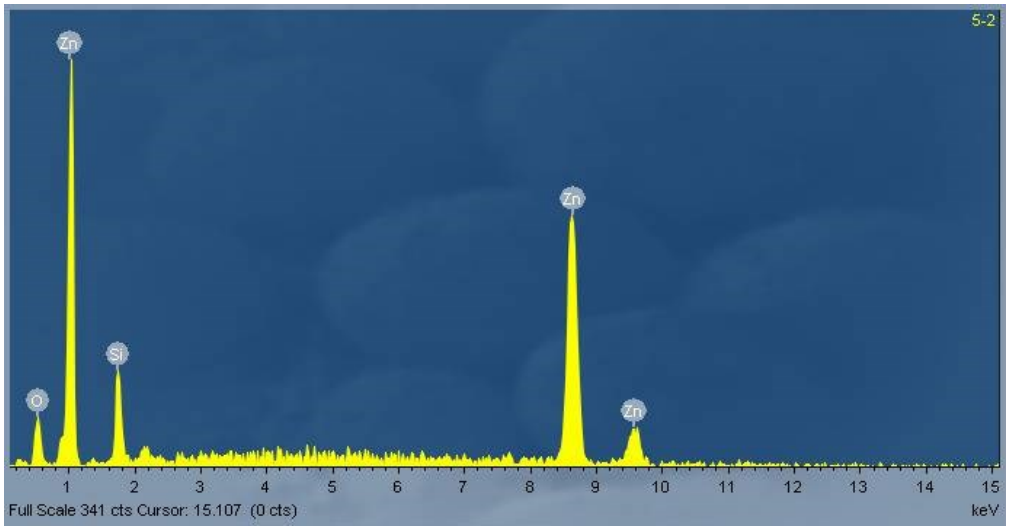

Figure 3.4 EDX spectrum of ZnO samples synthesized with zinc nitrate and HMTA at 195°C in ethanol solvent on silicon (100) substrate

The EDX spectrum of figure 3.4 corresponds to ZnO nanostructures grown for 2 hours in ethanol using zinc nitrate and HMTA at 195°C on silicon (100) substrate. Figure 3.4 indicates three emission peaks of metallic zinc (Zn) and a smaller peak of oxygen (O). Additionally, the spectrum revealed the existence of silicon (Si) which derives from the silicon substrate.

Although the spectrum of figure 3.4 does not include any other peaks, there were spectra in which small gold (Au) and carbon (C) signals existed, as it is depicted in figure 3.5. The Au signal is present due to the sputtering of the samples for SEM observation. As far as the C signal is concerned, its presence is due to the carbon tape used for the fixation of the samples in the SEM chamber.

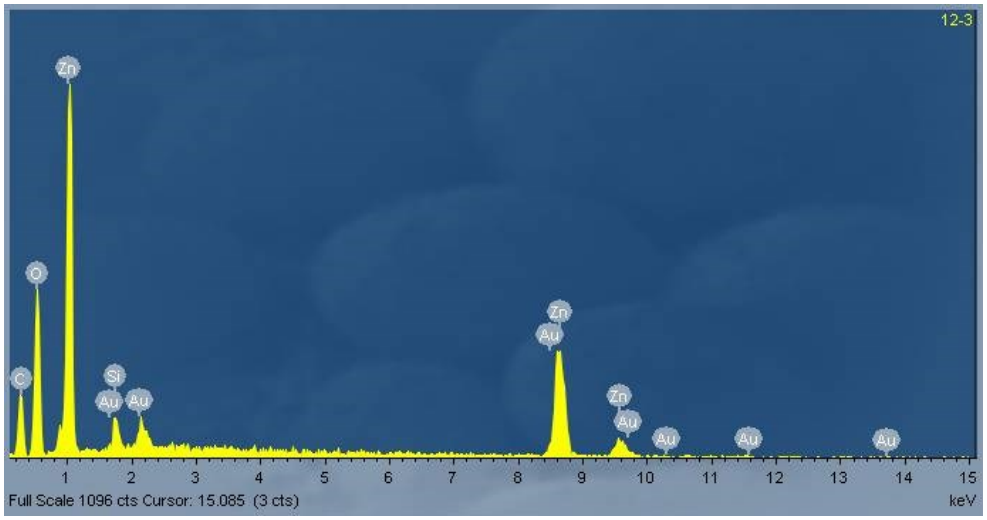

Figure 3.5 EDX spectrum of ZnO samples synthesized with zinc acetate and HMTA at 95°C in ouzo solvent on silicon (100) substrate

At this point it should be noted that all the samples exhibited the same behavior regarding the elements' peaks, independent of the temperature, the solvent and the zinc salt used.

3.1.3 Structural characterization – XRD

Figure 3.6 presents a typical XRD pattern for 2θ 30° to 70°. The obtained diffraction peaks were compared with the database of Joint Committee on Powder Diffraction Standards (JCPDS) and were matched with the ones for the hexagonal wurtzite phase of ZnO (JCPDS 36-1451) [90].

The XRD pattern of figure 3.6 corresponds to ZnO nanostructures grown for 2 hours in aqueous solution using zinc acetate and HMTA at 95°C on silicon (100). The presence of strong and narrow diffraction peaks indicate that the synthesized ZnO nanoparticles are crystalline. In addition, diffraction peaks from other species were not found, indicating that zinc oxide nanoparticles synthesized by zinc salts and HMTA were free from byproducts.

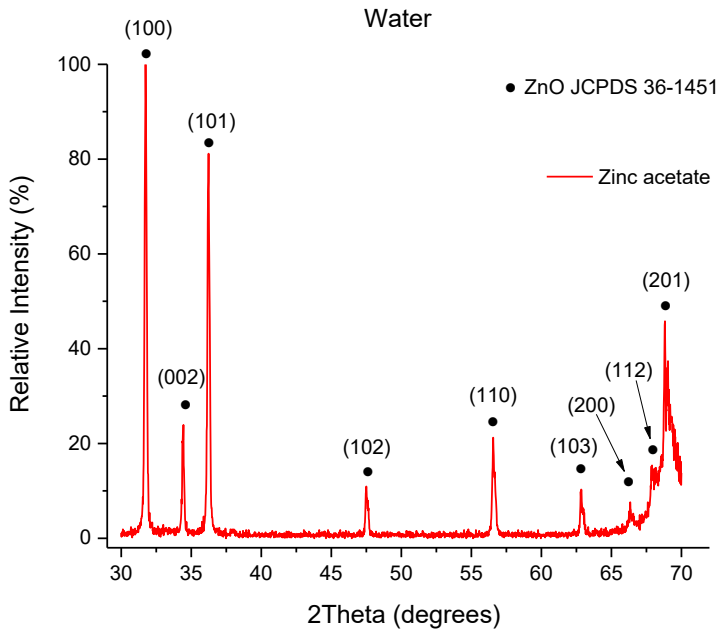

Figure 3.6 XRD spectrum of the sample synthesized with zinc acetate and HMTA for 2 h at 95°C on silicon (100) substrate

All the samples prepared in this group of experiments, by using either zinc nitrate or acetate and HMTA, at different temperatures and solvents, revealed the same diffraction peaks.

3.1.4 Optical characterization – PL

In order to perform PL measurements, the samples prepared using zinc salts and HMTA, were excited by a He-Cd cw laser (325nm) and the spectra were obtained at RT (295K) as well as at 13K in a wavelength range of 335nm to 750nm.

According to the literature [37], [40], [44], [68], [69], a typical PL spectrum of ZnO at RT consists mainly of UV emission, which is attributed to the exciton recombination that takes place in ZnO, and is corresponding to the near band edge emission at ~3.37eV. Another emission often observed in a PL spectrum at RT, is a so called broad visible emission, which is attributed to defects' or impurities'.

Figure 3.7 illustrates the PL spectra of the samples synthesized using zinc salts and HMTA at four different solvents at 95°C for 2 hours. The spectra were recorded at RT and at 13K, respectively.

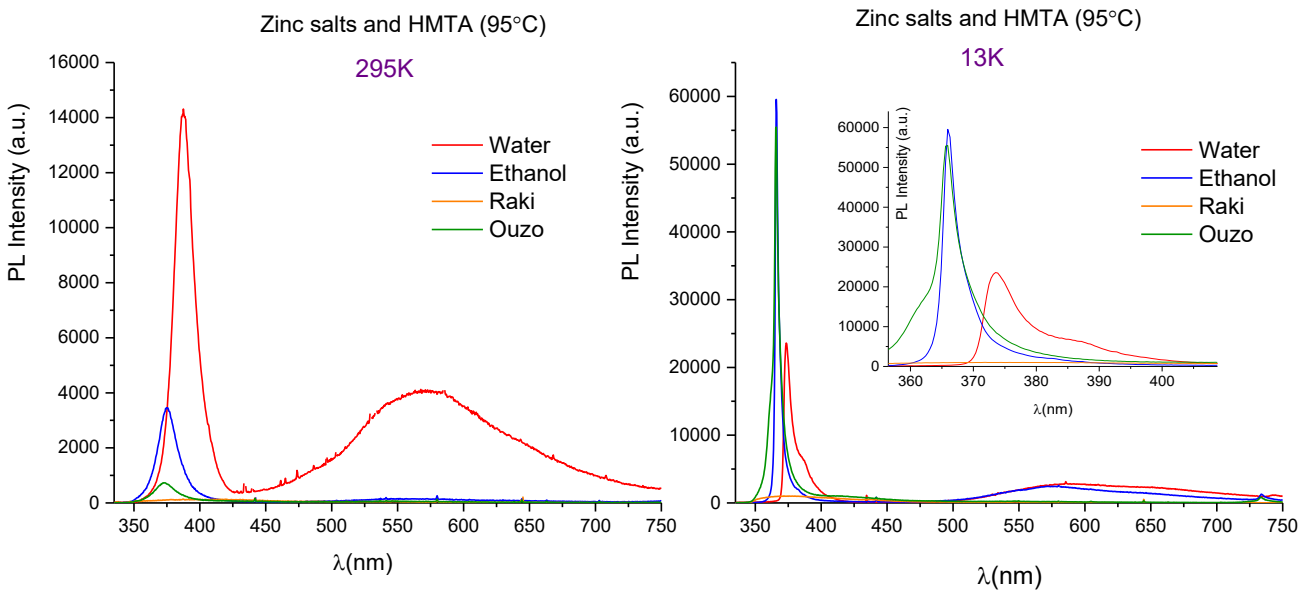

Figure 3.7 Typical PL spectra of the samples prepared with zinc salts and HMTA in four different solvents at 95°C for 2 hours. Left: PL spectra obtained at RT. Right: PL spectra obtained at 13K.

From figure 3.7 it is clear that at RT and at 13K almost all the samples exhibited the UV emission mentioned above. The only sample that did not exhibit any special behavior was the one synthesized in raki.

At RT the UV emission is centered at 388nm for water, 375nm for ethanol and 372nm for ouzo, which corresponds to energies of ~3.196eV, ~3.307eV and ~3.333eV, respectively.

At 13K the UV emission is centered at 374nm for water and 366nm for ethanol and ouzo. These wavelengths correspond to ~3.316eV and ~3.388eV, respectively and are closer to the value of ~3.37eV that is the estimated near band edge (NBE) emission of bound exciton (D^0X) of ZnO.

Moreover, at both spectra, one can see a broad band emission from 450nm to 700nm.

At RT, the sample prepared in aqueous solution exhibits the higher PL intensity, which at lower temperature (13K) becomes about 2 times higher.

As it was mentioned in the experimental section, the same samples were also prepared at 195°C for 2 hours. Typical PL spectra of these samples are presented in figure 3.8.

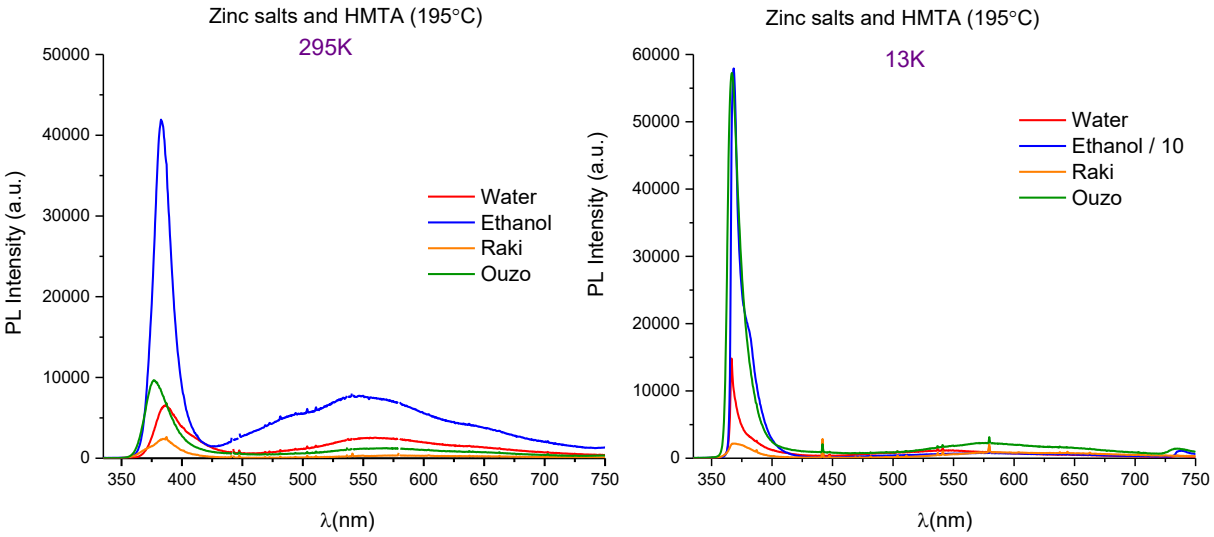

Figure 3.8 Typical PL spectra of the samples prepared with zinc salts and HMTA in four different solvents at 195°C for 2 hours. Left: PL spectra obtained at RT. Right: PL spectra obtained at 13K.

One can see from figure 3.8 that at higher synthesis temperature, the ZnO samples exhibit the characteristic UV emission of ZnO.

At RT the PL spectrum includes the UV as well as the broad visible emission (450nm-650nm), while at 13K the visible emission is very weak.

The UV emission, at RT, is centered at 387nm for water and raki, 382nm for ethanol and 377nm for ouzo and the corresponding energies are 3.204eV, 3.246eV and 3.289eV, respectively.

In addition, at 13K, the UV peaks are centered at 367nm for water and ouzo, and at 368nm for ethanol and raki. The corresponding energies are 3.379eV (water, ouzo) and 3.370eV (ethanol, raki), respectively.

It is observed that ZnO synthesized in ethanol at 195°C exhibits the strongest UV emission, which at 13K becomes almost 14 times higher.

3.2. ZnO structures synthesized with zinc salts and baking ammonia

In the second set of experiments, ZnO was synthesized on Silicon (100) substrates using solutions of zinc nitrate or zinc acetate and baking ammonia at four different solvents: water, ethanol, raki and ouzo. Each reaction was carried out at 95°C and 195°C.

The morphological and structural characteristics of the synthesized samples, as well as their optical properties are analytically presented below.

3.2.1 Morphology – SEM

- *Synthesis temperature: 95°C*

Figure 3.9 presents the SEM images of the ZnO samples prepared for 2 hours at 95°C using zinc nitrate or zinc acetate and baking ammonia.

The synthesized structures present noticeably differences from the respective ones synthesized using HMTA.

Figure 3.9a) shows the formation of agglomerated flakes using aqueous solution of zinc nitrate and baking ammonia. The flakes have average width and edge length of about 60nm and 400nm, respectively. When zinc acetate substituted zinc nitrate, agglomerated flakes with mean width ~100nm and edge length ~600nm, were formed (figure 3.9b)). The substrate coverage at both cases was ~60-70%.

Decomposing zinc nitrate and baking ammonia in ethanol resulted in the formation of flakes with average width ranging between ~150-400nm and edge length of ~1-2μm, as depicted in figure 3.9c). The substitution of zinc nitrate by zinc acetate results in the formation of flakes [figure 3.9d)], with an average width and edge length of about 100nm and 600nm, respectively. Both substrates present coverage of about 70-80%.

Under the presence of raki as solvent, the zinc nitrate-baking ammonia reaction resulted in sphere-like morphologies with rough surface and diameter of about 2μm. When zinc nitrate was replaced by zinc acetate, the morphology remained the same, and the average diameter was ~1-2μm. The substrates coverage remained about the same (~70%) (figures 3.9e), 3.9f)).

In case of ouzo, there is difference between the morphologies formed using different zinc sources. The zinc nitrate-baking ammonia reaction, led to sphere-like structures with mean diameter of ~2 μm [figure 3.9g)], while the zinc acetate-baking ammonia reaction resulted in

agglomerated flakes structures (figure 3.9h)). In both cases, the substrate coverage, ranges between 70-80%.

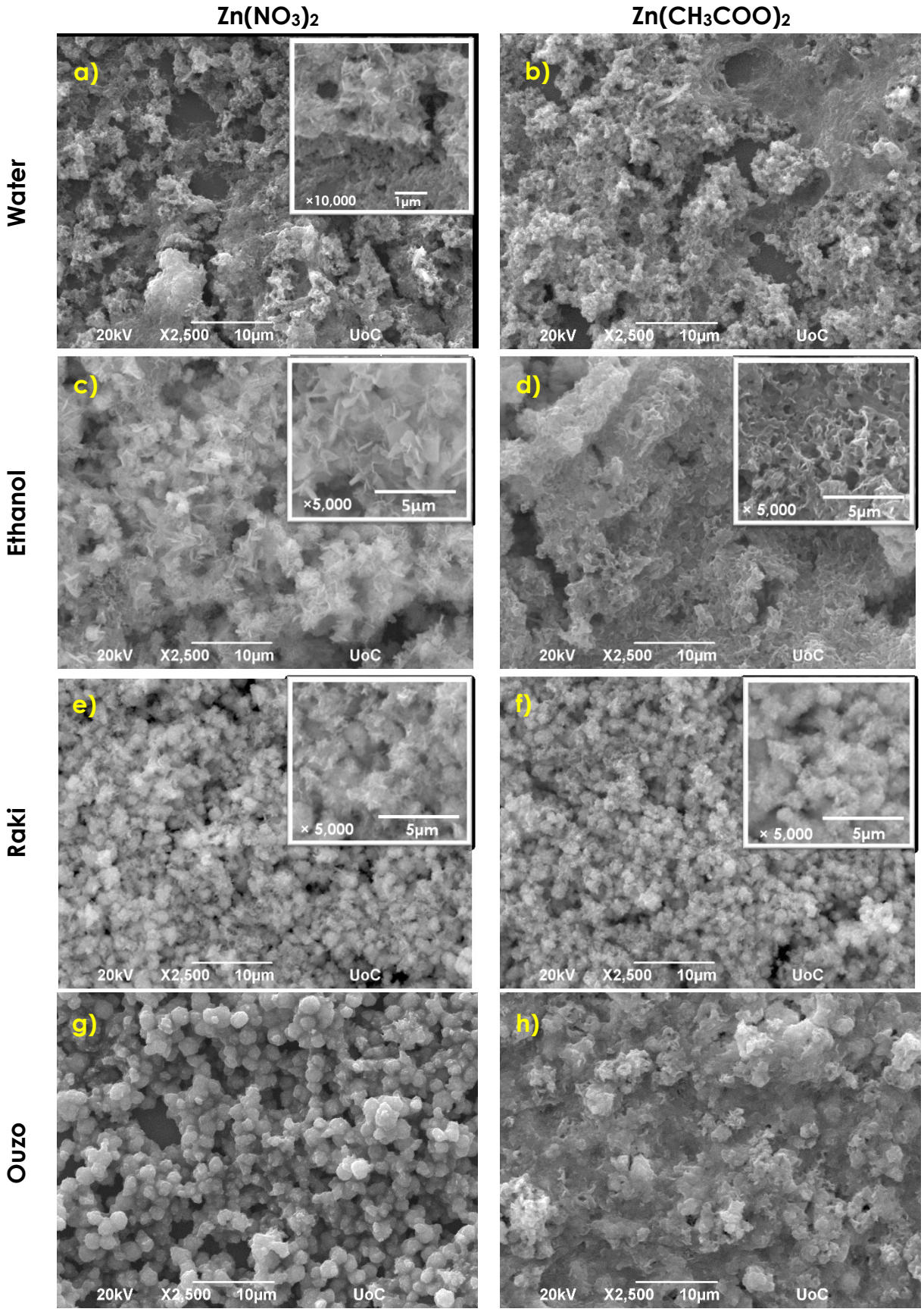

Figure 3.9 SEM images of ZnO samples synthesized at 95 °C with zinc nitrate or zinc acetate and baking ammonia

In this group of experiments again some extra syntheses were carried out when zinc salts and baking ammonia were dissolved in water solvent. Except from the equimolar aqueous solutions of zinc nitrate or acetate and baking ammonia, solutions with Zn:baking ammonia ratio 1: (1/6) were prepared and used for the ZnO structures' fabrication.

It can be observed from figure 3.10 that by varying the ratio, the morphology of the deposit for each zinc precursor, may do not differ from the equimolar reaction, but there is a change in the size of nanoparticles as well as the substrate coverage.

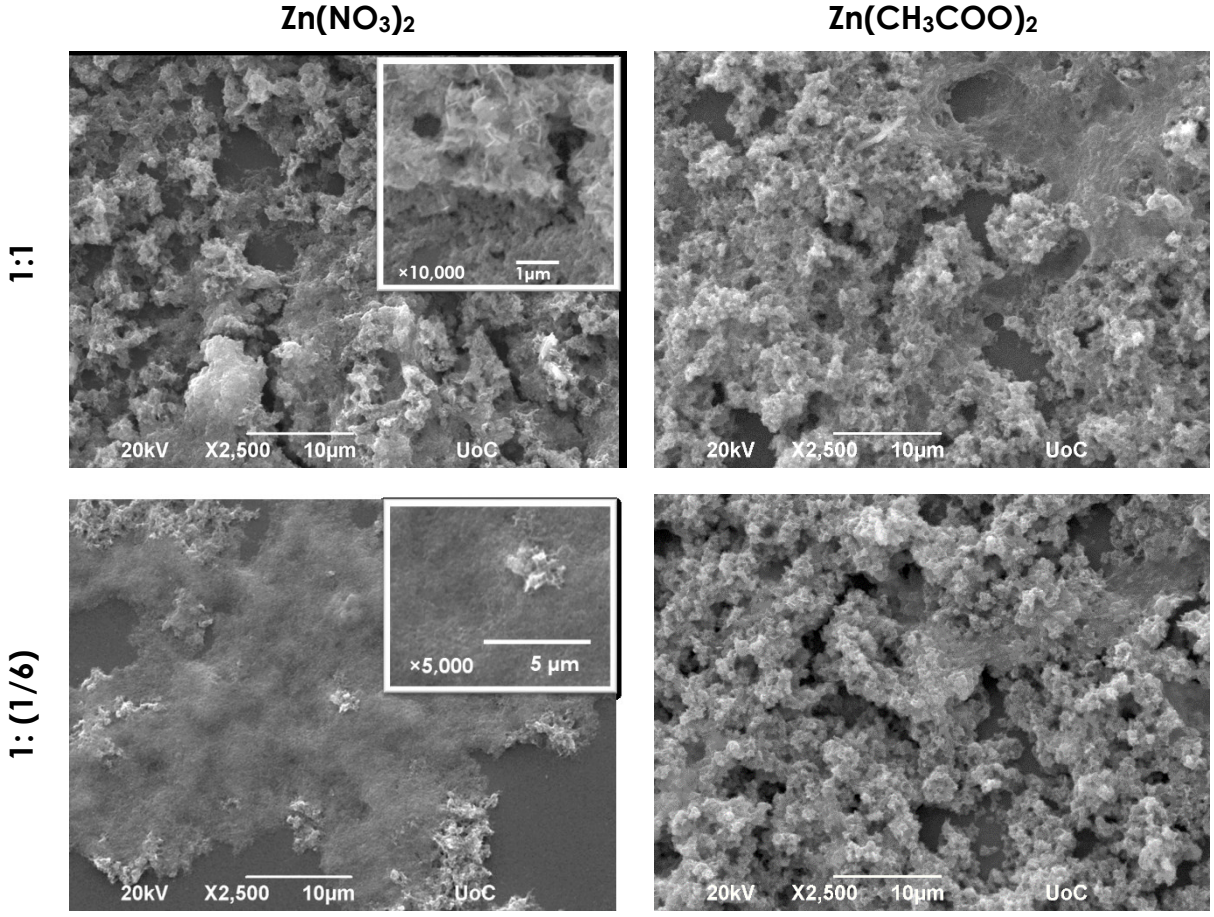

Figure 3.10 Comparison of ZnO samples prepared with different reagent's ratio in water solvent at 95 °C

When the Zn:baking ammonia ratio is 1: 1/6, in the case of zinc nitrate, the agglomerated flakes have not been so well developed as in the equimolar reaction. On the other hand, when zinc acetate is used, there is not obvious difference in the morphology of the samples.

In addition, when the equimolar reaction takes place, the substrate is well covered. The fact that the substrate coverage decreases when the Zn:baking ammonia ratio is 1: 1/6, leads to the conclusion that the chemical synthesis of ZnO according to the reaction 2.1 is slower.

- *Synthesis temperature: 195°C*

SEM images of the samples synthesized at 195°C using zinc nitrate or zinc acetate and baking ammonia are presented in figure 3.11.

When distilled water was used as solvent, the presence of zinc nitrate resulted in agglomeration of flakes (figure 3.11a)). The average width and edge length are ~100nm and ~400nm, respectively. On the other hand, the solution of zinc acetate and baking ammonia in water led to flowerlike architectures (figure 3.11b)), which consist of tip nanorods with length of several microns (~2-3μm) and a typical width of around 500nm. Some individual tip rods can also be observed with mean length of ~5-6μm and width of about 400nm. Except of the different morphologies, another difference, is that the substrate coverage decreases to 60% under the presence of zinc acetate.

Decomposition of zinc nitrate and baking ammonia in ethanol ends up with the formation of nonhomogeneous ZnO flowerlike structures, which are consisting of tip rods (figure 3.11c)) Some of the flowerlike structures are composed of dense rods and have diameter ranging between 2-3μm, while some other consist of more spare rods having length of ~1μm and width of about 300nm. Furthermore, when zinc nitrate was replaced by zinc acetate, ZnO rods with hexagonal cross section were formed (figure 3.11d)). The average length and width were 1-2μm and ~300nm-1μm, respectively. The substrate coverage remained stable at 70%.

Figures 3.11e) and 3.11f), depict the influence of raki on the morphology of the samples. Sphere-like architectures, with rough surface and mean diameter of ~2μm, were observed in both zinc sources. The substrate coverage was ~75-80%.

Finally, when the reaction was performed by decomposing zinc nitrate and baking ammonia in ouzo, sponge-like ZnO spheres, with 1-2μm diameter were formed (figure 3.11g)). The architecture changed, under the presence of zinc acetate, to agglomerated flakes with typical width and edge length of ~100nm and 1μm, respectively (figure 3.11h)).

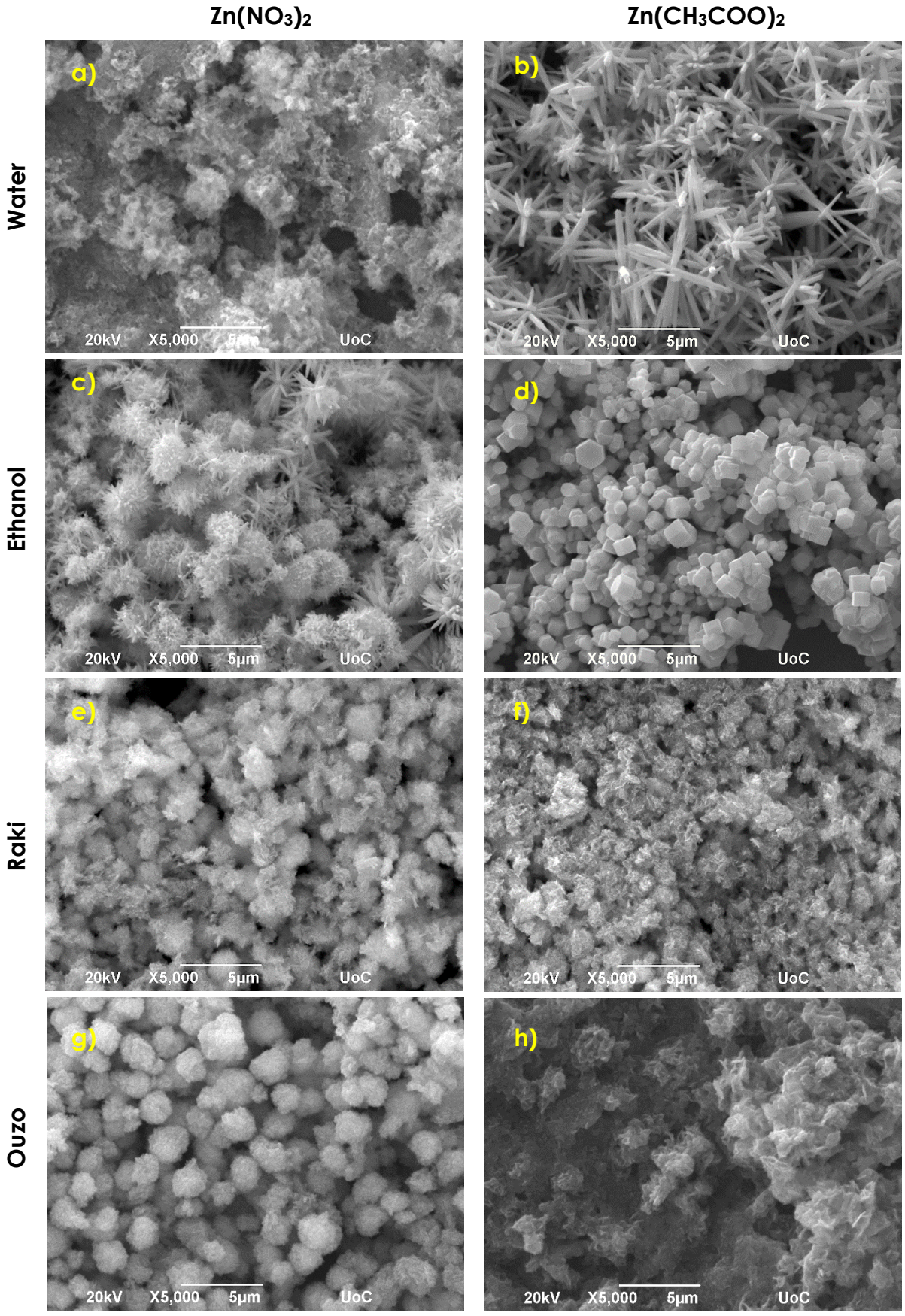

Figure 3.11 SEM images of ZnO samples synthesized at 195 °C with zinc nitrate or zinc acetate and baking ammonia

To sum up, the above SEM images revealed the diversity in the morphology depending on whether zinc nitrate or zinc acetate was used, at each solvent respectively.

The morphology of the ZnO nano-structures was altered upon changing the growth temperature from 95°C to 195°C. For example, when ethanol was the solvent, the flakes developed at 95°C (figures 3.10c)-d)) transformed into flower-like and hexagonal rods with a 100 °C increase in temperature (figures 3.11c)-d)).

Table 3.2 summarizes the morphologies as well as the reaction conditions.

Table 3.2 Summarized morphologies and reaction conditions when using baking ammonia

Morphology	Zinc source	Solvent	Temperature (°)
Agglomerated flakes	Zinc nitrate	Water	95
Agglomerated flakes	Zinc acetate	Water	95
Agglomerated flakes	Zinc nitrate	Water	195
Flowerlike/tip rods	Zinc acetate	Water	195
Flakes	Zinc nitrate	Ethanol	95
Flakes	Zinc acetate	Ethanol	95
Flowerlike	Zinc nitrate	Ethanol	195
Hexagonal rods	Zinc acetate	Ethanol	195
Spherelike	Zinc nitrate	Raki	95
Agglomerated flakes	Zinc acetate	Raki	95
Spherelike	Zinc nitrate	Raki	195
Spherelike	Zinc acetate	Raki	195
Spherelike	Zinc nitrate	Ouzo	95
Agglomerated flakes	Zinc acetate	Ouzo	95
Spongelike spheres	Zinc nitrate	Ouzo	195
Agglomerated flakes	Zinc acetate	Ouzo	195

3.2.2 Qualitative elemental analysis – EDX

The qualitative elemental analysis of the sample prepared with zinc nitrate and baking ammonia in raki at 95°C revealed the existence of zinc metal (Zn), oxygen (O), silicon elements (Si). The corresponding EDX spectrum is illustrated in figure 3.12.

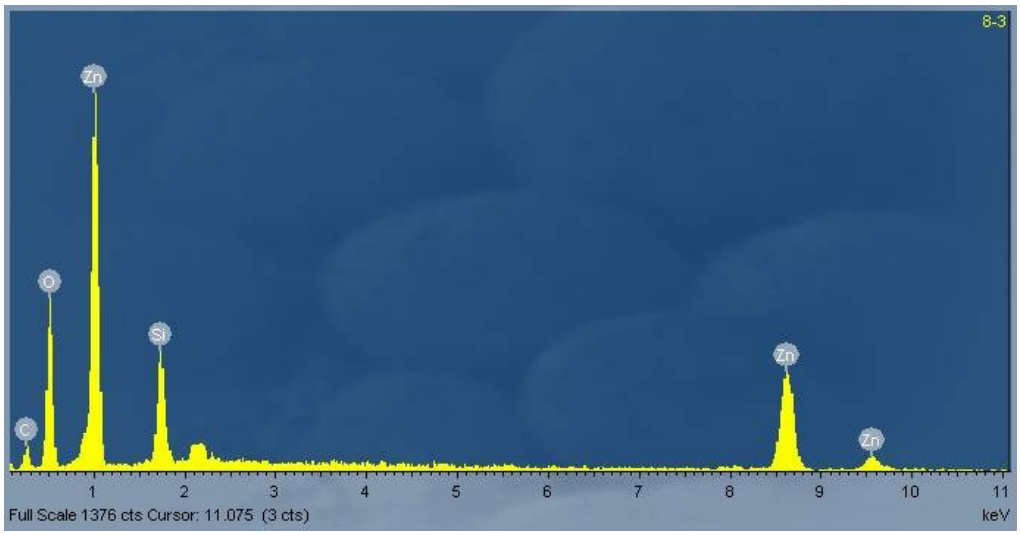

Figure 3.12 EDX spectrum of ZnO samples synthesized with zinc nitrate and baking ammonia at 95°C in raki solvent on silicon (100) substrate

Although the chemical reagent of HMTA was substituted by the baking ammonia, the EDX spectrum indicates that the resulted sphere-like morphologies are consisting of Zn and O elements.

3.2.3 Structural characterization – XRD

Figure 3.13 presents a typical XRD pattern of a sample, resulted from this set of experiments.

The XRD pattern of figure 3.13 corresponds to ZnO nanostructures synthesized in ouzo using zinc nitrate and baking ammonia at 95°C for 2 hours on silicon (100) substrate. The appeared diffraction peaks, marked with black dots, were matched to hexagonal wurtzite phase of ZnO (JCPDS 36-1451) [90], while the respective crystal planes were recognized. In addition, a peak of low intensity was observed which according to the JCPDS card no. 38-0385, matches to $Zn(OH)_2$ [91].

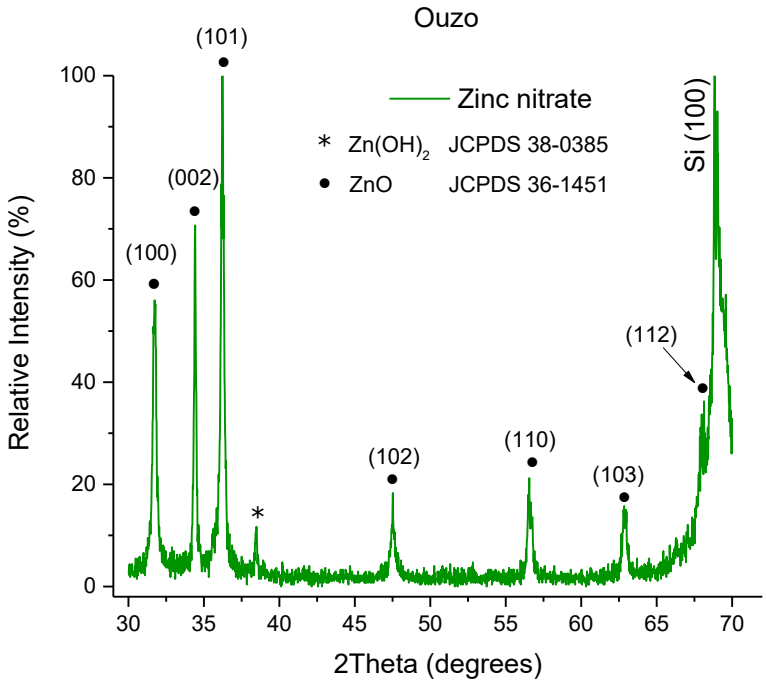

Figure 3.13 XRD spectrum of the sample synthesized with zinc nitrate and baking ammonia for 2 h at 95°C on silicon (100) substrate

Although, the presence of strong and narrow peaks indicate that the synthesized ZnO nanoparticles were crystalline, the extra XRD peak denotes the existence of byproducts. Therefore, in this set of experiments, there was not complete transformation of $Zn(OH)_2$ to ZnO, either due to the low temperature of the reaction-synthesis, or the duration of the synthesis was not adequate.

3.2.4 Optical characterization – PL

The samples synthesized using zinc salts and baking ammonia, were also characterized by PL measurements, in order to investigate if the characteristic UV emission of ZnO was present. The spectra were obtained at RT (295K) as well as at 13K in the wavelength range from 335nm to 750nm.

Typical PL spectra of the samples synthesized using four different solvents at 95°C for 2 hours are presented in figure 3.14.

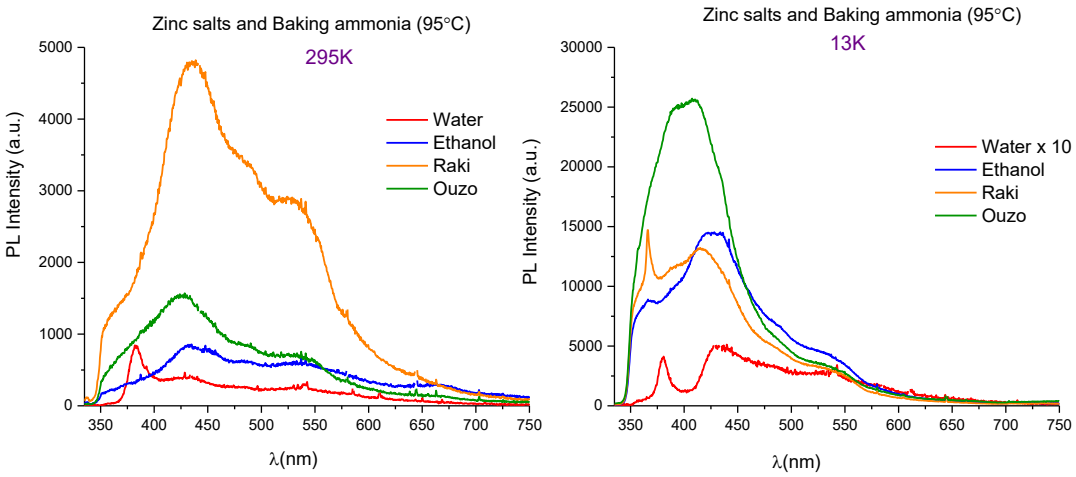

Figure 3.14 Typical PL spectra of the samples prepared with zinc salts and baking ammonia in four different solvents at 95°C for 2 hours. Left: PL spectra obtained at RT. Right: PL spectra obtained at 13K.

As it can be observed, only the sample synthesized in aqueous solution exhibited a low intensity UV emission, characteristic of ZnO. The emission is centered at 382nm, corresponding at 3.246eV. The samples prepared in ethanol, raki and ouzo did not emit in UV spectral region.

On the other hand at 13K, the solvent that allowed ZnO synthesis with UV emission was raki that in the previous group of experiments did not emit at all. The UV emission for water is centered at 381nm, and 366nm for raki, corresponding to energies of 3.255eV and 3.388eV, respectively.

When the synthesis temperature increased at 195°C, the PL performance of the samples was improved, as it can be seen from figure 3.15.

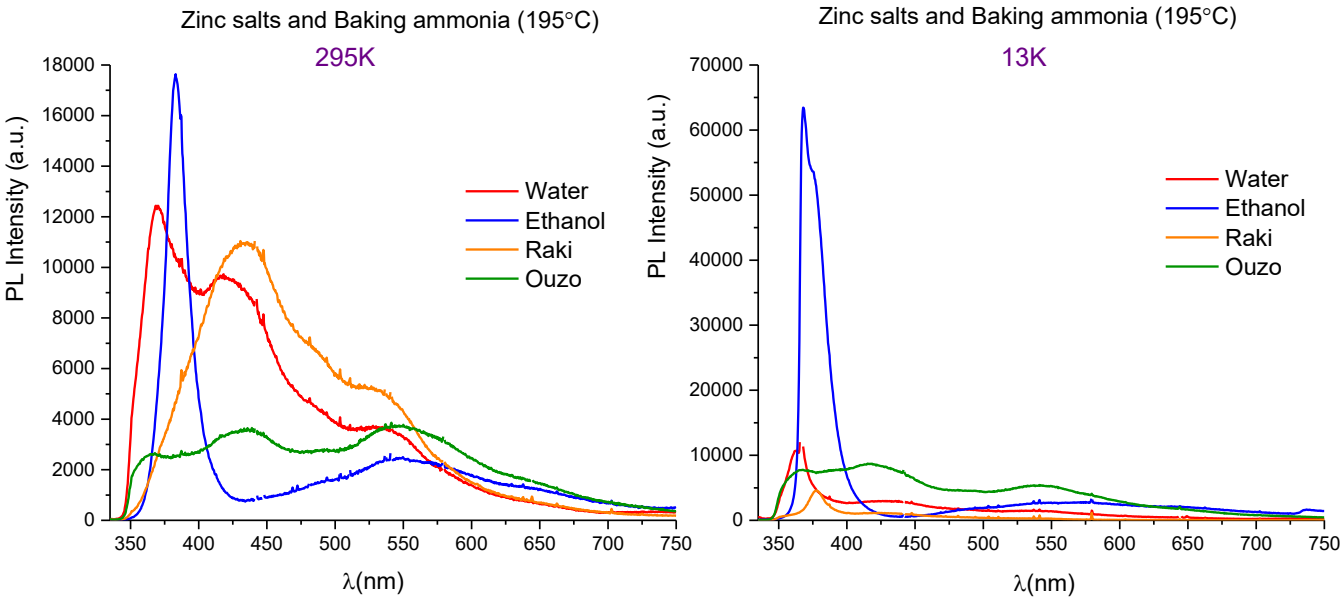

Figure 3.15 Typical PL spectra of the samples prepared with zinc salts and baking ammonia in four different solvents at 195°C for 2 hours. Left: PL spectra obtained at RT. Right: PL spectra obtained at 13K.

At RT, the ZnO sample synthesized in ethanol has a strong UV emission, accompanied with a weak visible emission. The UV emission is centered at 382nm for water and 387nm for ethanol, corresponding to 3.246eV and 3.204eV, respectively.

At low temperature (13K), the UV emission of ZnO samples synthesized in water is centered at 363nm for water, 368nm for ethanol and 378nm for raki, corresponding to energies of 3.416eV, 3.370eV and 3.280eV, respectively.

The best PL performance of all the samples was exhibited when ethanol was used and it was increased about 4 times when the PL temperature decreased at 13K.

3.3. ZnO structures synthesized with zinc powder and HMTA

In the third set of experiments, ZnO was synthesized on Silicon (100) substrates by dissolving zinc powder and HMTA at five different solvents: water, ethanol, soda water, lemon beverage and hydrogen peroxide (28% w/w) at 195 °C.

The morphological and structural characteristics of the synthesized samples, as well as their optical properties are analytically presented below.

3.3.1 Morphology – SEM

SEM images are presented in figure 3.16.

Zinc powder with 0.05g of HMTA dissolved in water resulted in sunflower-like ZnO structures with diameter ranging between 2-5μm (figure 3.16a)). As it is shown in figure 3.16b), the increase of the amount of HTMA (0.15g) did not affect the geometry of the structures, while their diameter was increased up to ~7μm. One noticeable difference is that when 0.05g of HMTA was used, the sunflower-like structures were not well developed and as a result their size varies. Their growth rate was lower and thus small and larger structures co-exist. In contrast, the 0.15g of HMTA help the homogenous growth of structures. The impact of growth rate is depicted on the substrate coverage (~70-80%), which is decreased upon increase of HMTA.

Figures 3.16c) and 3.16d) illustrate the influence of ethanol in the formation of ZnO structures. Mushroom-like architectures were developed for both amounts of HMTA. Similar morphologies have been previously reported by Jinzhou Yin et al. [92]. The substrate coverage increases from 40 to 60% with increasing the amount of amine.

Decomposing zinc powder and HMTA in soda water, led to the formation of tip rods with mean length of about 8μm and width 1μm, as it is depicted in figure 3.16e). Simultaneously with the presence of tip rods, agglomerated rods with hexagonal cross section were also formed, as it can be observed from the inset of the figure. The 0.15g of HMTA created the presence of rodlike structures with hexagonal cross section and flowerlike structures composed by flakes with diameter ~5μm (figure 3.16f)). As far as the rod-like structures are concerned, their length is about ~6μm and their width is ~700nm. The substrate coverage is about the same (80-85%).

When the synthesis was performed by decomposing zinc powder and HMTA in lemon beverage, flakes were formed for both amounts of HMTA (figures 3.16g) and 3.16h)). The 0.05g of HMTA gave flakes with width ~100nm and edge length ~500nm, while the respective dimensions when 0.15g of HMTA was used, were ~100nm and ~600nm.

Finally, the hydrogen peroxide (2.8% w/w) resulted in flakes and agglomerated hexagonal rods when 0.05g of HMTA was used (figure 3.16i)). The width and edge length of flakes are about 250nm and 2μm, respectively, while the rods have length of ~1-2μm and width of ~800nm. An increase in the amount of HMTA (0.15g) resulted in clusters of rods, shown in figure 3.16j), with an average diameter of 5μm and tip rods with length of about 6μm and width ~2μm.

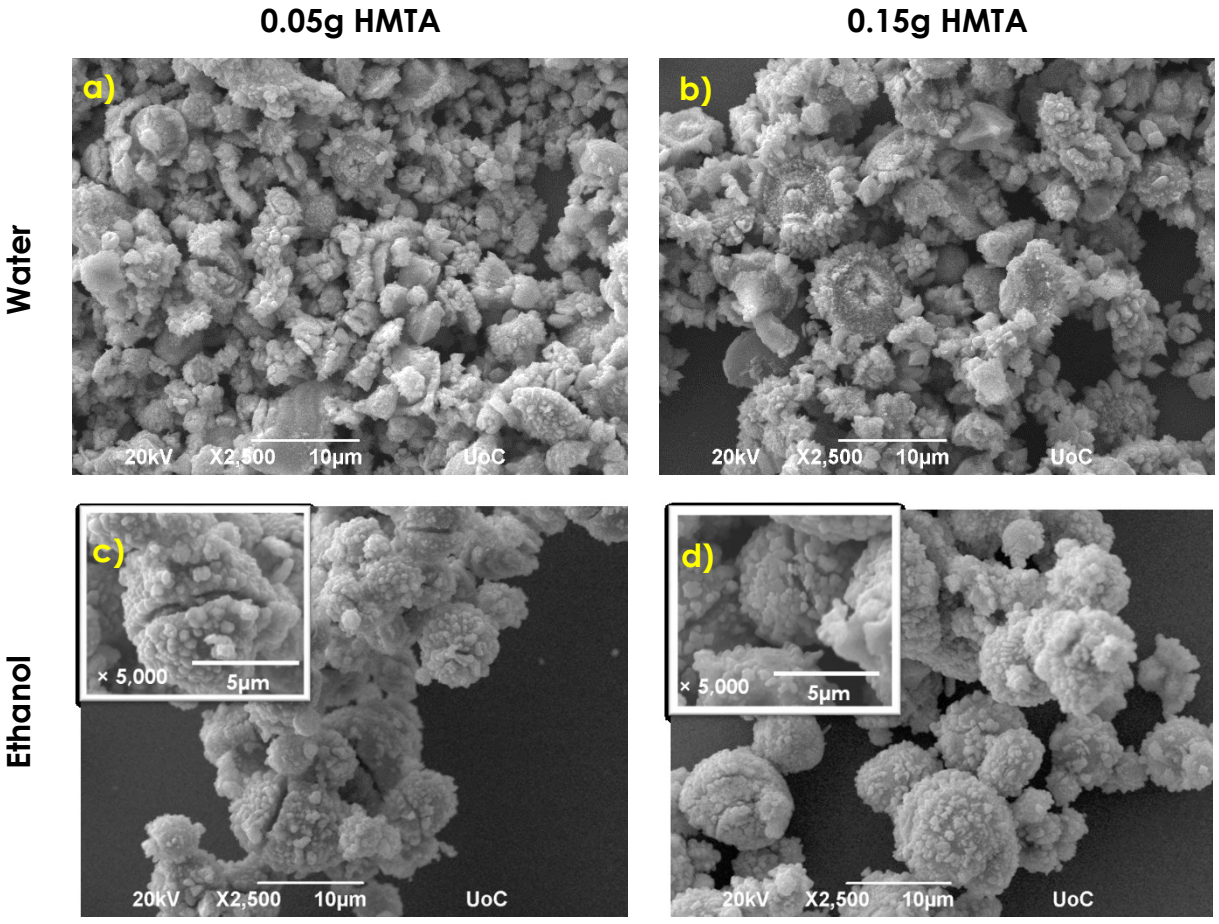

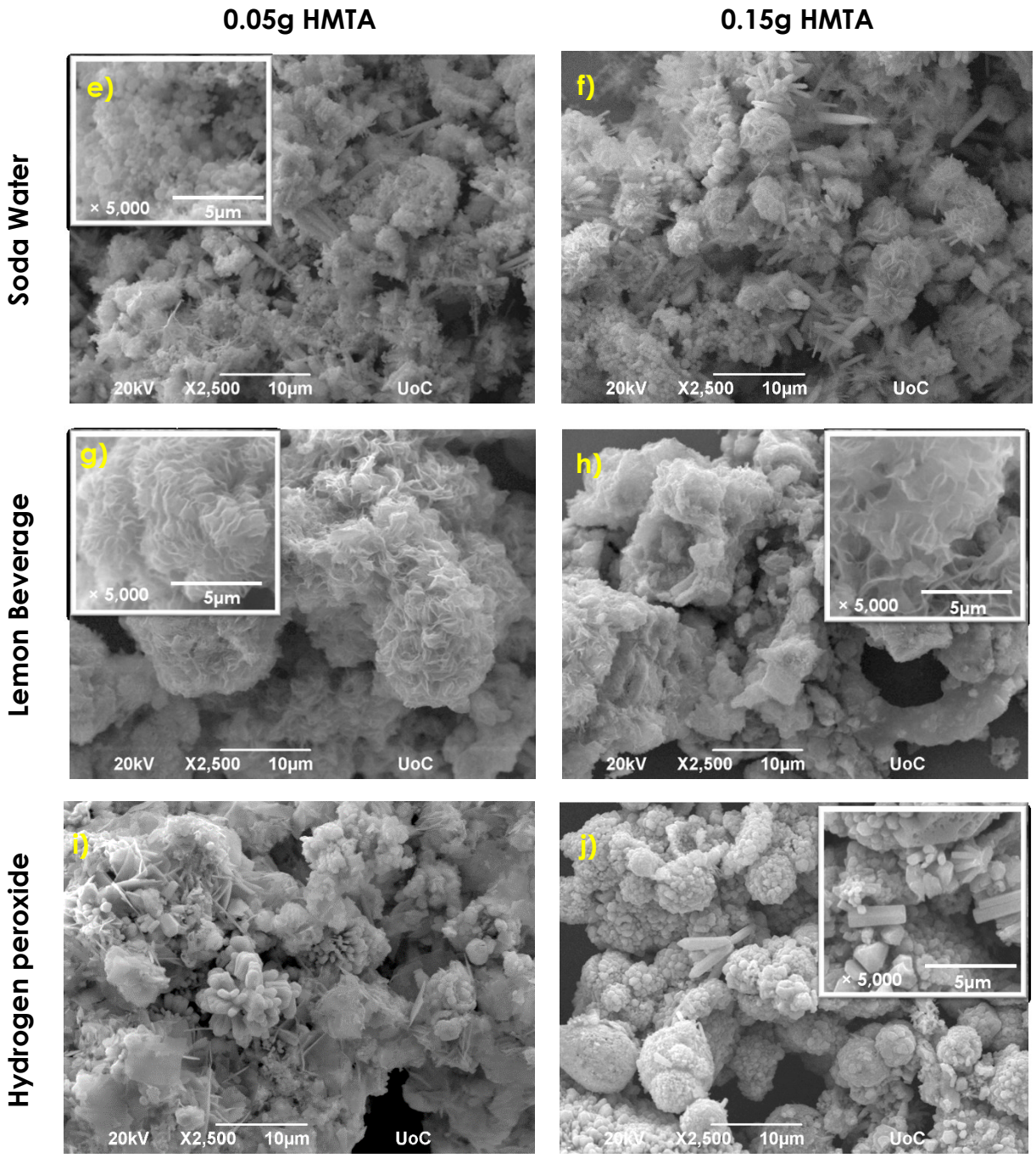

Figure 3.16 SEM images of ZnO samples synthesized at 195 °C with zinc powder and HMTA

3.3.2 Qualitative elemental analysis – EDX

The qualitative elemental composition of the nanoparticles, prepared in this set of experiments, was analyzed through EDX.

Figure 3.17 depicts the EDX spectrum of the sample prepared with zinc powder and 0.15g of HMTA for 24 hours at 195°C in soda water.

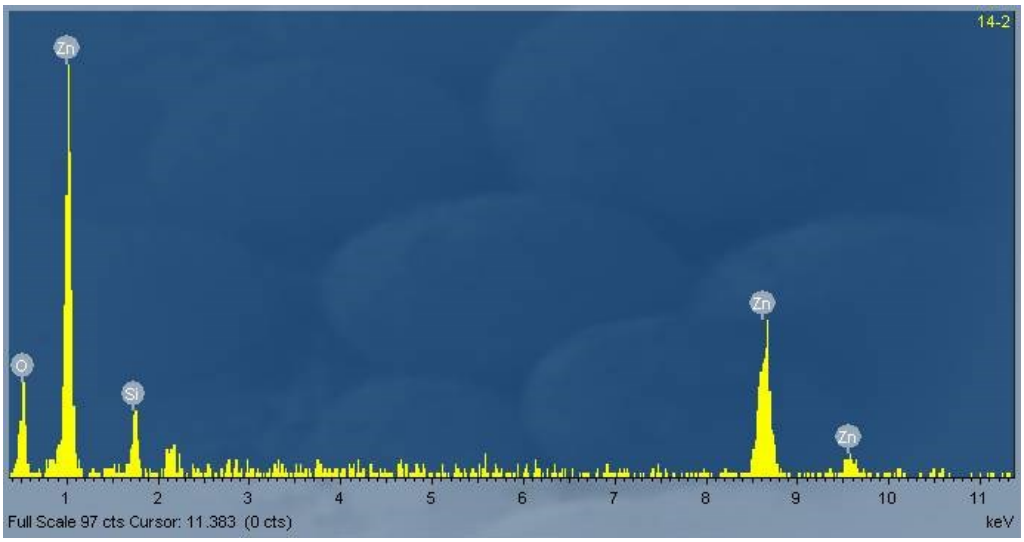

Figure 3.17 EDX spectrum of ZnO samples synthesized with zinc powder and 0.15g of HMTA at 195°C in soda water solvent on silicon (100) substrate

Similarly to the EDX spectra of the previous set of experiments, the peaks, presented in figure 3.17, correspond to zinc metal (Zn), oxygen (O) and silicon (Si).

The presence of Si element derived from the silicon substrate onto which the ZnO nanostructures were deposited.

3.3.3 Structural characterization – XRD

X-ray diffraction was applied to further confirm the zinc oxide phase of the synthesized nanoparticles. Typical XRD patterns of the samples synthesized in water, ethanol, soda water, lemon beverage and hydrogen peroxide (2.8% w/w) are presented in figure 3.18.

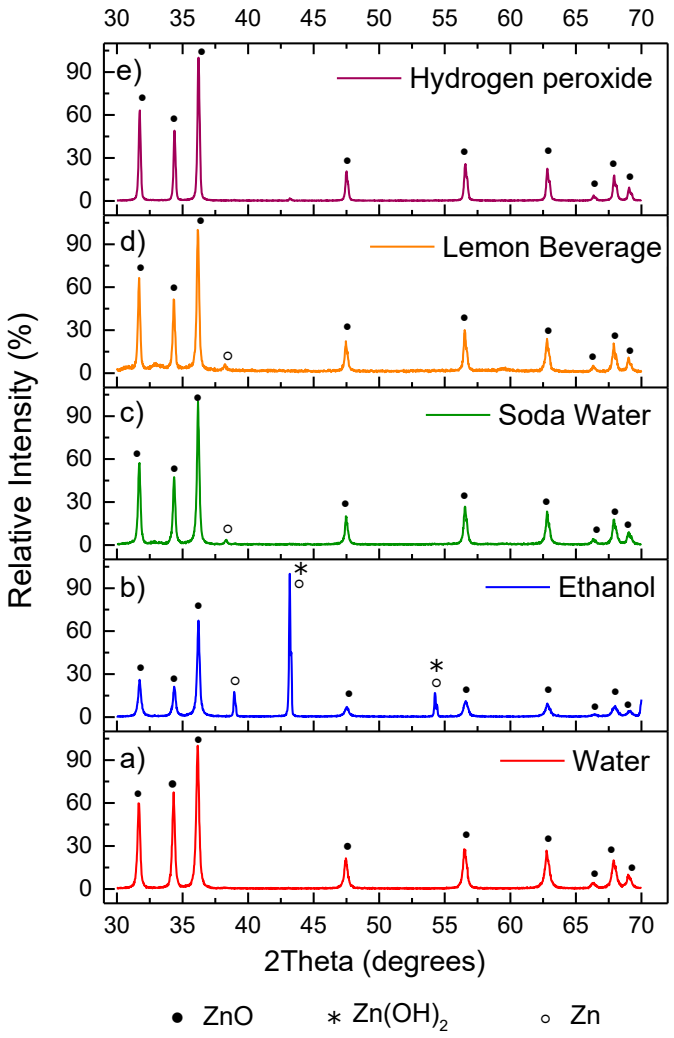

Figure 3.18 Typical XRD patterns of the samples prepared with zinc powder and HMTA at 195°C for 24 hours in five different solvents

Figure 3.18a) illustrates the XRD pattern of the sample prepared with zinc powder and HMTA in aqueous solution. The peaks centered at 31.64°, 34.32°, 36.16°, 47.46°, 56.48°, 62.76°, 66.38°, 67.88°, 68.98° correspond to (100), (002), (101), (102), (110), (103), (200), (112) and (210) crystal planes of the hexagonal wurtzite ZnO (JCPDS 36-1451) [37]. Black dots mark the peaks attributed to ZnO. Pure ZnO was formed, as no characteristic diffraction peaks from other materials were detected. Moreover, the

high intense diffraction peaks indicate the crystalline nature of ZnO particles.

In contrast, when ethanol was used as solvent, there was not complete transformation of zinc metal to ZnO, as it is indicated by the respective XRD pattern of figure 3.18b). The extra peaks obtained were matched to Zn (JCPDS 87-0713) as well as to $Zn(OH)_2$ (JCPDS 38-0387) and are marked with "o" and "*", respectively [93]–[95]. The presence of such peaks denotes that some portion of zinc powder either did not react at all with HMTA or it partially reacted resulting in the formation of $Zn(OH)_2$. Further decomposition of $Zn(OH)_2$ did not achieved and thus the XRD peaks appeared. Maybe a longer duration of the synthesis procedure or even higher temperature would be necessary for the complete transformation.

Figure 3.18c) represents the XRD pattern of the sample prepared with soda water. As it can be observed, exactly the same reflections resulted and with lemon beverage solution (figure 3.18d)). Sharp diffraction peaks characteristic of the ZnO wurtzite hexagonal phase (JCPDS 36-1451) as well as a reflection of very low intensity, attributed to $Zn(OH)_2$, can be observed in the XRD patterns. Thus under the presence of soda water and lemon beverage solvents the zinc powder did not fully transformed to ZnO.

Last but not least, the XRD pattern of the sample synthesized in hydrogen peroxide (2.8% w/w) does not seem to differ from that of water solvent. Once more the ZnO of hexagonal wurtzite phase is identified.

In conclusion, in this set of experiments, the samples synthesized in water and hydrogen peroxide revealed the pure phase of ZnO, while all the others include byproducts, such as Zn or $Zn(OH)_2$. Ethanol was the solvent that presented the maximum difficulty in converting Zn powder to ZnO, as the diffraction peaks of the byproducts were of higher density.

3.3.4 Optical characterization – PL

The samples synthesized using zinc powder and HMTA, were characterized by PL measurements, in order to investigate if the characteristic UV emission of ZnO was present. The RT (295K) as well as the 13K spectra were obtained in the wavelength range from 335nm to 750nm.

Typical spectra recorded at RT and 13K are presented in figure 3.19.

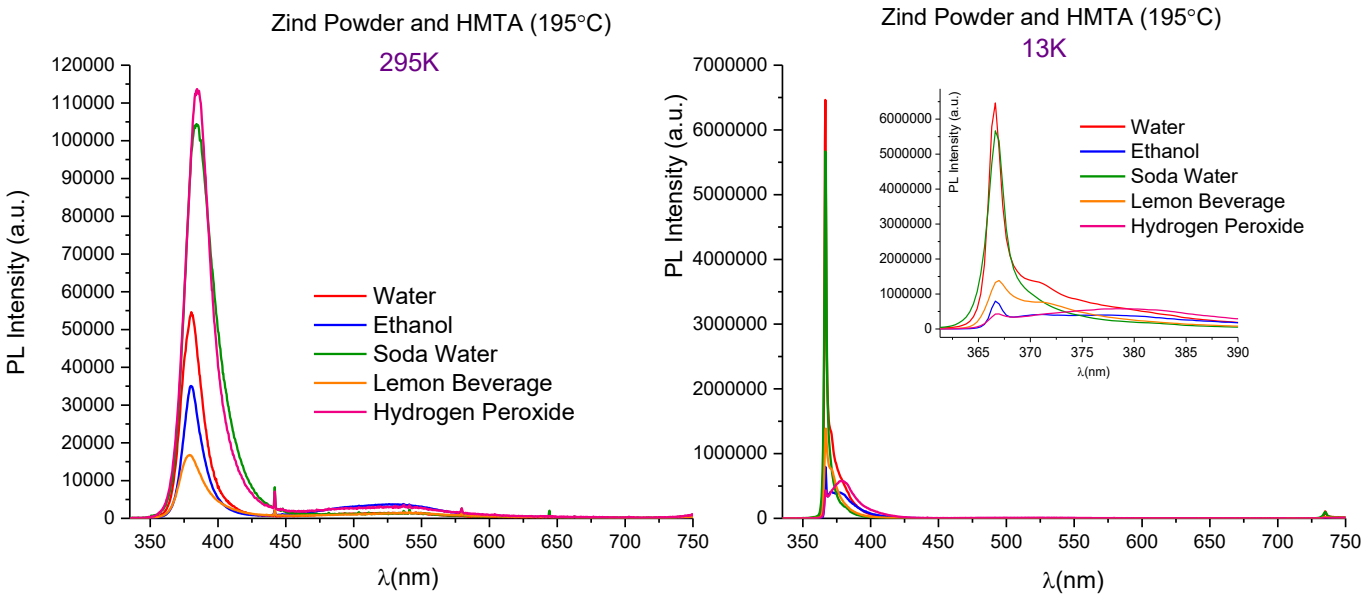

Figure 3.19 Typical PL spectra of the samples prepared with zinc powder and HMTA in five different solvents at 195°C for 24 hours. Left: PL spectra obtained at RT. Right: PL spectra obtained at 13K.

All the samples synthesized in different solvents, exhibited the characteristic UV emission of ZnO at both temperatures.Additionally, at RT, a very weak broad emission at visible spectral region is observed.

At RT the UV emission is centered at 380nm for water and ethanol, at 384nm for soda water, at 379nm for lemon beverage and at 385nm for hydrogen peroxide (2.8% w/w), corresponding to the energies of 3.263eV, 3.229eV, 3.272eV and 3.221eV, respectively.

At 13K all the peaks attributed to exciton recombination are centered at 367nm, which corresponds to 3.380eV.

The higher PL intensity, at RT, is exhibited by the sample prepared with hydrogen peroxide (2.8% w/w), which increases by four times at 13K.

3.4. ZnO structures synthesized with zinc powder and baking ammonia

In the fourth set of experiments, ZnO was synthesized on Silicon (100) substrates by dissolving zinc powder and baking ammonia at five different solvents: water, ethanol, soda water, lemon beverage and hydrogen peroxide (28% w/w), respectively. Except from the solvent, another parameter that was changing was the amount of baking ammonia. Each synthesis procedure was carried out at 195 °C.

The morphological and structural characteristics of the synthesized samples, as well as their optical properties are analytically presented below.

3.4.1 Morphology – SEM

Figure 3.20 summarizes all the SEM images of the samples synthesized in this group of experiments.

More specifically, in aqueous solution of zinc powder and baking ammonia, sunflower-like structures of ZnO with mean diameter ~3-5μm were formed (figure 3.20a)), while the addition of more baking ammonia led to inhomogeneous morphologies as it can be observed in figure 3.20b). Nanorods with hexagonal cross section having length of ~8μm and width of ~800-900nm co-existed with flowerlike structures that were composed of flakes and had mean diameter of ~5μm.

Figure 3.20c) presents the mushroom-like architectures formed by the reaction of zinc powder with 0.05g of baking ammonia in ethanol. Similar morphologies but with rough surfaces result when the amount of baking ammonia was increased (figure 3.20d)). The substrate coverage is decreased as the amount of amine is increasing.

Dissolving zinc powder with 0.05g of baking ammonia in soda water led to the formation of rods, with average length ~4μm and width 600nm, as well as structures composed of flakes with mean width and edge length being 100nm and 600 nm, respectively (figure 3.20e)). Figure 3.20f) illustrates the result of increasing the amount of baking ammonia; Rod-like structures with hexagonal cross section were developed. Furthermore, the substrate coverage was increased (~90%).

By simply substituting soda water with lemon beverage, structures consisting from flakes were formed at both baking ammonia amounts. The substrate coverage increased from 50% to 80% (figure 3.20g), and figure 3.20h))

Finally, structures of irregular shape consisting of hexagonal rods, was the result of hydrogen peroxide influence on zinc power and baking ammonia, as it is shown in figures 3.20i) and 3.20j).

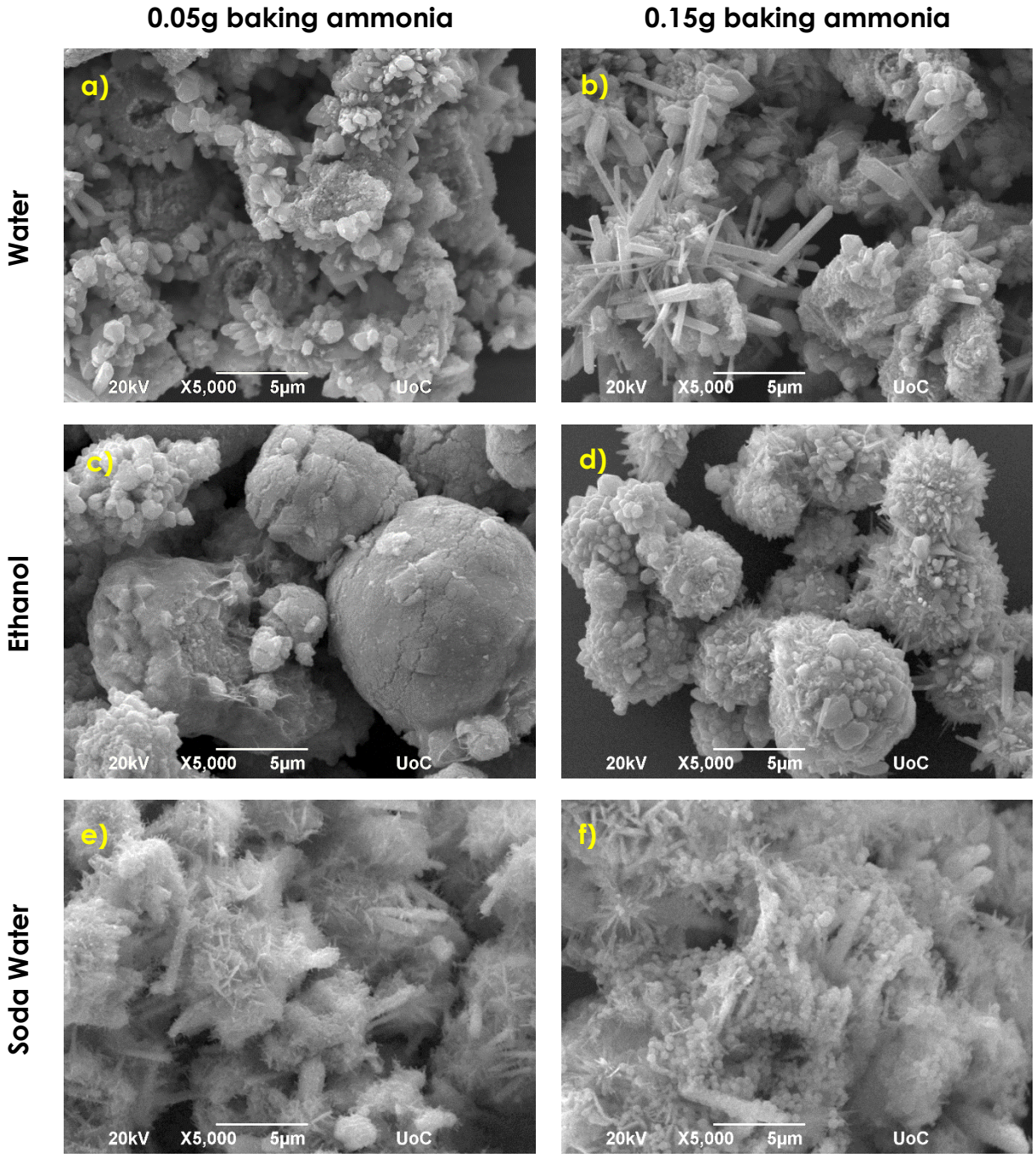

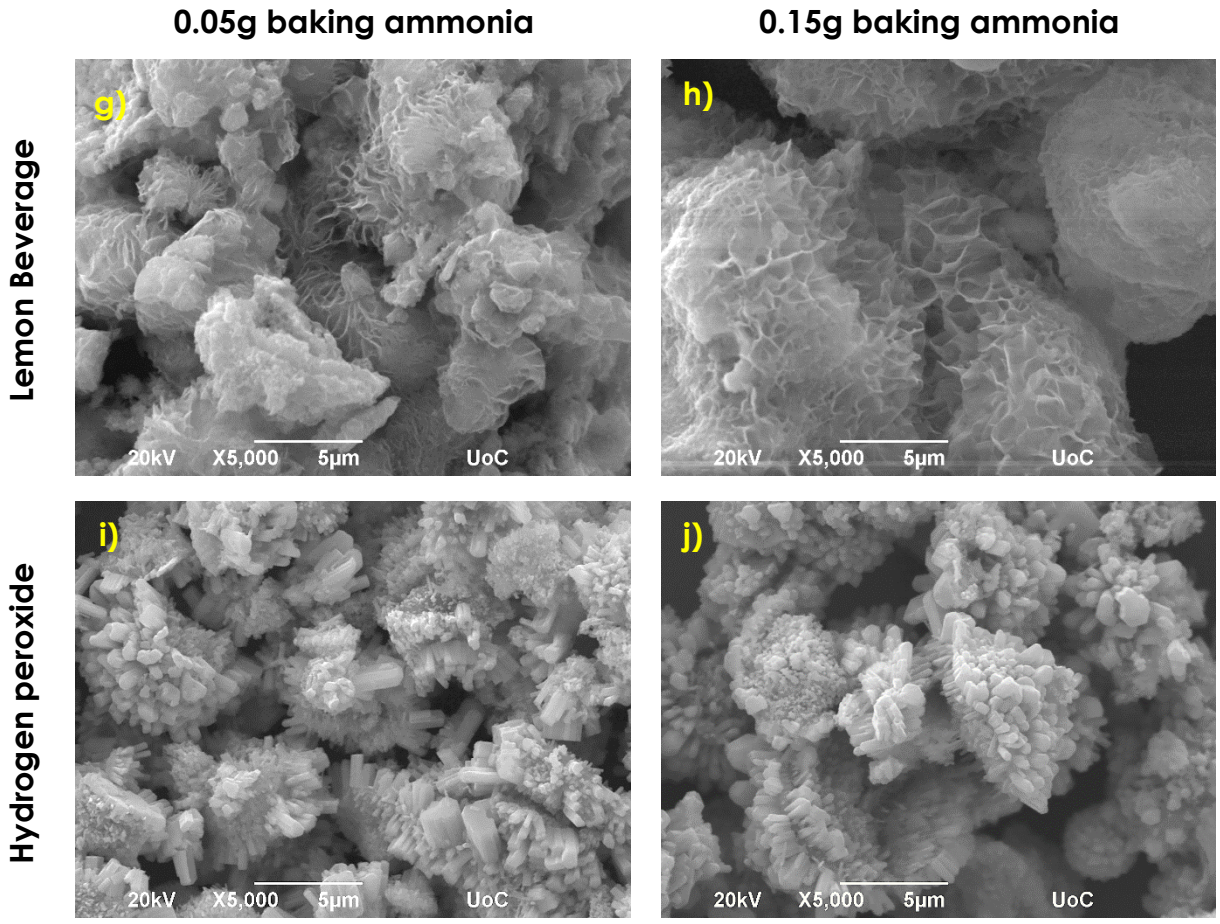

Figure 3.20 SEM images of ZnO samples synthesized at 195 °C with zinc powder and baking ammonia

3.4.2 Qualitative elemental analysis – EDX

EDX analysis was performed for the elemental analysis of the above samples.

Figure 3.21 illustrates a typical spectrum resulted from the EDX analysis of the sample prepared with zinc powder and 0.05g of baking ammonia in lemon beverage, that was used as solvent, at 195 °C.

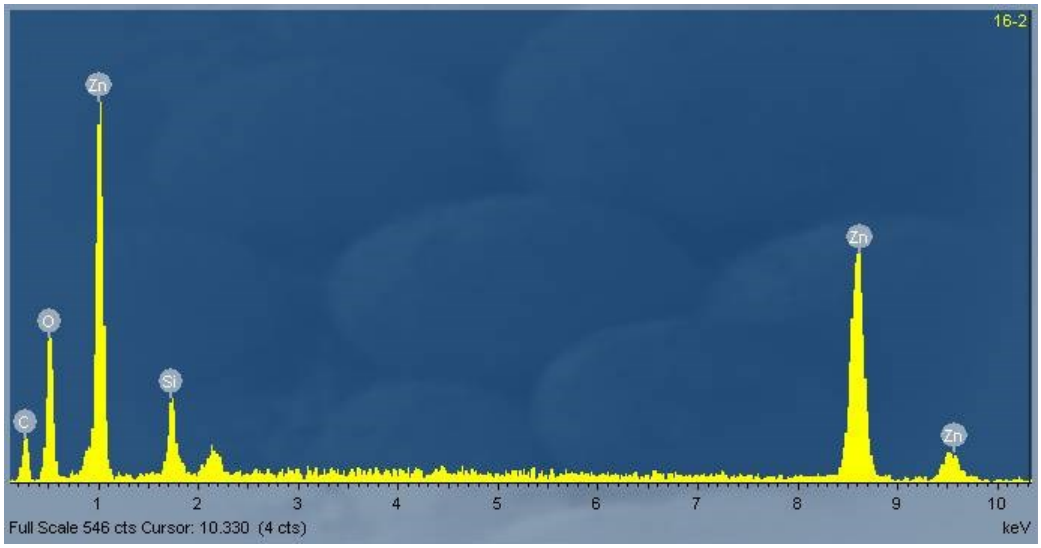

Figure 3.21 EDX spectrum of ZnO samples synthesized with zinc powder and 0.05g of baking ammonia at 195°C in lemon beverage solvent on silicon (100) substrate

The results confirmed the presence of zinc metal (Zn), oxygen (O), silicon (Si) as well as carbon. Si element derived from the silicon substrate on which the deposition of ZnO nanostructures took place, while the C element came from the carbon tape used to fix the samples in the SEM chamber.

3.4.3 Structural characterization – XRD

Figure 3.22 presents the XRD patterns of the prepared samples in water, ethanol, soda water, lemon beverage and hydrogen peroxide (2.8% w/w).

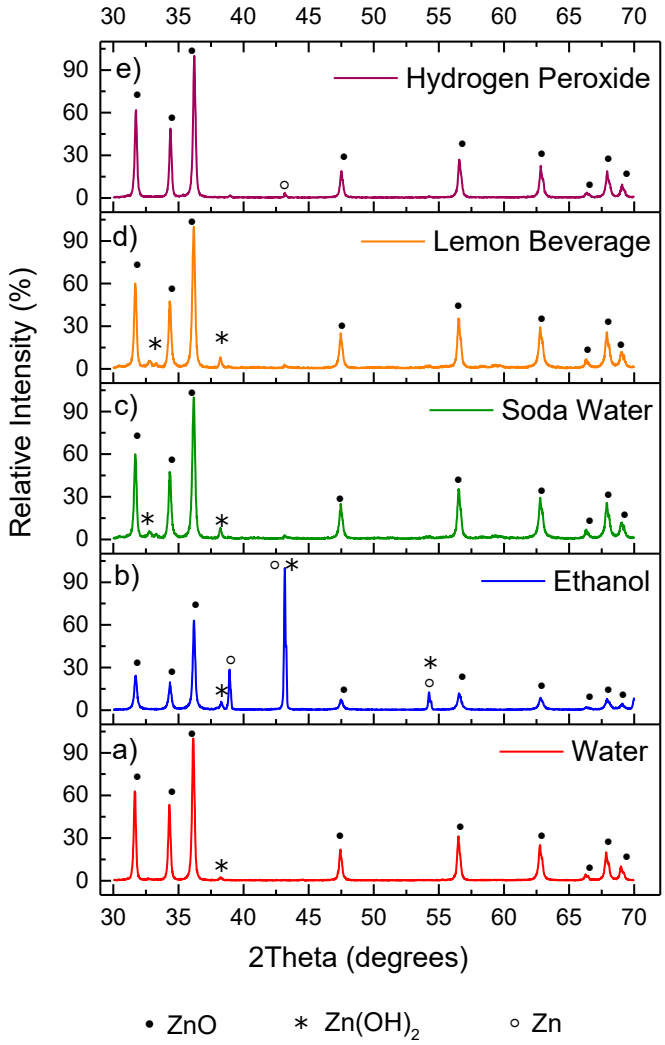

Figure 3.22 Typical XRD patterns of the samples prepared with zinc powder and baking ammonia at 195°C for 24 hours in five different solvents

The XRD pattern of the sample prepared with zinc powder and baking ammonia in aqueous solution is depicted in figure 3.22a). The peaks are shown at 31.66°, 34.4°, 36.14°, 47.44°, 56.5°, 62.78°, 66.26°, 67.84°, 68.98° and are corresponding to (100), (002), (101), (102), (110), (103), (200), (112) and (210) crystal planes of the hexagonal wurtzite ZnO (JCPDS 36-1451) [37]. Black dots mark the peaks attributed to ZnO. The star "*"

symbol is used to declare the low intensity peak that corresponds to $Zn(OH)_2$, according to the JCPDS card no. 38-0387 [95]. Thus as the XRD pattern indicates, in the aqueous solutions of the reactants, no pure ZnO was formed as $Zn(OH)_2$ did not completely transformed into ZnO.

The substitution of solvent with ethanol, also leads to the conclusion that there was not complete transformation of zinc metal to ZnO, as it is indicated by the respective XRD pattern of figure 3.21b). The extra peaks obtained were matched to Zn (JCPDS 87-0713) as well as to $Zn(OH)_2$ (JCPDS 38-0387) and are marked with "o" and "*", respectively [93]–[95]. The presence of such peaks denotes that some portion of zinc powder either did not react at all with HMTA or it partially reacted resulting in the formation of $Zn(OH)_2$. Further decomposition of $Zn(OH)_2$ was not achieved and thus the XRD peaks appeared. Maybe a longer duration of the synthesis procedure or even higher temperature would be necessary for the complete transformation.

Figures 3.22c) and 3.22d) represent the XRD patterns of the samples synthesized using soda water and lemon beverage, respectively. One can observe that the resulted diffraction peaks are the same. Sharp diffraction peaks, characteristic of the ZnO wurtzite hexagonal phase (JCPDS 36-1451), as well as peaks of very low intensity, attributed to $Zn(OH)_2$, can be observed in the XRD patterns. This lead to the conclusion that under the presence of soda water and lemon beverage solvents, the zinc powder did not fully transformed to ZnO.

Last but not least, the XRD pattern of the sample synthesized in hydrogen peroxide (2.8% w/w) solution is characterized by high intense diffraction peaks of ZnO, indicating the high crystallinity of ZnO, but a very weak diffraction peak of zinc metal can be also observed.

In conclusion, in this group of experiments, the XRD patterns did not reveal the formation of pure phase of ZnO. In all the samples the existence of byproducts was detected, but ethanol was the solvent with the strongest diffraction peaks attributed to impurities.

3.4.4 Optical characterization – XRD

For the PL spectroscopy measurements, the samples, prepared with zinc powder and baking ammonia, were excited by a He-Cd cw laser (325nm) and the spectra were obtained at RT (295K) as well as at 13K in the wavelength range from 335nm to 750nm.

Typical PL spectra of the prepared samples are illustrated in figure 3.23.

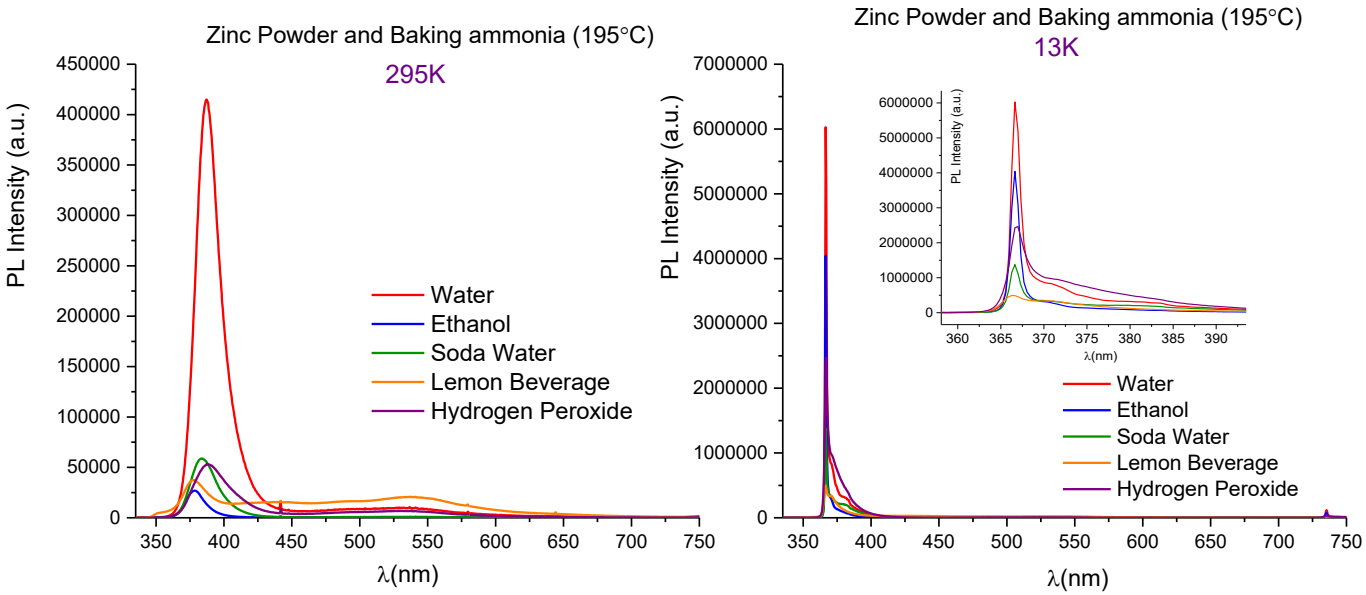

Figure 3.23 Typical PL spectra of the samples prepared with zinc powder and baking ammonia in five different solvents at 195°C for 24 hours. Left: PL spectra obtained at RT. Right: PL spectra obtained at 13K.

One can easily notice, that all the samples, independently of the solvent, exhibited the characteristic UV emission of ZnO at both temperatures. Furthermore, at RT a very weak broad emission at visible spectral region is observed

At RT the UV emission is centered at 387nm for water and hydrogen peroxide (2.8% w/w), at 379nm for ethanol, at 384nm for soda water and at 378nm for lemon beverage, corresponding to the energies of 3.204eV, 3.272eV, 3.229eV and 3.280eV, respectively.

At 13K the peaks present at UV spectral region are centered at 367nm for water, ethanol, soda water and hydrogen peroxide (2.8% w/w) and at 366nm for lemon beverage. The corresponding energies are 3.380eV and 3.390eV.

The higher PL intensity at RT exhibits the sample prepared with water, which increases its intensity by 15 times at 13K.

3.5. ZnO structures synthesized only with zinc powder

This is the fifth and last group of executed experiments. Without the use of either HMTA or baking ammonia, the zinc powder was simply dissolved at 195°C in four different solvents; water, ethanol, soda water, and hydrogen peroxide.

The morphological and structural characteristics of the synthesized samples, as well as their optical properties are analytically presented below.

3.5.1 Morphology – SEM

SEM images of the ZnO samples, prepared with only zinc powder, are presented in figure 3.24, at two different magnifications.

Sunflower structures of different sizes figures 3.24a), 3.24b), resulted from the aqueous solution of zinc powder at 195°C. The average diameter of these structures is ~6.5 μm. Also, it is obvious that there is no homogeneity, as some structures have irregular shape and do not form sunflowers. The substrate coverage can be estimated about 40-50%.

Figures 3.24c), 3.24d) reveal only a partial coverage of the substrate area (~30-35%), while again there is no homogeneity. Small and larger rods, as well as hexagonal flakes are formed.

Reaction of zinc powder with soda water solvent gave flowerlike structures with mean diameter of ~10μm. These flowerlike structures consist of flakes that have average width ~250nm and edge length ~2μm (figures 3.24e, 3.24f)). The substrate is 85-90% covered.

Last but not least, the hydrogen peroxide (2.8 % w/w) solvent created inhomogeneity regarding the morphologies (figures 3.24g), 3.24h)). Tip rods with typical lengths of ~8μm and width of 500nm were formed and co-existed with spherelike structures, which were composed of rods with mean length 1-2μm and width 500nm, respectively.

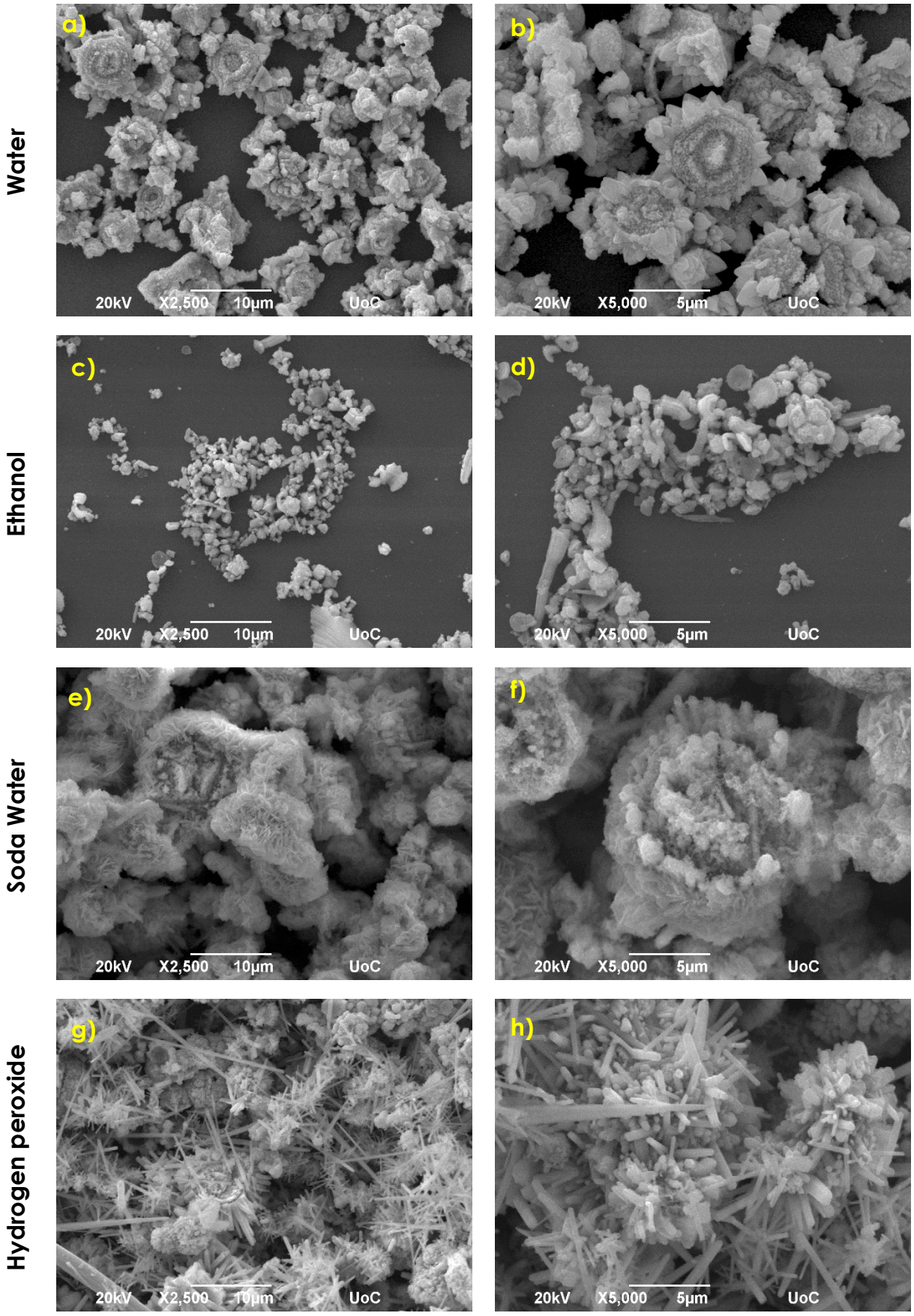

Figure 3.24 *SEM images* of ZnO samples synthesized at 195 °C with only zinc powder

3.5.2 Qualitative elemental analysis – EDX

The EDX spectrum of figure 3.25 corresponds to the sample fabricated by dissolving zinc powder in hydrogen peroxide (2.8% w/w) at 195°C for 24 hours.

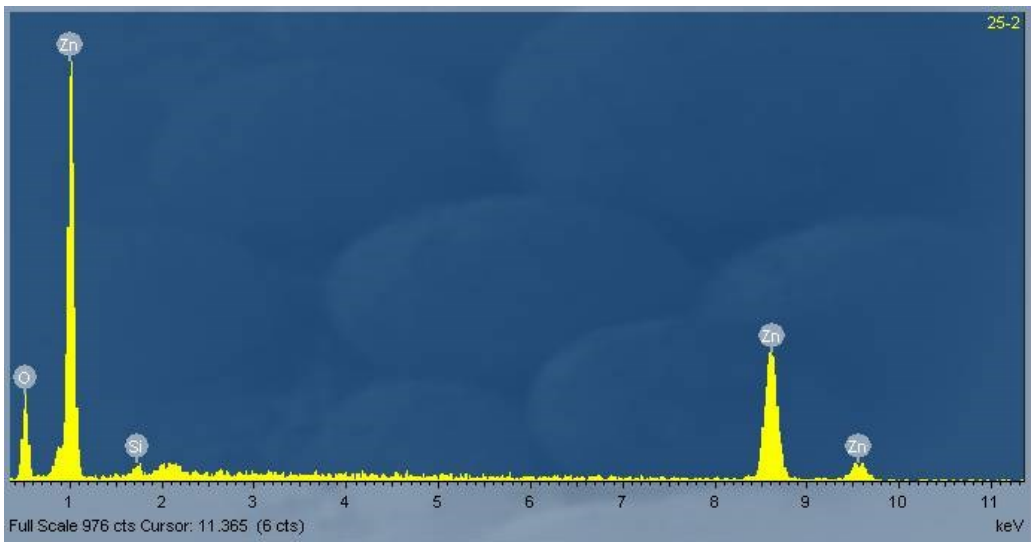

Figure 3.25 EDX spectrum of ZnO samples synthesized with zinc powder at 195 °C in hydrogen peroxide (2.8% w/w) solvent on silicon (100) substrate

Again three strong zinc metallic (Zn) signals and one weak signal of oxygen (O) are presented. The peak of silicon (Si) element derives from the silicon substrate.

Similarly to the previous, only one typical EDX spectrum is presented in this group of experiments, because all the fabricated samples exhibited the same behavior.

3.5.3 Structural characterization – XRD

For further characterization of the samples synthesized in the last group of experiments XRD was performed, and the respective patterns are presented in figure 3.26.

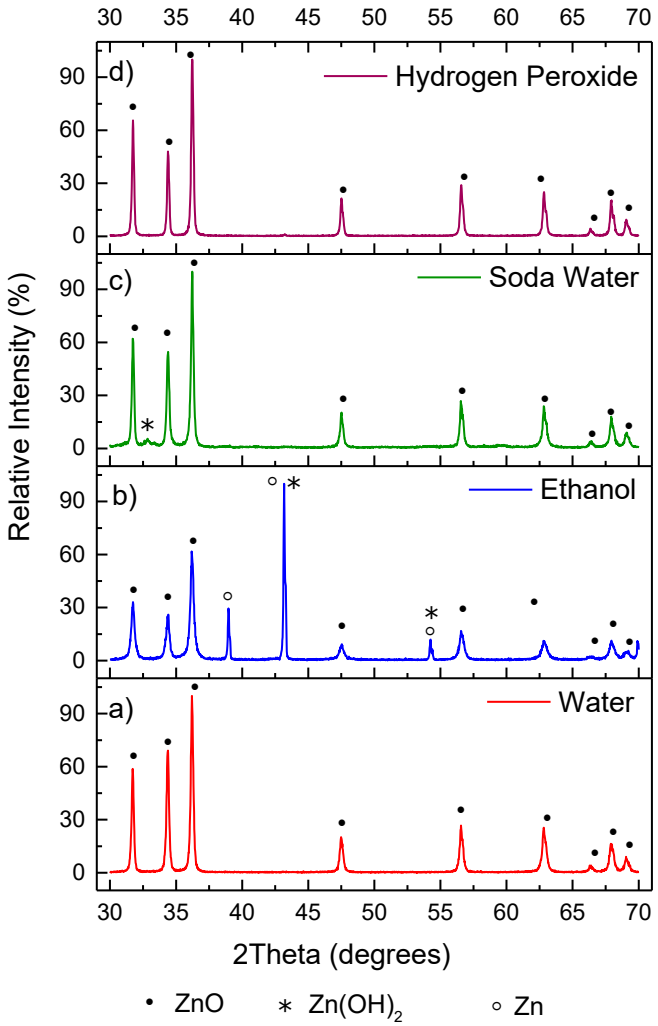

Figure 3.26 XRD patterns of the samples prepared with zinc powder at 195°C for 24 hours in four different solvents

The XRD pattern of aqueous solution of zinc powder at 195°C (figure 3.26a)), shows reflections at 31.72°, 34.38°, 36.2°, 47.48°, 56.56°, 62.82°, 66.3°, 67.9°, 69.04° which are corresponding to (100), (002), (101), (102), (110), (103), (200), (112) and (210) crystal planes of the hexagonal wurtzite ZnO (JCPDS 36-1451) [37]. Black dots mark the peaks attributed to ZnO. Pure ZnO was formed, as no characteristic diffraction peaks from byproducts were detected. Moreover, the high intense diffraction peaks

indicate the well crystalline nature of ZnO particles. Exactly the same behavior is followed by the sample of ZnO synthesized in hydrogen peroxide (2.8% w/w) solvent, as it is depicted in figure 3.26d).

On the other hand, the use of ethanol as the solvent, resulted in partially formed ZnO. The respective XRD pattern of figure 3.26b) indicates that there is coexistence of Zn, $Zn(OH)_2$ and ZnO phase, as the diffraction peaks of these compounds exist were matched with the JCPDS cards of no. 38-0387 and no. 87-0713, respectively. The fact that ethanol did not fully transformed Zn to ZnO means that either the reaction time was short or the temperature of the synthesis was low.

Last but not least, figure 3.26c) reveals that the soda water solvent, also did not result in pure ZnO, as a small diffraction peak $Zn(OH)_2$ can be observed.

However, ethanol was the solvent that resulted to the more and higher intensity peaks of other chemical compounds, leading to the conclusion that is was the only solvent that did not help to the formation of ZnO by this environmental friendly approach.

3.5.4 Optical characterization – PL

PL measurements were also performed to the samples synthesized with only zinc powder, in order to investigate if the characteristic UV emission of ZnO was present. The spectra were obtained at RT (295K) as well as at 13K in the wavelength range from 335nm to 750nm.

Figure 3.27 presents the PL spectra of the prepared samples.

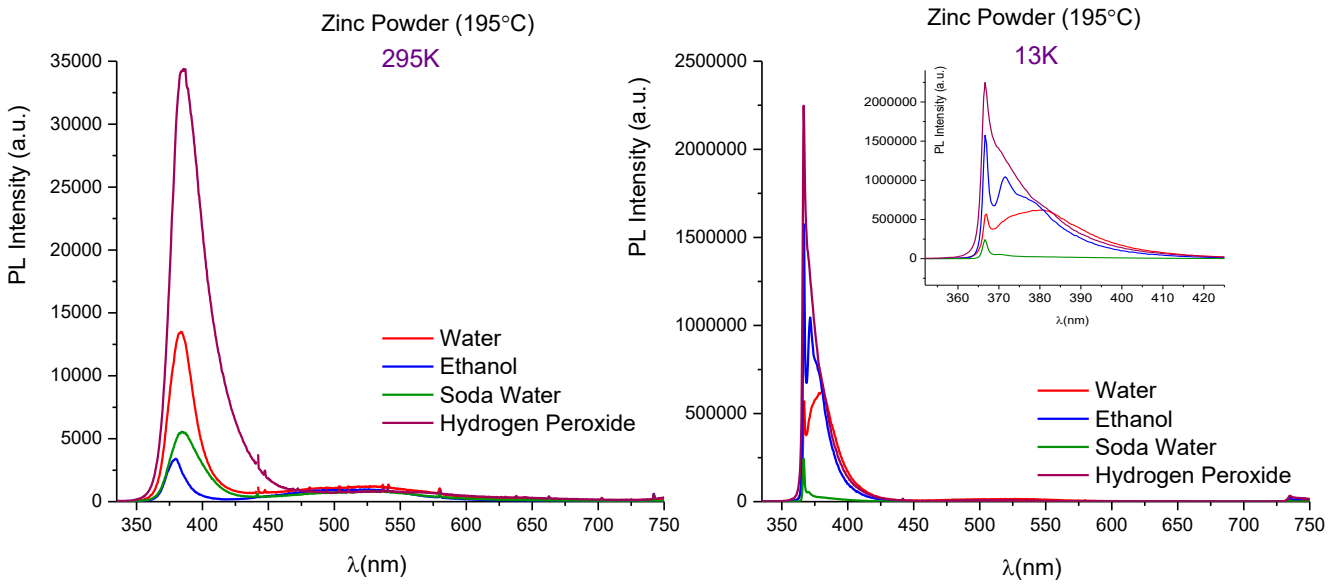

Figure 3.27 Typical PL spectra of the samples prepared with zinc powder and HMTA in five different solvents at 195°C for 24 hours. Left: PL spectra obtained at RT. Right: PL spectra obtained at 13K.

As it can be seen all the samples, independent of the solvent used, exhibited the characteristic UV emission of ZnO at both temperatures, while at RT a very weak broad emission at visible spectral region is also observed.

At RT the UV emission is centered at 384nm for water and soda water, at 380nm for ethanol and at 386nm for hydrogen peroxide (2.8% w/w), corresponding to the energies of 3.229eV, 3.263eV and 3.212eV, respectively.

At 13K all the UV emissions are centered at 367nm, which corresponds to 3.380eV.

The sample prepared with hydrogen peroxide (2.8% w/w) exhibits the higher PL intensity at RT, which increases by 63 times at 13K.

3.5.5 Raman Spectroscopy

All the prepared samples exhibited the same behavior regarding the Raman spectroscopy measurements. Figure 3.28 shows a typical Raman spectrum of ZnO nanostructures grown on Si(100) substrates for 2 hours or 24 hours, at either 95°C or 195°C, using any combination of reagents (Zn salts, solvents etc.). The observed phonon frequencies, indicating the presence of ZnO according to the literature [96], [97] are: 334 cm^{-1} (multiple-phonon scattering processes), 378 cm^{-1} (A1(TO)), 409 cm^{-1} (E1(TO)), 436 cm^{-1} (E2(high)) and 582 cm^{-1} (E1(LO)).

Among these peaks, the E2(high) mode at 436 cm^{-1}, having the strongest intensity, corresponds to the band characteristic of the wurtzite phase.

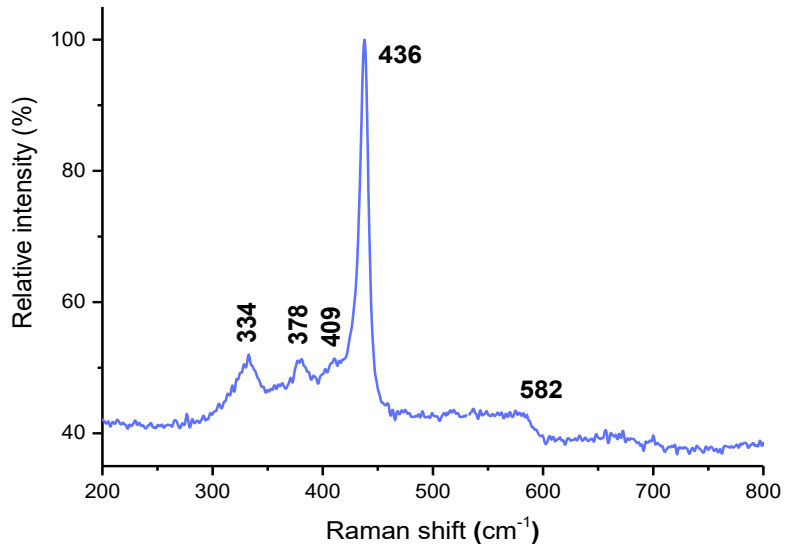

Figure 3. 28 Typical Raman spectrum of ZnO nanostructures grown on ACG on Si(100)

Therefore, the recorded Raman spectrum clearly demonstrates that the composed ZnO particles have hexagonal wurtzite structure of good crystal quality, a result which is in agreement with the XRD analysis.

3.6. Analysis of the photoluminescence (PL) measurements

So far, the PL performance of all the samples, synthesized in the previous five groups of experiments, was examined. There were samples that exhibited very strong PL performance, while some others did not show any special behavior. In order to conclude which group of experiments resulted to the best PL performance, the best samples of each group of experiments are compared below, regarding their PL emission.

Figure 3.28 illustrates the room temperature PL spectra of different ZnO samples.

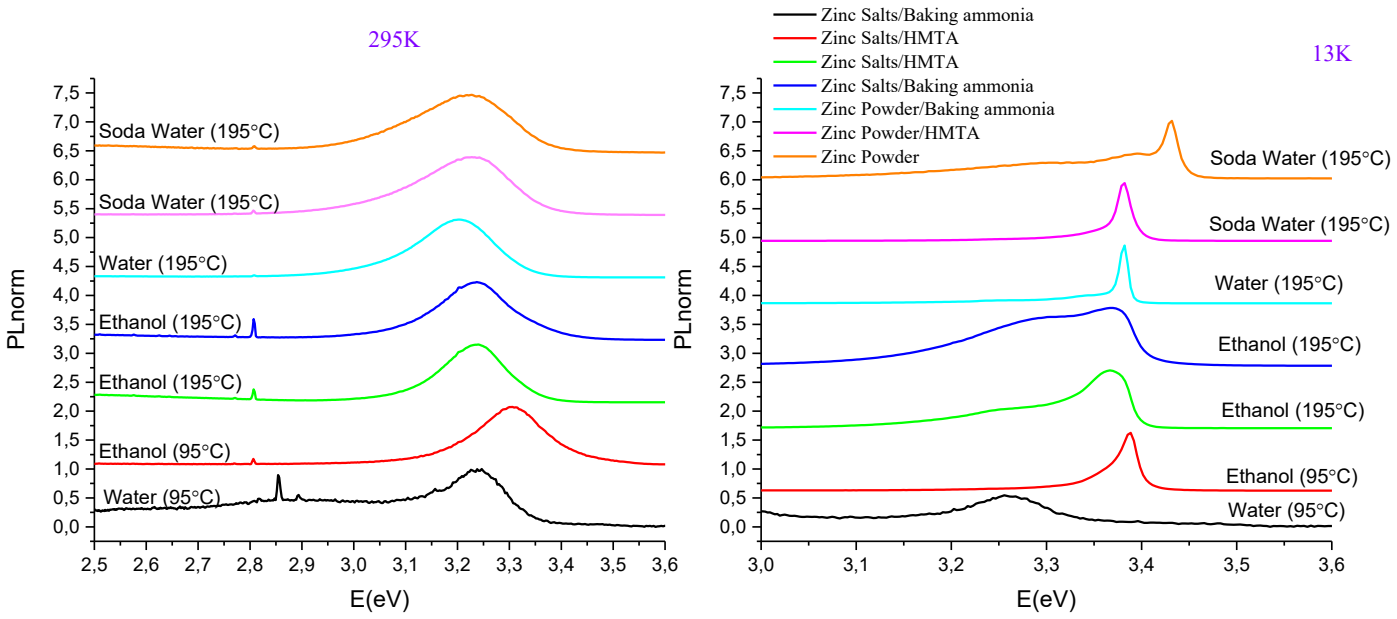

Figure 3.29 Comparison of the PL spectra (at RT and 13K) of the ZnO samples prepared in different groups of experiments.

As it can be observed, the UV emission changes from 3.224eV (Light blue line: Zinc Powder/Baking ammonia in water) to 3.303eV (Red line: Zinc Salts/HMTA in ethanol solution (195°C)), due to the non-stoichiometry of the sample. Last but not least, the FWHM is about 200meV, for all samples.

From low temperature PL spectra (13K), a strong emission is observed at ~3.38eV corresponding to free exciton (FX). The sample synthesized in aqueous solution of zinc salts and baking ammonia (Black line) has not FX emission, while the sample prepared with zinc powder in soda water solvent shows a blue shift 50meV from the FX peaks. This probably happens due to non-stoichiometric ZnO growth.

The observation of FX, the high PL intensity and the small FWHM indicate good crystal quality of ZnO nanostructures, even in the samples grown in solvents like soda water.

The best PL performance was exhibited by:

- ZnO synthesized by zinc salts and HMTA at 95°C in ethanol solution.
- ZnO synthesized by zinc powder and baking ammonia at 195°C in aqueous solution.
- ZnO synthesized by zinc powder and HMTA at 195°C in soda water solution.

The PL analysis, of ZnO sample synthesized by zinc powder in soda water solvent, using Gaussian fit is presented in figure 3.29. The emission is centered at 3.379eV, while the FWHM is only 15meV (estimated by the Gaussian fit). The strong and narrow PL emission indicates the good crystalline structure of the as-prepared ZnO.

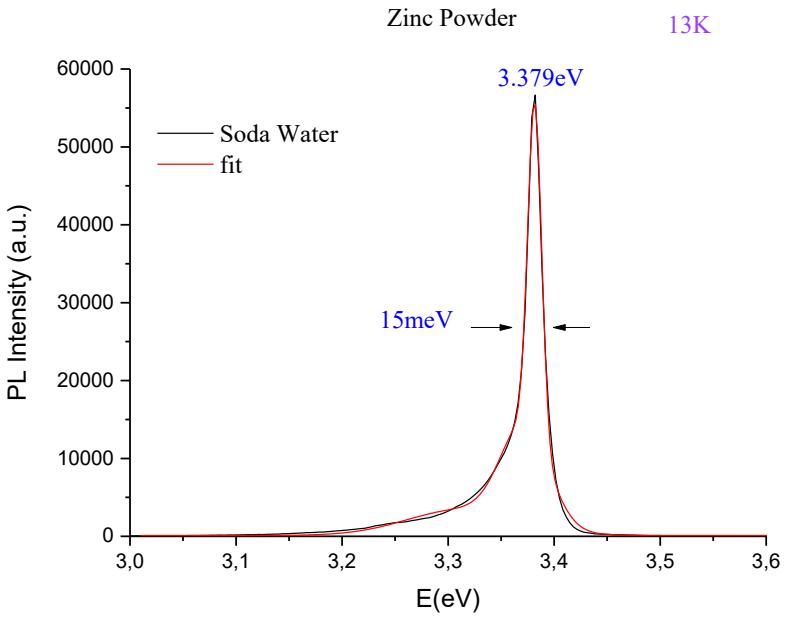

Figure 3.30 The PL analysis of ZnO sample, synthesized by zinc powder in soda water solvent, using Gaussian fit. The PL spectrum is recorded at 13K.

Chapter 4 – Conclusions

This Master thesis focused on the synthesis of ZnO nanostructures on Silicon(100) substrate, following environmental friendly approaches, and study of their structural and optical properties.

The synthesis of ZnO nanostructures was based on an aqueous solution chemical (ACG) method, a low cost, environmental friendly technique that does not require any complicate or expensive equipment, at mild temperatures. Moreover, it is the first time that ZnO was synthesized following the ACG approach at temperatures as high as 195°C max., using eco-friendly solvents, such as water or mild alcohol solutions;Five different sets of experiments were carried out and more than seventy samples were synthesized.

In the first set of experiments, zinc nitrate and zinc acetate (zinc salts) and HMTA reacted in water, ethanol, raki and ouzo. Each synthesis was executed at 95°C and 195°C for 2 hours. The morphology of the ZnO samples was characterized by diversity, depending on the zinc precursor and the solvent used as well as the synthesis temperature. Higher temperature led to the formation of structures with better crystal structure. A typical example is the sample prepared in raki, as the flake-like structure was converted to hexagonal rods when the synthesis temperature increased from 95°C to 195°C. Regarding the structural morphology of the prepared samples, XRD patterns revealed the hexagonal wurtzite phase of ZnO. The PL measurements of the samples synthesized at 95°C showed that the higher intensity was attributed to the sample synthesized in aqueous solutions, while the increase in the synthesis temperature made ethanol the best candidate. Key role to this plays the quite similar morphology of the respective ZnO structures.

The second set of experiments, consisted from ZnO samples synthesized with solutions of zinc salts and baking ammonia, prepared in water, ethanol, raki and ouzo. Once more, the synthesis temperature was set to either 95°C or 195°C, while the duration of each experiment was 2 hours. The derived morphologies were different from the ones resulted when HMTA was used instead of baking ammonia. The structural characterization of the synthesized samples revealed the existence of $Zn(OH)_2$ byproducts along with ZnO. Furthermore, according to the PL spectra, only water and ethanol were the solvents that made possible the UV emission at RT.

After the substitution of HMTA by baking ammonia, the zinc salts were substituted by zinc powder. Thus, the third set of experiments, included ZnO samples prepared by dissolving zinc powder and HMTA in water, ethanol, soda water, lemon beverage and hydrogen peroxide (2.8% w/w). SEM images proved that different solvents led to different structures, while the XRD patterns revealed the hexagonal wurtzite phase of ZnO. However, some solvents did not led to the formation of pure ZnO, since other chemical compounds were present and depicted in the respective XRD patterns. Only water and hydrogen peroxide resulted on pure ZnO, while ethanol was the solvent having the more reflection peaks corresponding to other materials. All the samples exhibited RT UV emission, but soda water and hydrogen peroxide presented the strongest ones.

The simple substitution of HMTA by baking ammonia and the use of zinc source in the same solvents like before, constituted the fourth set of experiments. Upon changing the solvent and the amount of baking ammonia, different ZnO morphologies derived. All the XRD patterns were dominated by diffraction peaks of other chemical compounds, but again ethanol had the more and of higher intensity impurities' peaks. UV was emitted by all the samples at RT with the higher PL intensity being attributed by ZnO synthesized in water.

Finally, the fifth set of experiments includes all the samples prepared by decomposition of zinc powder in water, ethanol, soda water and hydrogen peroxide (2.8% w/w). The morphologies were not the same between the different solvents, while the structural characterization revealed the hexagonal wurtzite phase of ZnO. Samples prepared with water and hydrogen peroxide gave pure ZnO, while ethanol sample presented the more and higher intensity peaks of Zn and $Zn(OH)_2$. All the samples were characterized by RT UV emission, which corresponded to NBE emission of ZnO, but the one prepared in hydrogen peroxide solvent had the strongest.

It is worth mentioning that, in comparison to other research groups, edible alcoholic distillations were used as solvents, in order to synthesize different morphologies of ZnO, enriched with dopants coming from the characteristic ingredients of each drinking alcohol.

Moreover, we present nano- and micro-structures of ZnO, without further annealing which resulted in sharp photoluminescence characteristic peaks at room temperature, with intensities much higher than the ones recorded so far.

It is concluded that ZnO nanostructures can be synthesized based on an environmental green synthesis approach, using non-toxic reagents, exhibiting remarkable PL properties.

References

[1] M. Ojeda, B. Chen, D. Y. C. Leung, J. Xuan, and H. Wang, "A hydrogel template synthesis of TiO2 nanoparticles for aluminium-ion batteries," *Energy Procedia*, vol. 105, pp. 3997–4002, 2017.

[2] Y. Tian, D. Liu, F. Luo, and H. Qi, "A rapid and convenient method for the preparation of thermochromic VO2 thin fi lms," *Mater. Res. Bull.*, vol. 94, pp. 100–103, 2017.

[3] S. Sel, O. Duygulu, U. Kadiroglu, and N. E. Machin, "Synthesis and characterization of nano-V2O5 by flame spray pyrolysis , and its cathodic performance in Li-ion rechargeable batteries," *Appl. Surf. Sci.*, vol. 318, pp. 150–156, 2014.

[4] P. A. Shinde, A. C. Lokhande, A. M. Patil, and C. D. Lokhande, "Facile synthesis of self-assembled WO3 nanorods for high-performance electrochemical capacitor," *J. Alloys Compd.*, vol. 770, pp. 1130–1137, 2019.

[5] Y. H. Navale *et al.*, "Rapid synthesis strategy of CuO nanocubes for sensitive and selective detection of NO2," *J. Alloys Compd.*, vol. 708, pp. 456–463, 2017.

[6] D. Gupta, S. R. Meher, N. Illyaskutty, and Z. C. Alex, "Facile synthesis of Cu2O and CuO nanoparticles and study of their structural , optical and electronic properties," *J. Alloys Compd.*, vol. 743, pp. 737–745, 2018.

[7] M. Pudukudy and Z. Yaakob, "Facile solid state synthesis of ZnO hexagonal nanogranules with excellent photocatalytic activity," *Appl. Surf. Sci.*, vol. 292, pp. 520–530, 2014.

[8] J. Chen and L. Shao, "MASS PRODUCTION OF NANOPARTICLES BY HIGH GRAVITY REACTIVE PRECIPITATION TECHNOLOGY WITH LOW COST," *China Particuology*, vol. 1, no. 2, pp. 64–69, 2003.

[9] S. Kaviya and E. Prasad, "Eco-friendly synthesis of ZnO nanopencils in aqueous medium: A study of photocatalytic degradation of methylene blue under direct sunlight," *RSC Adv.*, vol. 6, no. 40, pp. 33821–33827, 2016.

[10] F. Yakuphanoglu, "Transparent metal oxide films based sensors for solar tracking applications," *Compos. Part B Eng.*, vol. 92, pp. 151–159, 2016.

[11] C. Rodwihok, S. Choopun, P. Ruankham, A. Gardchareon, S. Phadungdhitidhada, and D. Wongratanaphisan, "UV sensing properties of ZnO nanowires/nanorods," *Appl. Surf. Sci.*, 2017.

[12] R. Dalvand, S. Mahmud, J. Rouhi, and C. H. Raymond Ooi, "Well-aligned ZnO nanoneedle arrays grown on polycarbonate

substrates via electric field-assisted chemical method," *Mater. Lett.*, vol. 146, pp. 65–68, 2015.

[13] L. Gou and C. J. Murphy, "Solution-phase synthesis of Cu2O nanocubes," *Nano Lett.*, vol. 3, no. 2, pp. 231–234, 2003.

[14] G. A. M. Ali, M. M. Yusoff, E. R. Shaaban, and K. F. Chong, "High performance MnO2 nanoflower supercapacitor electrode by electrochemical recycling of spent batteries," *Ceram. Int.*, vol. 43, no. 11, pp. 8440–8448, 2017.

[15] A. V. Nikam, B. L. V. Prasad, and A. A. Kulkarni, "Wet chemical synthesis of metal oxide nanoparticles: A review," *CrystEngComm*, vol. 20, no. 35, pp. 5091–5107, 2018.

[16] H. J. Kim and J. H. Lee, "Highly sensitive and selective gas sensors using p-type oxide semiconductors: Overview," *Sensors Actuators, B Chem.*, vol. 192, pp. 607–627, 2014.

[17] D. Vernardou, E. Spanakis, G. Kenanakis, E. Koudoumas, and N. Katsarakis, "Hydrothermal growth of V2O5 photoactive films at low temperatures," *Mater. Chem. Phys.*, vol. 124, no. 1, pp. 319–322, 2010.

[18] J. Huang, Z. Yin, and Q. Zheng, "Applications of ZnO in organic and hybrid solar cells," *Energy Environ. Sci.*, vol. 4, pp. 3861–3877, 2011.

[19] Y. Panahi, H. Mellatyar, M. Farshbaf, Z. Sabet, T. Fattahi, and A. Akbarzadehe, "Biotechnological applications of nanomaterials for air pollution and water/wastewater treatment," *Mater. Today Proc.*, vol. 5, no. 7, pp. 15550–15558, 2018.

[20] C. G. Granqvist, A. Azens, P. Heszler, L. B. Kish, and L. Österlund, "Nanomaterials for benign indoor environments: Electrochromics for 'smart windows', sensors for air quality, and photo-catalysts for air cleaning," *Sol. Energy Mater. Sol. Cells*, vol. 91, no. 4, pp. 355–365, 2007.

[21] M. A. Zimmler, T. Voss, C. Ronning, and F. Capasso, "Exciton-related electroluminescence from ZnO nanowire light-emitting diodes," *Appl. Phys. Lett.*, vol. 94, no. 241120, pp. 1–4, 2009.

[22] C. Y. Liu, H. Y. Xu, Y. Sun, J. G. Ma, and Y. C. Liu, "ZnO ultraviolet random laser diode on metal copper substrate," *Opt. Express*, vol. 22, no. 14, pp. 16731–16737, 2014.

[23] R. Viter *et al.*, "Novel immune TiO2 photoluminescence biosensors for leucosis detection," *Procedia Eng.*, vol. 47, pp. 338–341, 2012.

[24] S. Gavalas *et al.*, "Vanadium oxide nanostructured thin films prepared by Aerosol Spray Pyrolysis for gas sensing and

thermochromic applications," *Mater. Sci. Semicond. Process.*, vol. 89, pp. 116–120, 2019.

[25] K. Ravichandran *et al.*, "Tuning the combined magnetic and antibacterial properties of ZnO nanopowders through Mn doping for biomedical applications," *J. Magn. Magn. Mater.*, vol. 358–359, pp. 50–55, 2014.

[26] J. Podporska-Carroll, E. Panaitescu, B. Quilty, L. Wang, L. Menon, and S. C. Pillai, "Antimicrobial properties of highly efficient photocatalytic TiO2 nanotubes," *Appl. Catal. B Environ.*, vol. 176–177, pp. 70–75, 2015.

[27] Ü. Özgür *et al.*, "A comprehensive review of ZnO materials and devices," *J. Appl. Phys.*, vol. 98, no. 041301, 2005.

[28] M. Premanathan, K. Karthikeyan, K. Jeyasubramanian, and G. Manivannan, "Selective toxicity of ZnO nanoparticles toward Gram-positive bacteria and cancer cells by apoptosis through lipid peroxidation," *Nanomedicine Nanotechnology, Biol. Med.*, vol. 7, no. 2, pp. 184–192, 2011.

[29] E. D. Sherly, J. J. Vijaya, N. C. S. Selvam, and L. J. Kennedy, "Microwave assisted combustion synthesis of coupled ZnO-ZrO2 nanoparticles and their role in the photocatalytic degradation of 2,4-dichlorophenol," *Ceram. Int.*, vol. 40, no. 4, pp. 5681–5691, 2014.

[30] M. Stan, A. Popa, D. Toloman, A. Dehelean, I. Lung, and G. Katona, "Enhanced photocatalytic degradation properties of zinc oxide nanoparticles synthesized by using plant extracts," *Mater. Sci. Semicond. Process.*, vol. 39, pp. 23–29, 2015.

[31] G. Sangeetha, S. Rajeshwari, and R. Venckatesh, "Green synthesis of zinc oxide nanoparticles by aloe barbadensis miller leaf extract: Structure and optical properties," *Mater. Res. Bull.*, vol. 46, no. 12, pp. 2560–2566, 2011.

[32] K. Elumalai and S. Velmurugan, "Green synthesis, characterization and antimicrobial activities of zinc oxide nanoparticles from the leaf extract of Azadirachta indica (L.)," *Appl. Surf. Sci.*, vol. 345, pp. 329–336, 2015.

[33] H. Agarwal, S. Venkat Kumar, and S. Rajeshkumar, "A review on green synthesis of zinc oxide nanoparticles – An eco-friendly approach," *Resour. Technol.*, vol. 3, no. 4, pp. 406–413, 2017.

[34] P. J. Lu, S. C. Huang, Y. P. Chen, L. C. Chiueh, and D. Y. C. Shih, "Analysis of titanium dioxide and zinc oxide nanoparticles in cosmetics," *J. Food Drug Anal.*, vol. 23, no. 3, pp. 587–594, 2015.

[35] A. Klini, S. Pissadakis, R. N. Das, E. P. Giannelis, S. H. Anastasiadis,

and D. Anglos, "ZnO-PDMS nanohybrids: A novel optical sensing platform for ethanol vapor detection at room temperature," *J. Phys. Chem. C*, vol. 119, no. 1, pp. 623–631, 2015.

[36] M. L. Zhang, F. Jin, M. L. Zheng, J. Liu, Z. S. Zhao, and X. M. Duan, "High efficiency solar cell based on ZnO nanowire array prepared by different growth methods," *RSC Adv.*, vol. 4, no. 21, pp. 10462–10466, 2014.

[37] G. Kenanakis, M. Androulidaki, E. Koudoumas, C. Savvakis, and N. Katsarakis, "Photoluminescence of ZnO nanostructures grown by the aqueous chemical growth technique," *Superlattices Microstruct.*, vol. 42, pp. 473–478, 2007.

[38] A. Kolodziejczak-Radzimska and T. Jesionowski, "Zinc oxide-from synthesis to application: A review," *Materials (Basel).*, vol. 7, no. 4, pp. 2833–2881, 2014.

[39] E. Hasabeldaim, O. M. Ntwaeaborwa, R. E. Kroon, V. Craciun, E. Coetsee, and H. C. Swart, "Surface characterization and cathodoluminescence degradation of ZnO thin films," *Appl. Surf. Sci.*, vol. 424, pp. 412–420, 2017.

[40] S. S. Kurbanov, H. C. Jeon, Z. S. Shaymardanov, R. Y. Rakhimov, and T. W. Kang, "Photoluminescence from porous textured ZnO films grown by chemical bath deposition," *J. Lumin.*, vol. 170, pp. 168–173, 2016.

[41] H. Morkoç and Ü. Özgür, "General Properties of ZnO," in *Zinc Oxide: Fundamentals, Materials and Device Technology*, 2009, pp. 1–76.

[42] V. A. Coleman and C. Jagadish, "Chapter 1 Basic Properties and Applications of ZnO," in *Zinc Oxide Bulk, Thin Films and Nanostructures*, 2006, pp. 1–20.

[43] A. Hernandez Battez *et al.*, "CuO , ZrO2 and ZnO nanoparticles as antiwear additive in oil lubricants," *Wear*, vol. 265, pp. 422–428, 2008.

[44] A. B. Djurišić and Y. H. Leung, "Optical Properties of ZnO Nanostructures," *Small J.*, vol. 2, no. 8–9, pp. 944–961, 2006.

[45] D. P. Norton *et al.*, "ZnO : growth , doping & processing," *materialstoday*, vol. 7, no. 6, pp. 34–40, 2004.

[46] D. Depla, S. Mahieu, and J. E. Greene, "Chapter 5 - Sputter Deposition Processes," in *Handbook of Deposition Technologies for Films and Coatings*, Third Edit., Elsevier Ltd., 2010, pp. 253–296.

[47] "6.4 Physical Processes for Layer Deposition." [Online]. Available: https://www.tf.uni-

kiel.de/matwis/amat/elmat_en/kap_6/backbone/r6_4_1.html.

[48] N. Hardy, "What is thin film deposition by thermal evaporation?," 2013. [Online]. Available: http://www.semicore.com/news/71-thin-film-deposition-thermal-evaporation.

[49] "Thermal evaporation in vacuum." [Online]. Available: https://www.icmm.csic.es/fis/english/evaporacion_resistencia.html.

[50] R. Eason, *Pulsed Laser Depodition of Thin Films*. Wiley and Sons, Inc., 2006.

[51] "Pulsed laser deposition." [Online]. Available: https://en.wikipedia.org/wiki/Pulsed_laser_deposition.

[52] S. A. Kandjani, S. Mirershadi, and A. Nikniaz, "Inorganic – Organic Perovskite Solar Cells," in *Solar Cells-New Approaches and Reviews*, L. A. Kosyachenko, Ed. INTECH, 2015.

[53] L. E. Scriven, "Physics and applications of dip and spin coating," *Mater. Res. Soc. Proc.*, vol. 121, pp. 717–729, 1988.

[54] X.-T. Yan and Y. Xu, "Chemical Vapour Deposition," London: Springer, 2010, pp. 1–28.

[55] Wikipedia, "Chemical vapor deposition." [Online]. Available: https://en.wikipedia.org/wiki/Chemical_vapor_deposition.

[56] L. Vayssieres, "On the design of advanced metal oxide nanomaterials," *Int. J. Nanotechnol.*, vol. 1, no. 1–2, pp. 1–41, 2004.

[57] M. Mahdavi, F. Namvar, M. Bin Ahmad, and R. Mohamad, "Green biosynthesis and characterization of magnetic iron oxide (Fe3O4) nanoparticles using seaweed (Sargassum muticum) aqueous extract," *Molecules*, vol. 18, no. 5, pp. 5954–5964, 2013.

[58] A. Manikandan, R. Sridhar, S. Arul Antony, and S. Ramakrishna, "A simple aloe vera plant-extracted microwave and conventional combustion synthesis: Morphological, optical, magnetic and catalytic properties of CoFe2O4 nanostructures," *J. Mol. Struct.*, vol. 1076, pp. 188–200, 2014.

[59] D. Devipriya and S. M. Roopan, "Cissus quadrangularis mediated ecofriendly synthesis of copper oxide nanoparticles and its antifungal studies against Aspergillus niger, Aspergillus flavus," *Mater. Sci. Eng. C*, vol. 80, pp. 38–44, 2017.

[60] C. R. Rambo and H. Sieber, "Novel synthetic route to biomorphic Al2O3 ceramics," *Adv. Mater.*, vol. 17, no. 8, pp. 1088–1091, 2005.

[61] A. Diallo, E. Manikandan, V. Rajendran, and M. Maaza, "Physical & enhanced photocatalytic properties of green synthesized SnO2

nanoparticles via Aspalathus linearis," *J. Alloys Compd.*, vol. 681, pp. 561–570, 2016.

[62] R. Yuvakkumar, J. Suresh, A. J. Nathanael, M. Sundrarajan, and S. I. Hong, "Rambutan (Nephelium lappaceum L.) peel extract assisted biomimetic synthesis of nickel oxide nanocrystals," *Mater. Lett.*, vol. 128, pp. 170–174, 2014.

[63] M. Kumaresan, K. Vijai Anand, K. Govindaraju, S. Tamilselvan, and V. Ganesh Kumar, "Seaweed Sargassum wightii mediated preparation of zirconia (ZrO2) nanoparticles and their antibacterial activity against gram positive and gram negative bacteria," *Microb. Pathog.*, vol. 124, pp. 311–315, 2018.

[64] Q. Li, V. Kumar, Y. Li, H. Zhang, T. J. Marks, and R. P. H. Chang, "Fabrication of ZnO Nanorods and Nanotubes in Aqueous Solutions," *Chem. Mater.*, vol. 17, no. 5, pp. 1001–1006, 2005.

[65] M. K. Liang, M. J. Limo, A. Sola-Rabada, M. J. Roe, and C. C. Perry, "New Insights into the Mechanism of ZnO Formation from Aqueous Solutions of Zinc Acetate and Zinc Nitrate," *Chem. Mater.*, vol. 26, no. 14, pp. 4119–4129, 2014.

[66] X. M. Sun, X. Chen, Z. X. Deng, and Y. D. Li, "A CTAB-assisted hydrothermal orientation growth of ZnO nanorods," *Mater. Chem. Phys.*, vol. 78, no. 1, pp. 99–104, 2003.

[67] L. S. Panchakarla, A. Govindaraj, and C. N. R. Rao, "Formation of ZnO nanoparticles by the reaction of zinc metal with aliphatic alcohols," *J. Clust. Sci.*, vol. 18, no. 3, pp. 660–670, 2007.

[68] A. Zhao *et al.*, "Synthesis of ordered ZnO nanorods film on zinc-coated Si substrate and their photoluminescence property," *Mater. Chem. Phys.*, vol. 99, no. 1, pp. 50–53, 2006.

[69] A. Umar, S. H. Kim, Y. H. Im, and Y. B. Hahn, "Structural and optical properties of ZnO micro-spheres and cages by oxidation of metallic Zn powder," *Superlattices Microstruct.*, vol. 39, no. 1–4, pp. 238–246, 2006.

[70] Q.-L. Ma, R. Xiong, B.-G. Zhai, and Y. M. Huang, "Water assisted conversion of ZnO from metallic zinc particles," *Key Eng. Mater.*, vol. 538, pp. 38–41, 2013.

[71] "CFR-Code of Federal Regulations Title 21." [Online]. Available: https://www.accessdata.fda.gov/scripts/cdrh/cfdocs/cfCFR/CFRSearch.cfm?fr=184.1137.

[72] "Ammonium carbonate." [Online]. Available: https://en.wikipedia.org/wiki/Ammonium_carbonate.

[73] B. J. Inkson, *Scanning Electron Microscopy (SEM) and Transmission*

Electron Microscopy (TEM) for Materials Characterization. Elsevier Ltd, 2016.

[74] Wikipedia, "Electron microscope." [Online]. Available: https://en.wikipedia.org/wiki/Electron_microscope.

[75] "Module 3 : Microscopic techniques Lecture 17 : Electron Microscopy-I." [Online]. Available: https://nptel.ac.in/courses/102103044/module3/lec17/5.html.

[76] M. Joshi, A. Bhattacharyya, and S. W. Ali, "Characterization techniques for nanotechnology applications in textiles," *Indian J. Fibre Text. Res.*, vol. 33, no. 3, pp. 304–317, 2008.

[77] A. Baroon, Ed., *Physical Methods in Chemistry and Nano Science*.

[78] B. L. Dutrow, "X-ray Powder Diffraction (XRD)." [Online]. Available: https://serc.carleton.edu/research_education/geochemsheets/techniques/XRD.html.

[79] W. D. Callister and D. G. Rethwisch, *Materials Science and Engineering - An introduction*. John Wiley & Sons, Inc., 2010.

[80] K. S. Yoshio Waseda, Eiichiro Matsubara, *X - Ray Diffraction Crystallography*. Springer, 2011.

[81] "X-ray Powder Diffraction." [Online]. Available: https://slideplayer.com/slide/6143092/.

[82] "Bragg's Law." [Online]. Available: https://en.wikipedia.org/wiki/Bragg%27s_law.

[83] Wikipedia, "Bragg's law." [Online]. Available: https://en.wikipedia.org/wiki/Bragg%27s_law.

[84] Wikipedia, "Raman spectroscopy." [Online]. Available: https://en.wikipedia.org/wiki/Raman_spectroscopy.

[85] "What is Raman Spectroscopy ?" [Online]. Available: https://www.nanophoton.net/raman/raman-spectroscopy.html.

[86] HoribaScientific, "LabRAM HR Evolution 123456." [Online]. Available: http://www.horiba.com/uk/scientific/products/raman-spectroscopy/raman-spectrometers/raman-microscopes/hr-evolution/labram-hr-evolution-17309/.

[87] R. F. Pierret, *Advanced Semiconductor Fundamentals*, Second Edi. Boston, MA, USA: Addison-Wesley Longman Publishing Co., Inc.

[88] E. C. Larkins and J. S. Harris, "2 - Molecular Beam Epitaxy of High-Quality GaAs and AlGaAs," in *Molecular Beam Epitaxy*, 1st ed., R. F. C. Farrow, Ed. Noyes Publications, 1995, pp. 114–274.

[89] J. Zhang, L. Sun, J. Yin, H. Su, C. Liao, and C. Yan, "Control of ZnO

morphology via a simple solution route," *Chem. Mater.*, vol. 14, no. 10, pp. 4172–4177, 2002.

[90] I. Fatimah, "Biosynthesis and characterization of ZnO nanoparticles using rice bran extract as low-cost templating agent," *J. Eng. Sci. Technol.*, vol. 13, no. 2, pp. 409–420, 2018.

[91] G. Kenanakis, M. Androulidaki, D. Vernardou, N. Katsarakis, and E. Koudoumas, "Photoluminescence study of ZnO structures grown by aqueous chemical growth," *Thin Solid Films*, vol. 520, no. 4, pp. 1353–1357, 2011.

[92] J. Yin, F. Gao, C. Wei, and Q. Lu, "Water Amount Dependence on Morphologies and Properties of ZnO nanostructures in Double-solvent System," *Sci. Rep.*, vol. 4, pp. 1–7, 2014.

[93] D. L. T. Nguyen *et al.*, "Selective CO2 Reduction on Zinc Electrocatalyst: The Effect of Zinc Oxidation State Induced by Pretreatment Environment," *ACS Sustain. Chem. Eng.*, vol. 3, pp. 11377–11385, 2017.

[94] C.-H. Lu, T.-Y. Chao, Y.-F. Chiu, S.-Y. Tseng, and H.-C. Hsu, "Enhanced optical confinement and lasing characteristics of individual urchin-like ZnO microstructures prepared by oxidation of metallic Zn," *Nanoscale Res. Lett.*, vol. 9, no. 1, p. 178, 2014.

[95] S. Pung, W. Lee, and A. Aziz, "Kinetic Study of Organic Dye Degradation Using ZnO Particles with Different Morphologies as a Photocatalyst Kinetic Study of Organic Dye Degradation Using ZnO Particles with Different Morphologies as a Photocatalyst," *Int. J. Inorg. Chem.*, vol. 2012, pp. 1–9, 2012.

[96] G. Kenanakis, D. Vernardou, and N. Katsarakis, "Light-induced self-cleaning properties of ZnO nanowires grown at low temperatures," "*Applied Catal. A, Gen.*, vol. 411–412, pp. 7–14, 2012.

[97] Z. Zhaochun, H. Baibiao, Y. Yongqin, and C. Deliang, "Electrical properties and Raman spectra of undoped and Al-doped ZnO thin films by metalorganic vapor phase epitaxy," *Mater. Sci. Eng. B*, vol. 86, pp. 109–112, 2001.